HEATHGATE RESOURCES
Natural Attenuation Project

From Lab Tests
to
FME Aquifer
– Geochemical Modeling –

Report submitted to

Heathgate Resources Pty. Ltd. (HGR)
Suite 1, Level 4, 25 Grenfell Street, Adelaide, S. A. 5000, AUSTRALIA

by

Umwelt- und Ingenieurtechnik GmbH Dresden (UIT)
Zum Windkanal 21, D-01109 Dresden, GERMANY

Contact: Dr. Harald Kalka
Phone: +49-351-8 86 46 40
Fax: +49-351-8 86 57 73
e-mail: h.kalka@uit-gmbh.de

28 November 2008

REPORT

Natural Attenuation Project

From Lab Tests to FME Aquifer

– Geochemical Modeling –

AUTHORS: Dr. Harald Kalka
Dr. Jana Nicolai

REPORTED TO: Heathgate Resources Pty. Ltd. (HGR)
Suite 1, Level 4, 25 Grenfell Street, Adelaide, S.A. 5000
AUSTRALIA

SUBMITTED BY: Umwelt- und Ingenieurtechnik GmbH Dresden
Zum Windkanal 21
01109 Dresden, GERMANY

CONTENTS

APPENDIX

1 INTRODUCTION

1.1 Main Task and General Approach

In order to fulfill regulatory requirements regarding the Natural Attenuation (NA) processes in post-mining aquifers at Four Mile East (FME) investigation work was started in April/May 2008. This work is undertaken by ANSTO (column leaching), UIT (technical guidance, geochemical modeling) and HGR (batch tests, reporting, provision of testing material, facilitation of testing). The broader work program will be completed in mid to end 2009.

NA. In the present study, 'Natural Attenuation' means (i) the immobilization of uranium in the aquifer downstream the FME leaching area, and (ii) the post-mining groundwater restoration. The fate of uranium strongly depends on the hydro-geochemical conditions like pH, redox potential, and mineral composition. The aim of this study is (i) to understand these processes qualitatively and quantitatively by modeling batch and column tests performed with site-specific material, and (ii) to upscale the lab parameters for aquifer simulations.

Modeling Framework. The general approach consists of two separate models as shown in Fig. 1.1: (i) the 3D hydrogeological model (MODFLOW) and (ii) the geochemical model (reactive transport along a flow path). The MODFLOW calculations performed by Heathgate Resources [HGR08] provide the hydraulic input for the geochemical model which simulates rock-water interactions and the fate of uranium within the aquifer. The necessary parameters are taken from lab tests with site-specific material.

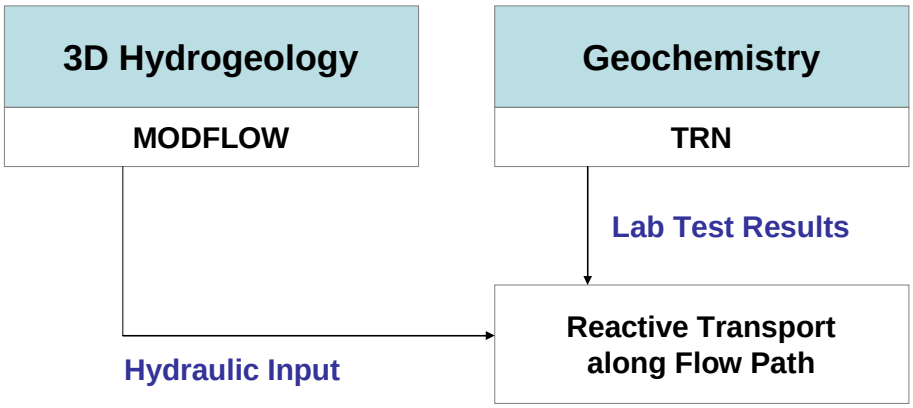

Fig. 1.1 Conceptual model for the NA problem in FME

The geochemical modeling performed by UIT is based on (i) PHREEQC and (ii) the reactive transport model TRN. It consists of two parts:

Part I: Interpretation of Column and Batch Tests
Part II: Reactive Transport Simulations in FME aquifer

Part I lays the foundations for subsequent aquifer studies in Chapter 4. Since uranium chemistry is highly complex (and still under world-wide investigation) we focus on the

main processes to give a 'robust' description of the experiments (with a minimum of assumptions and free parameters).

TRN Model. A reactive transport model was provided by UIT to describe the experiments and the geochemistry in the FME aquifer. It combines transport with geochemistry (thermodynamics and kinetics). In particular, the model/program consists of three main parts:

- transport module (advection & dispersion)
- chemical equilibrium module (based on PHREEQC routines)
- kinetic module (for mineral dissolution)

The present report contains a brief description of the reactive transport model TRN. The TRN code is a member of a family of other geochemical/limnological/microbiological models developed by UIT in the last 12 years. It is written in C++ and uses special chemistry classes which include the numerical routines of PHREEQC. TRN is able to handle more complex systems than PHREEQC.

TRN is easy to handle; it is equipped with online graphics and visualization tools. The user is able to interact with the running system and check easily intermediate results. About 20 % of the source code deals with plausibility tests. In particular, at every time step TRN checks the local and global mass balance (in single cells and the whole column). Any inconsistency generates an error message file.

1.2 Report Structure

The report is structured in 5 Chapters and extended by an appendix.

Chapter 2 – Column Tests.

Column data are obtained in July 2008. In order to understand the main geochemical processes almost 1 000 calculations are performed with TRN. As a result, the full gamut of redox processes that arises when a front of highly-oxidized water collides with reduced water/minerals could be reduced to a clear and manageable picture.

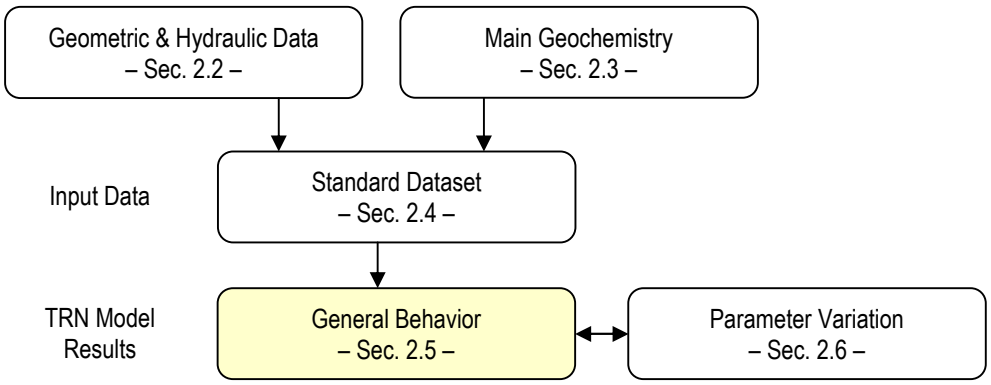

Fig. 1.2 Structure of Chapter 2 'Column Tests'

The structure of Chapter 2 is depicted in Fig. 1.2. After discussion of the geometric and hydraulic data in Sec. 2.2 and the main geochemical processes in Sec. 2.3 the model input for TRN is defined in Sec. 2.4. This so-called 'Standard Dataset' is used for the simulation of the column test; the results are described in Sec. 2.5. Finally, in order to better understand the chosen dataset and the geochemistry a lot of parameter variations were performed; the extract of these variations is presented in Sec. 2.6.

Chapter 3 – Batch Tests.

Batch data are obtained in September 2008. The batch tests are complementary to the column tests. In batch tests the residence time, i.e. the time while water and core material interact, is more than one order of magnitude greater than in the column tests (which have been performed at very high flow velocity). Online measurements of pH and ORP proved that after 4 days stirring equilibrium was attained. Thus, the transition into the final aqueous solution was simulated by the equilibrium model PHREEQC. The model results are described in Sec. 3.3.

Batch and column tests are based on the same fundamental assumptions and model parameters. This was achieved in a long run of single calculations and by a permanent cross-checking of the input datasets for batch and column tests.

Chapter 4 – Aquifer Simulations.

The aquifer simulations are in the focus of the present report. The structure of Chapter 4 is depicted in Fig. 1.3. In Sec. 4.1 three main scenarios have been defined to study the inflow of aggressive lixiviant from the Ore Zone into the undisturbed Four Mile Embayment: one scenario for transport studies and two scenarios for post mining studies ('Worst Case' and 'Real Case'). The generation of the 'Real Case' is described separately in Sec. 4.2.

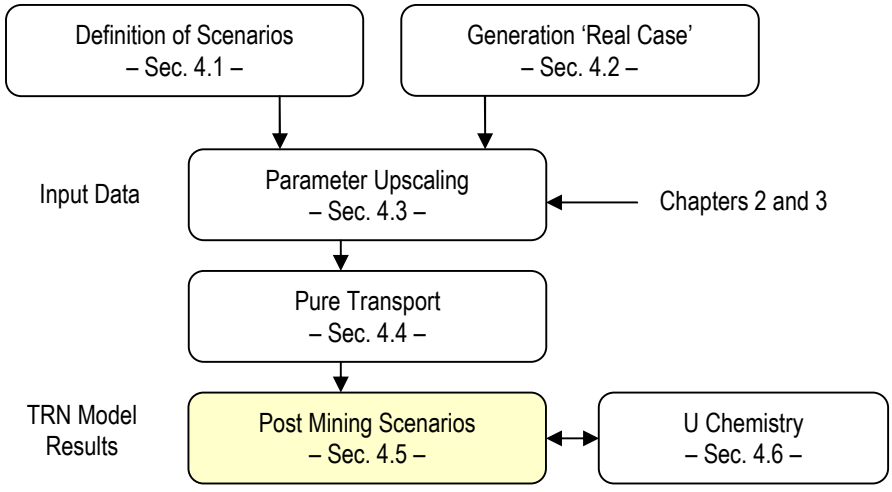

Fig. 1.3 Structure of Chapter 4 'Aquifer Simulations'

In Sec. 4.3 the input data for TRN are defined. This has been done by upscaling the obtained lab test parameters. In contrast to the column tests, we are now confronted with another space-time discretization and, hence, larger computation times (14 hours for

800 years forecast rather then 160 sec for 60 h column tests). The results are discussed in Sec. 4.4 and 4.5; all diagrams for the post-mining 'Worst Case' and 'Real Case' are presented in Appendix D. Finally, the uranium geochemistry is discussed in Sec. 4.6.

Chapter 5 – Summary and Conclusions.

Appendix A and B – Mathematical Model and Program Description

These chapters describe the reactive transport model TRN. Within the present report it has been used for the simulation of column tests and aquifer scenarios.

Appendix C – Core composition for column tests (taken from [AN07])

Appendix D – Model results (in form of diagrams) for the post-mining 'Worst Case' and 'Real Case'

Appendix E – Discussion of the impact of uncontrolled fractured rock flow

Abbreviations

1D	1-dimensional
3D	3-dimensional
ADR	Advection-Dispersion-Reaction Equation
ANSTO	Australian Nuclear Science and Technology Organization
CEC	Cation Exchange Capacity
CSIRO	Australia's National Science Agency
DIC	Dissolved Inorganic Carbon
DO	Dissolved Oxygen
Eh	Redox Potential in mV (relative to SHE)
ENA	Enhanced Natural Attenuation
FM	Four Mile
FME	Four Mile East (newly discovered uranium deposit)
GUI	Graphical User Interface
GW	Groundwater (also gw)
HGR	Heathgate Resources Pty. Ltd., Adelaide, South Australia
ISL	In-situ Leaching
IX	Ion Exchange
Lix	Lixiviant (also lix)
M	Mol per Liter (concentration unit: 1 M = 1 mol/L)
mM	Millimol per Liter (concentration unit: 1 mM = 1 mmol/L)
MNA	Monitored Natural Attenuation
NA	Natural Attenuation
ODE	Ordinary Differential Equation
ORP	Oxidation-Reduction Potential (in short: redox potential)
PDE	Partial Differential Equation
SHE	Standard Hydrogen Electrode
SI	Saturation Index
TRN	Reactive Transport Model developed by UIT and applied in this report
UIT	Umwelt- und Ingenieurtechnik GmbH Dresden, Germany
U-IX	Ion Exchange for Uranyl species
USGS	U.S. Geological Survey

2 COLUMN TESTS

2.1 Short Overview

ANSTO performed column tests [AN08] to simulate the inflow of aggressive lixiviant (pH = 1.7, ORP = 800 mV, U = 50 ppm) into a clean aquifer at pre-mining conditions (pH = 7, ORP = 0 mV). In contrast to reality, however, the columns were filled with groundwater of higher ORP (about 300 mV) – see Fig. 2.1. Thus, the NA effect of strong reductive conditions found in the field is weakened in the lab tests.

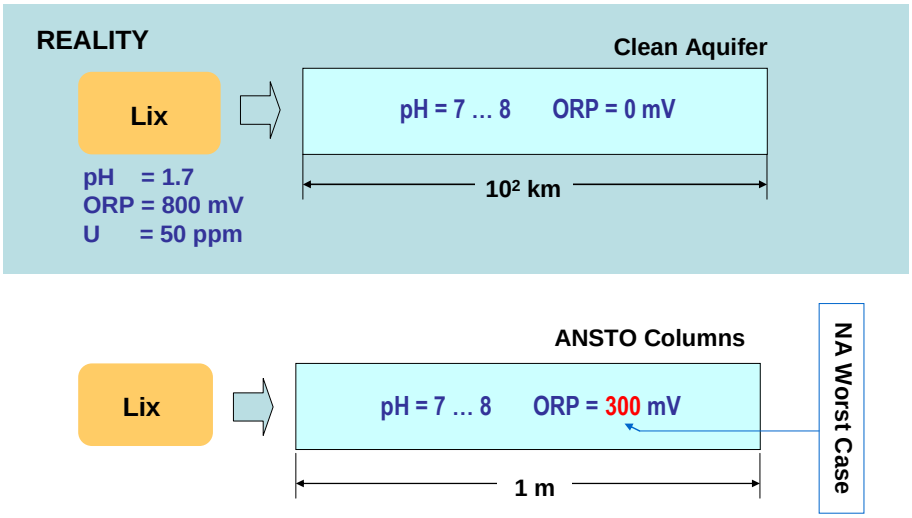

Fig. 2.1 Inflow of lixiviant into pre-mining aquifer (reality and lab tests)

Column Setup. Due to the special setup shown in Fig. 2.2 the inflow water is directed via a relatively large storage volume (tubes etc.) before it enters the column. When the experiment starts the initial groundwater in this storage volume will be replaced by the lixiviant successively (and avoids a sharp-front lix inflow). In order to simulate this effect the reactive transport model TRN (described in Chapters A and B) was modified by adding a storage/mix box in front of the first column cell.

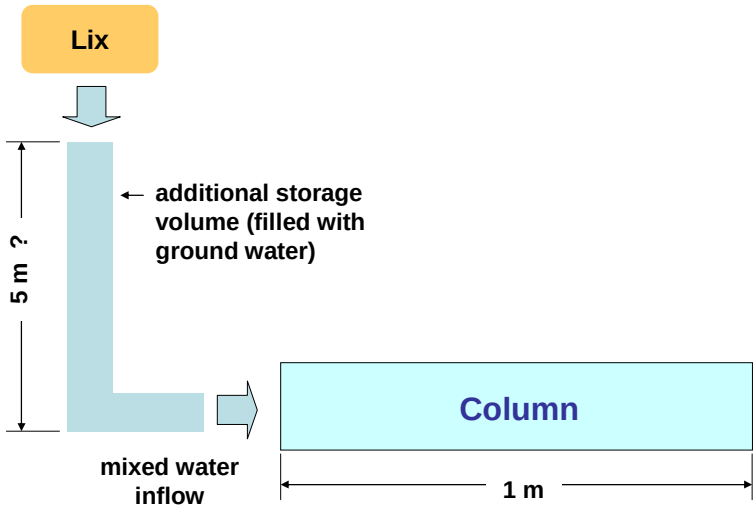

Fig. 2.2 Typical setup for ANSTO column tests

2.2 Geometric and Hydraulic Data

The geometric and hydraulic parameters of a typical column are

total length	L	= 1.00 m		
diameter	d	= 3.7 cm	$\Rightarrow$	$A_{col} = \pi d^2/4 = 10.75\ cm^2$
			$\Rightarrow$	$V_{col} = A_{col}\, L = 1.075\ dm^3$
flow rate	Q	= 0.9 mL/min		

The porosity and other relevant quantities depend on the packing material. For example, the packing material in column NA02 is characterized by [AN07]

material mass	m_m	= 1.683 kg
material density	ρ_m	$= m_m / V_{col} = 1.57\ g/cm^3$
mineral density	ρ_s	$= 2.64\ g/cm^3$

These parameters define the total porosity

$$\varepsilon_T = 1 - \frac{\rho_m}{\rho_s} = 0.41 \tag{2.1}$$

The effective porosity $\varepsilon_{eff} = 0.30$ was taken from the site-specific hydrogeological model [HGR08]. According to the dual-porosity concept, we have

$$\varepsilon_T = \varepsilon_{eff} + \varepsilon_{res} \tag{2.2}$$

with

effective porosity	$\varepsilon_{eff} = 0.30$	(for the mobile water phase)
residual porosity	$\varepsilon_{res} = 0.11$	(for the stagnant water phase)

Using the effective porosity and the flow rate Q, the pore velocity v is given by

$$v = \frac{Q}{\varepsilon_{eff} A_{col}} = 2.9\ \frac{m}{day} \tag{2.3}$$

The numerical solution of the 1D transport requires a space-time discretization. For this reason the column are divided into N = 20 cells. Cell length and timestep are defined as follows:

$$\Delta x = \frac{L}{N} = 0.05\ m \tag{2.4}$$

$$\Delta t = \frac{\Delta x}{v} = 0.3\ h \tag{2.5}$$

It should be noted that the last condition (2.5) excludes numerical dispersion in the transport calculations (see Sec. A.2.1).

Finally, the unknown value of the storage volume in the mixing box (inflow tube) was adjusted to $V_{mix} = 0.15$ dm^3.

Tracer Test. The hydraulic conditions and parameters were tested by the tracer 'chloride'. Fig. 2.3 shows the breakthrough curve in column NA02 for two cases: without and with an 'inflow mix' in front of the column (setup shown in Fig. 2.2). Only the latter approach describes the hydraulic conditions appropriately.

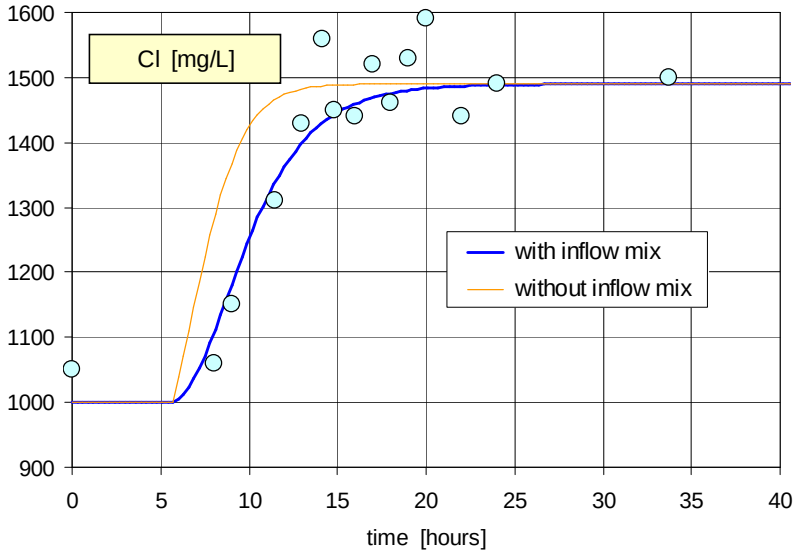

Fig. 2.3 Breakthrough curve of chloride in column NA02 (model with and without inflow mix)

Remark 1. Potassium does not act as tracer because it is influenced by ion exchange.

Remark 2. Is it possible to describe the measured breakthrough by enhancing the dispersivity alone (without a storage/mix box in front of the column)? The answer is no. Dispersivity and storage/mix box act differently: If the dispersivity α_L is enhanced the breakthrough curve flattens, but the position of the midpoint does not change. The measured data, however, shows that the midpoint of the breakthrough curve has to be shifted by about 3 hours. This can only be achieved by adding a storage/mix box in front of the column.

2.3 Main Geochemical Processes

The reactive transport model TRN allows two principal concepts: single-porosity and dual porosity. In the present report we apply the *dual* porosity approach. For example, Fig. A.1 at page 68 displays a typical interplay between the mobile and stagnant water within the dual porosity approach (including reversible and irreversible reactions with minerals as well as ion exchange).

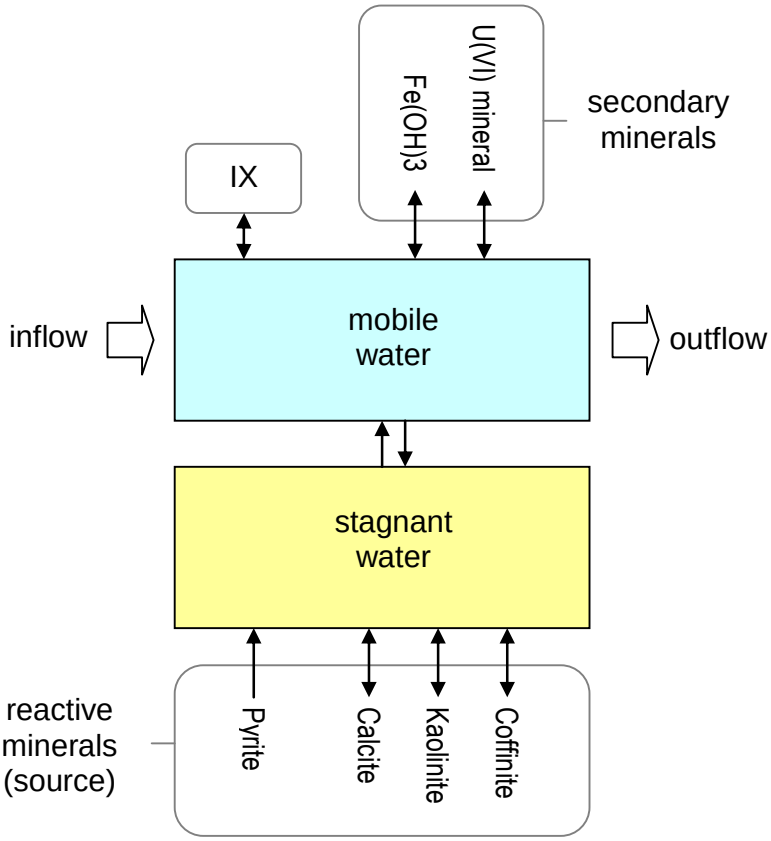

Fig. 2.4 Main geochemical transformations within the dual porosity approach (double arrows symbolize reversible processes)

Main Processes. In order to make the model as transparent as possible we focus on the *main* geochemical processes depicted in Fig. 2.4:

- dissolution of *reactive* minerals in the stagnant phase (as source of elements)
- precipitation/re-dissolution of *secondary* minerals in both phases
- ion exchange (IX) in the mobile phase

In Fig. 2.4, the double arrows symbolize reversible processes controlled by thermodynamic equilibrium. The advantage of any equilibrium approach is that it is based on a well-known thermodynamic database rather than on kinetic data (which are less available or unknown). Thus, in our model all reactions – except of pyrite dissolution – are equilibrium reactions based on log_k values taken from the PHREEQC database *wateq4f*. In this way, the number of free parameters is reduced significantly.

Reactive Minerals. The column tests indicate that there is – apart from ion exchange – a net production of several elements: Ca, Fe, S, Al, Si, and U. In our model so-called *reactive* minerals act as a source for these elements:

- Calcite $CaCO_3$ source for Ca (pH neutralization)
- Pyrite FeS_2 source for Fe and S (pe consumption)
- Kaolinite $Al_2Si_2O_5(OH)_4$ source for Al and Si
- Coffinite $USiO_4$ source for U

These 4 minerals equipped with an initial mass $m_0 > 0$ (in mol per liter pore water) dissolve in the stagnant water phase (which is per definition in direct contact with the solid phase). In principle, there are two possibilities to simulate the dissolution:

- by thermodynamics (based on log_k values contained in the PHREEQC database)
- by kinetics (based on a kinetic formula and additional parameters)

As mentioned above, the thermodynamic approach is more straightforward because no additional kinetic data are needed. It will be applied to calcite, kaolinite, and coffinite. Tab. 2.1 summarizes the content of the corresponding elements within the material of column 2. This data give us an upper bound for the initial mineral mass m_0 in the stagnant water compartment:

Calcite:	$m_0/V_{stgn} <$	130 mM	(with $V_{stgn} = \varepsilon_{res} V_{col}$)
Kaolinite:	$m_0/V_{stgn} <$	15 100 mM	
Coffinite:	$m_0/V_{stgn} <$	15 mM	
Pyrite:	$m_0/V_{stgn} <$	650 mM	

These are, in turn, upper bounds because (i) the elements are also constituents of other minerals, and (ii) the reactive efficiency is always less than 100 percent (due to restricted accessibility). Since the actual values for m_0 are not known beforehand; they will be adjusted to the column data (parameter variations are studied in Sec. **Fehler! Verweisquelle konnte nicht gefunden werden.**).

Tab. 2.1 Average content of Ca, C, Fe, S, and U in the core AKC029 for column 2 (data from Appendix C)

parameter	symbol	unit	Ca	C	Fe	S	Al	U
content	x_i	%	0.037	0.40	0.528	0.15	2.91	0.026
mass	$m_i = x_i\, m_{col}$	g	0.62	6.7	8.9	2.5	49.0	0.44
mole mass	M_r	g/mol	40.04	12.01	55.85	32.06	26.98	238.03
moles in column	$n_i = m_i/M_r$	mmol	15.5	557	159	78	1 816	1.85
moles per stagnant water	$n_i / (\varepsilon_{res}\, V_{col})$	mol/L	0.13	4.64	1.32	0.65	15.1	0.015

Remark 1. If the U(IV) mineral coffinite is replaced by uraninite the model results do not alter (apart from an insignificant change of Si).

Remark 2. The mineral equilibrium is implemented in both domains: mobile *and* stagnant water (with the same mineral list). Fig. 2.4 depicts only the main idea behind the processes, i.e., in which domain Fe(III) und U(VI) minerals (secondary minerals) precipitate and in which domain the reactive minerals dissolve.

Pyrite Dissolution. The pure thermodynamic approach applied to calcite, kaolinite, and coffinite is not valid for the pyrite dissolution. Here, we apply the O_2 driven kinetics that is proportional to $[O_2]^{0.5}[H^+]^{-0.11}$ (taken from [WR94]; also cited as example in PHREEQC manual). Within our model, mineral dissolution is described by

(2.6) $$\frac{dm}{dt} = -\text{rate} \qquad \text{with initial condition:} \qquad m(t=0) = m_0$$

and with

(2.7) $$\text{rate} = r_0 \left(\frac{m}{m_0}\right) \sqrt{DO}\ [H^+]^{-0.11} \qquad \text{for} \quad SI\ (\text{pyrite}) < 0$$

where DO symbolizes the dissolved oxygen in mol/L. The dependence of m resembles a first-order kinetic. It simulates the general case of a *finite* amount of initial inventory m_0 (rather than an unlimited supply based on zero-order kinetics). The constant factor r_0 was adjusted to the column data (see parameter variations in Sec. 2.6). Please note: Pyrite dissolves only, if the saturation index SI < 0; otherwise, in case of oversaturation, there is no pyrite dissolution:

(2.8) $$\text{rate} = 0 \qquad \text{for} \quad SI\ (\text{pyrite}) \geq 0$$

In accord with the above equation, pyrite dissolution starts when O_2-rich water (lixiviant) enters the stagnant water compartment. For this reason we introduced the variable 'DO' as dissolved oxygen. As shown in Tab. 2.2, only the lixiviant contains dissolved oxygen with DO = 10^{-4} M; the oxygen content in the pore water is zero, DO = 0.

Remark. By using 'DO' instead of the master variable O_2 or O(0) in PHREEQC we bypass the (kinetic) redox reaction

(2.9) $$O_2(aq) + 4\,e^- + 4\,H^+ = 2\,H_2O \qquad \log k = 86$$

This enables us to maintain the observed relation between O_2 and ORP for the lixiviant:

(2.10) $$\text{measured data:} \quad pe \approx 12.5 \quad \Leftrightarrow \quad O_2(aq) \approx 8 \cdot 10^{-4}\ M$$

Conversely, if reaction (2.9) is involved in pure equilibrium calculations we have:

(2.11) $$\text{PHREEQC for} \quad pe = 12.5 \quad \Rightarrow \quad O_2(aq) \approx 3 \cdot 10^{-22}\ M$$

(2.12) $$\text{PHREEQC for} \quad O_2(aq) = 8 \cdot 10^{-4}\ M \quad \Rightarrow \quad pe = 18.2$$

Here 'reality' and equilibrium calculations differ by several orders of magnitudes. In other words, if we accept the measured pe = 12.5, then there is no O_2 (and no pyrite oxi-

dation at all); on the other hand, if we accept 1 mM O_2, then the calculated pe value overestimates the measured pe by 6 units. This problem has been solved by redox-decoupling, i.e. by inclusion of the variable 'DO' (which triggers the pyrite oxidation).

Secondary Minerals. In addition to the 4 reactive minerals there are also *secondary* minerals (e.g. Fe(III) and U(VI) minerals) that precipitate and re-dissolve in the mobile water depending on the pH-pe conditions. This process is thermodynamically controlled.

In particular, we consider two secondary minerals:

Ferrihydrite	$Fe(OH)_3$	from wateq4f
Soddyite	$(UO_2)_2SiO_4{:}2H_2O$	from [GL07]

These two secondary minerals define the minimum dataset.

If, for example, two other secondary minerals are added,

Schwertmannite	$Fe_8O_8(OH)_{4.8}(SO_4)_{1.6}$	from [BCM94]
Becquerelite	$Ca(UO_2)_6O_4(OH)_6{:}8H_2O$	from [GL08]

these minerals would precipitate instead of Ferrihydrit and Soddyite (since Schwertmannite and Becquerelite are less soluble). However, this does not change the general picture (see variations in Sec. 2.6).

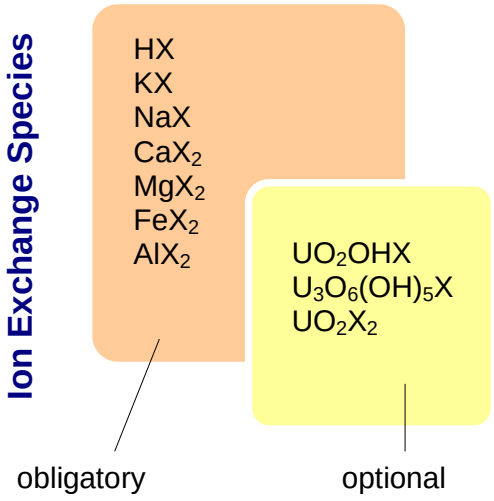

Fig. 2.5 Ion exchange species used in the model (U(VI) species are optionally)

Ion Exchange. The mineralogical analysis of FME material in [AN07] affirms the presence of clay minerals (predominantly in form of Kaolinite and Montmorillonite). Clay minerals act as ion exchanger. Therefore, in all calculations ion exchange for the cations H^+, K^+, Na^+, Ca^{2+}, Mg^{2+}, Fe^{2+}, and Al^{3+} is taken into account (see Fig. 2.5).

Besides the thermodynamic data (log_k values from wateq4f) the ion exchange model requires the input parameter "total cation capacity per pore volume"

$$C_{TOT} = \frac{n_{sites}}{V_P} = \frac{CEC \cdot m_{clay}}{V_P} \qquad (2.13)$$

Here, the cation exchange capacity CEC for a typical clay mineral (Montmorillonite) is

(2.14) $$CEC = \frac{n_{sites}}{m_{clay}} \approx 50 \frac{meq}{100\ g}$$

Assuming a low clay content between 1 % and 2 %, that is, $f = m_{clay}/m_m = 0.01 \ldots 0.02$, we obtain

(2.15) $$C_{TOT} = \frac{f \cdot \rho_m}{\varepsilon} CEC = \frac{1}{\varepsilon} \cdot 8 \ldots 16 \frac{meq}{L}$$

In the model calculations we choose $C_{TOT} = 13.5/\varepsilon$ meq/L as input. Here, the porosity ε is equal to ε_{eff} for the mobile water and ε_{res} for the stagnant water. Parameter variations of C_{TOT} are considered in Sec. 2.6.

Optionally, in addition to the ion-exchange species (defined in wateq4f) we also consider three uranyl species:

UO_2X_2	$UO_2^{+2} + 2X^- = UO_2X_2$	log_k = -11.7
UO_2OHX	$UO_2OH^+ + X^- = UO_2OHX$	log_k = 1.0
$U_3O_6(OH)_5X$	$(UO_2)_3(OH)_5^+ + X^- = U_3O_6(OH)_5X$	log_k = 11.35

where X denotes the exchange sites of the clay mineral. The required log_k values were taken from literature [MZS95] and re-normalized to fit the batch test data in Chapter 3. [Renormalization means that, in order to fit the batch data, only *one* log_k of the three species was adjusted by a shift Δ; the other two log_k's are then shifted by the same Δ. In this way, the internal relations of the triple are kept unchanged.]

Remark. As shown in Fig. 2.4, ion exchange (IX) is considered in the mobile phase (standard dataset). Additionally, in Sec. 2.6 calculations are performed for the opposite case where IX is located in the stagnant phase. The model allows both scenarios; however, the former fits the measured data more accurately.

Dual-Porosity Mass Transfer. The diffusion-like mass transfer between stagnant and mobile water is controlled by the rate parameter α in Eqs. (A.6) and (A.7), respectively. For the extreme case $\alpha = 0$ there is no interaction at all; otherwise, for $\alpha = \infty$ the double porosity approach converges to the single porosity model.

An estimate for α is given by van Genuchten's approach [VG85]

(2.16) $$\alpha = \frac{D \cdot \varepsilon_{res}}{(a \cdot f_{s\to 1})^2}$$

where $D \approx 10^{-9}$ m^2/s is the diffusion coefficient, a is the particle radius, and $f_{s\to 1} = 0.2$ a shape factor. Assuming $a = 3 \cdot 10^{-3}$ m, $\varepsilon_{res} = 0.11$ we get

(2.17) $$\alpha \approx 1.1\ h^{-1}$$

This value will be used in the present model calculations.

Thermodynamic Data. PHREEQC, which is embedded in the reactive transport model, uses the standard database *wateq4f*. For transparency reasons, this database is applied in its original form. Additional species that are not contained in *wateq4f* are added to the PHREEQC input files as header (the same header for all PHREEQC calculations during running TRN). Thus, we never change or disturb the original database file wateq4f.dat.

The list of all supplementary species, which are added to the input file header, is short. It contains two mineral phases and three ion exchange species:

```
PHASES
  Soddyite(e)
      (UO2)2SiO4:2H2O + 4H+ = 2UO2+2 + H4SiO4 + 2H2O
      log_k 6.43
  Becquerelite(e)
      Ca(UO2)6O4(OH)6:8H2O + 14H+ = Ca+2 + 6UO2+2 + 18H2O
      log_k 40.5

EXCHANGE_SPECIES
      UO2OH+ +  X-  = UO2OHX
            log_k       1.0
      (UO2)3(OH)5+ + X- = U3O6(OH)5X
                  log_k       11.35
      UO2+2 + 2X- = UO2X2
            log_k       -11.7
```

Together with the database *wateq4f*, this is the complete thermodynamic information we used in the present calculations.

2.4 Model Input – Standard Dataset

In this Section we define the *standard dataset* (or default dataset) used for the column simulations in Sec. 2.5. The subsequent Sec. 2.6 answers the question: What happens to the results if we make a particular change to the main parameters of this dataset?

Input Water. The calculations are based on two aqueous solutions: (i) groundwater (cell.sol) for the initial water in the column cells at t = 0, (ii) lixiviant (lix.sol) for the column feed. The model input was generated from measured data (raw data) using the hydrochemical code PHREEQC [PA99]. The water composition of both raw and input data is listed in Tab. 2.2.

Tab. 2.2 Model input for groundwater and lixiviant (ΔIB denotes the ion/charge balance error)

		groundwater (cell.sol)		lixiviant (lix.sol)	
		raw data	model input	raw data	model input
pH	-	7.78	7.33	1.67	1.67
ORP	mV-AgCl	100		552	
ORP	mV-SHE	308		762	
pE	-	5.0	5.0	12.5	12.5
T	°C	35	35	35	35
Ca	mg/L	84.4	84.4	115	115
Mg	mg/L	30.1	30.1	26.6	26.6
Na	mg/L	876	876	950	718
K	mg/L	44.3	44.3	606	606
SO4-S	mg/L	203	203	851	851
HCO3	M	0.005	0.005	0	<0.001
Cl	mg/L	1 050	1 001	1 490	1 490
Fe	mg/L	4.02	<0.01	1.73	1.73
Al	mg/L	1.67	1.67	4.76	4.76
U	mg/L	<1	0.001	52.9	52.9
Si	mg/L	16	16.0	28.3	28.3
DO	mM		0		0.1
ΔIB	%	-1.55	0	6.04	0

Here, charge balance was achieved by adjustment of Cl and Na for *cell.sol* and *lix.sol*, respectively. In contrast to the raw data the input solutions are in equilibrium with the amorphous mineral phases $Fe(OH)_3$ and $Al(OH)_3$. Additionally, the inflow solution *lix* is put into equilibrium with the atmosphere (open CO_2 system).

Main Parameters. The main model parameters of the standard dataset are as follows:

number of cells		N = 20
cell length		$\Delta x = 0.05$ m
time step		$\Delta t = 0.3$ h
total porosity		$\varepsilon_T = 0.41$
effective porosity	(for mobile water phase)	$\varepsilon_{eff} = 0.30$
residual porosity	(for stagnant water phase)	$\varepsilon_{res} = 0.11$
mobile/stagnant transfer rate (from Eq. (2.16))		$\alpha = 1.1\ h^{-1}$

longitudinal dispersivity	$\alpha_L = 0$
total ion exchange capacity	$C_{TOT} = 13.5/\varepsilon$ meq/L

Minerals. The list of reactive minerals (located in stagnant water) is defined by:

Pyrite	initial mass	$m_0/V_{stgn} = 100$ mM,	kinetic rate r_0
Calcite		$m_0/V_{stgn} = 40$ mM	SI = 0.8
Kaolinite		$m_0/V_{stgn} = 1.2$ mM	SI = 0.0
Coffinite		$m_0/V_{stgn} = 2.0$ mM	SI = 0.0

In case of calcite we allow supersaturation (which is not uncommon for natural waters). The kinetic rate for pyrite, $r_0 = 1.6 \cdot 10^{-5}$ M/s, was fitted to the high Fe and S release observed in the column tests. [Remark: The advantage of using m_0/V_{stagn} rather than m_0 is that the former quantity is independent of the cell size.]

The list of secondary minerals (located in mobile water) is defined by:

Ferrihydrit	$Fe(OH)3$	($m_0 = 0$)
Soddyite	$(UO_2)_2SiO_4{:}2H_2O$	($m_0 = 0$)

Ion Exchange. The initial amount of ion-exchange species (for the cations H^+, K^+, Na^+, Ca^{2+}, Mg^{2+}, Fe^{2+}, and Al^{3+}) is completely determined by equilibrium conditions, i.e. equilibrium with groundwater (cell.sol). Thus, the total capacity C_{TOT} is the only parameter of the ion exchange model. Ion exchange is placed in the *mobile* water phase (and not in the stagnant water). In the standard dataset, uranyl ion exchange is ignored.

Redox Conditions. The calculations are performed under definite redox conditions which differ for the mobile and stagnant water pores:

- stagnant water: pe ≈ 5 (“near-reducing” groundwater conditions)
- mobile water: pe = 5 ⇒ 12 (oxidizing conditions imported by lix)

Whereas the ‘reducing’ conditions within the *stagnant* water are fixed at the measured value pe = 5 (net effect of pyrite dissolution and lix intrusion), the pe in the *mobile* water evolves in good accord with the pe-pH relation in Eq. (2.9), i.e.

$$\text{(2.18)} \qquad pe = \frac{1}{4}\left[\,86 - 4\,pH + \log O_2\right] = \frac{86 + \log O_2}{4} - pH \;\approx\; \text{const} - pH$$

The ‘anti-correlated’ behavior of pH and pe is clearly seen in the two upper diagrams of Fig. 2.6 (dots and blue curves).

Remark. The effect of different redox conditions for the stagnant water is discussed in Sec. 2.6. For this purpose, two simulations are compared: (i) pe is kept fixed at 5, and (ii) pe develops freely.

2.5 Model Results – General Behavior (Standard Dataset)

In order to demonstrate the crucial role of geochemistry two model calculations are performed and compared:

(i)	without REAC	pure transport (only advection and dispersion)
(ii)	with REAC	transport plus reactions (mineral dissolution and precipitation, ion exchange, redox reactions etc.)

The results for column NA02 are shown in Fig. 2.6 to Fig. 2.8. Obviously, the experimental data can be described if, and only if, geochemistry is taken into account (blue curves). Please note the big deviations from the non-reaction "tracer model" (red curves) to the measured data. Here, chloride is the only species that acts as a tracer (see Fig. 2.8).

Most important: The geochemical model explains the retardation of pH, pe, and uranium and other elements in a simple and consistent way. The pH retardation results from both, dissolution of a carbonate mineral (calcite) and ion exchange. The U retardation is an effect of precipitation and re-dissolution of U(VI) minerals (and/or of uranyl ion exchange described in Sec. 2.6).

Similar results are obtained for the column NA01. [The columns NA03 and NA04 are not considered here due to the unknown flow velocities resulting from a leakage during the experiments.]

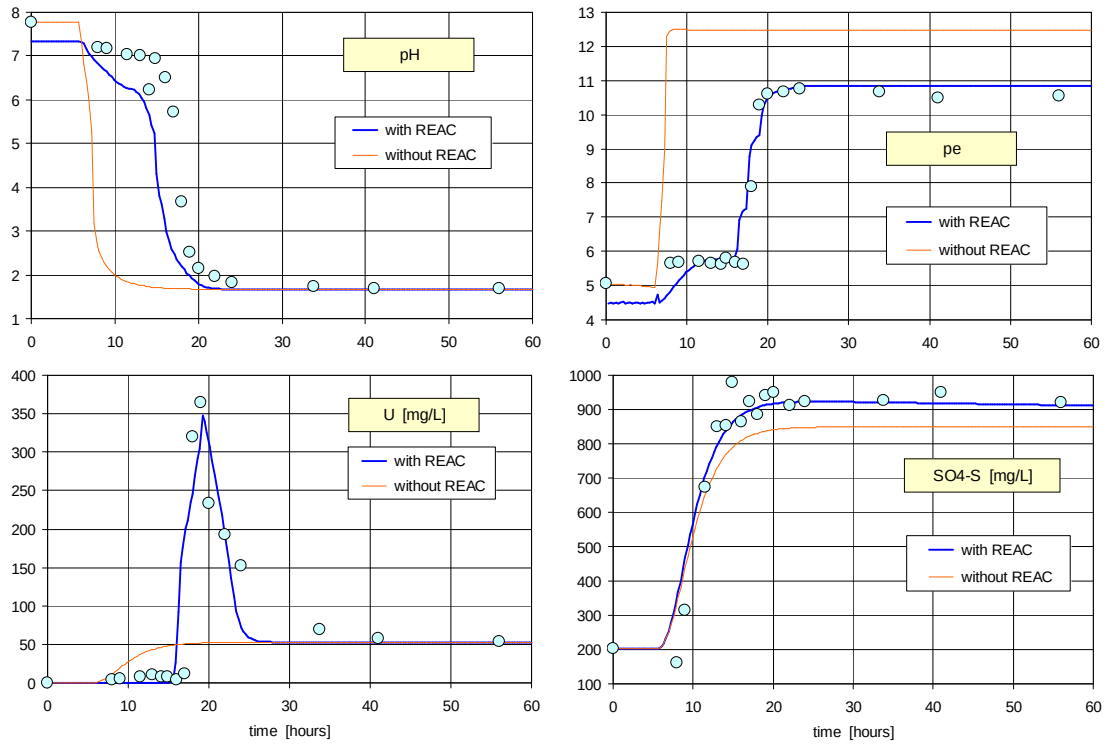

Fig. 2.6 Column outflow parameters pH, pe, U, and SO_4 – model and reality

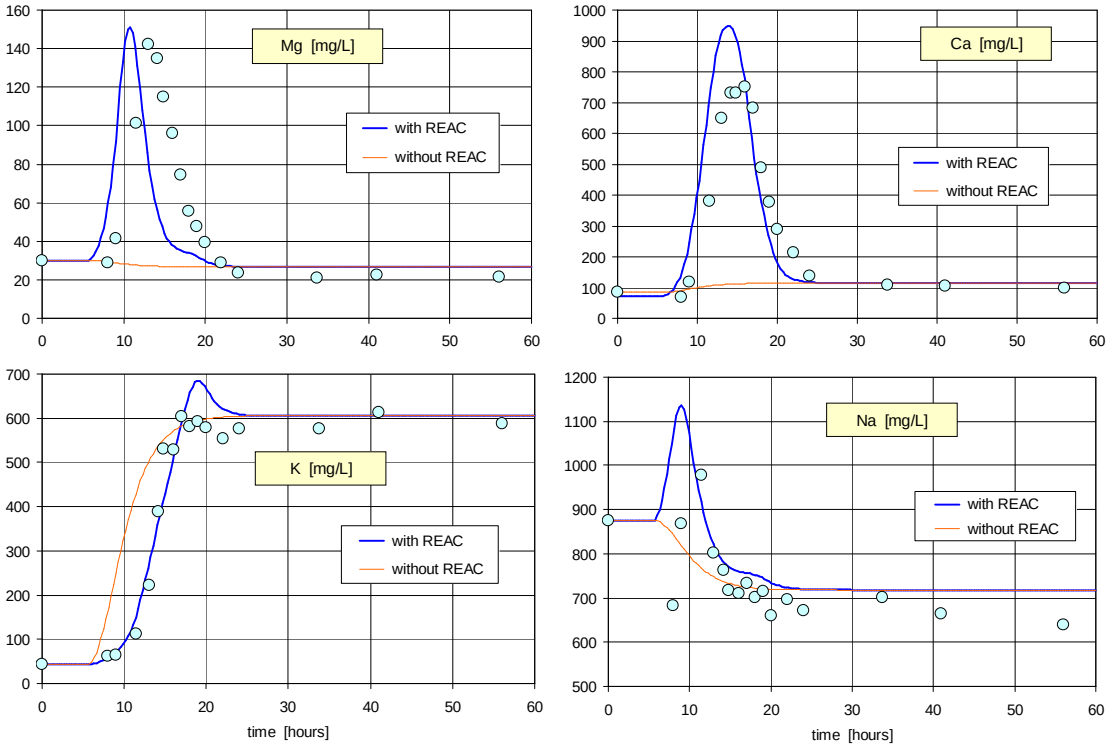

Fig. 2.7 Column outflow parameters Mg, Ca, K, and Na – model and reality

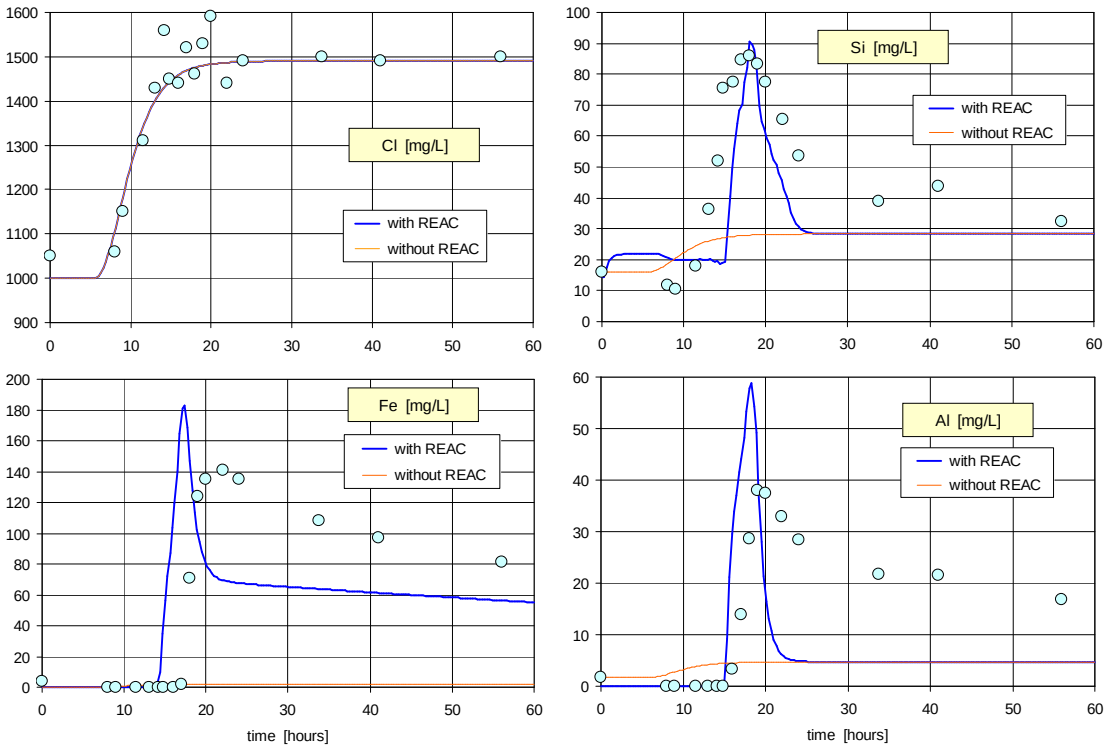

Fig. 2.8 Column outflow parameters Cl, Si, Fe, and Al – model and reality (In case of chloride both curves coincide: chloride acts as a tracer.)

U-Fe-Chemistry. The main geochemical transformations can be summarized as follows (see Fig. 2.9): The aggressive lixiviant enters the stagnant water zone and dissolves the reductive minerals pyrite and coffinite (pyrite is the principal reductant in the unaltered aquifer). Due to the contact with the O_2-rich mobile phase the released Fe(II) and U(IV) species oxidize and precipitate as Fe(III) and U(VI) minerals. As a result there is neither Fe nor U in the column outflow. However, this happens only in the initial period of the test. In the further process, pH drops below 3, the precipitation stops and all accumulated Fe(III) and U(VI) minerals re-dissolve (which produce the peaks in the curves). The greater the pH buffer the more the peaks are retarded. The pH is buffered by both ion exchange and calcite dissolution.

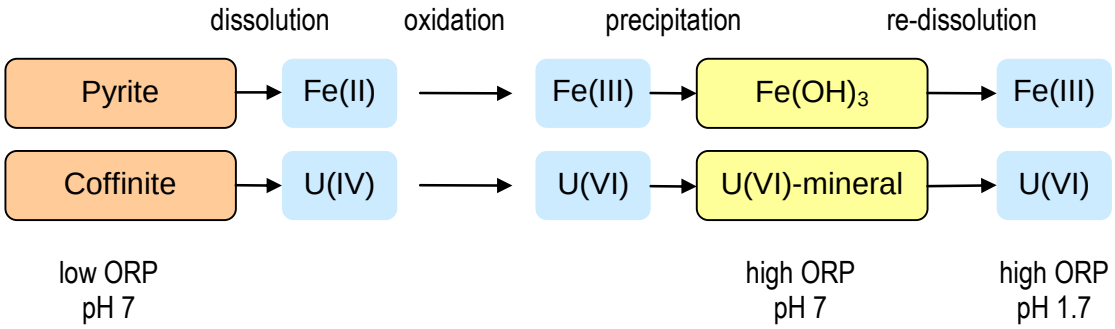

Fig. 2.9 Uranium-Iron-Chemistry in the columns

Remark. The obtained results are quite independent of the applied model concept. For example, our first attempt based on a *single*-porosity model with dissolution kinetics for several minerals (and more kinetic parameters) leads to the similar outcome.

Experimental & Theoretical Limits. In fact, the results show that experimental data and calculations are in due correspondence. A further improvement of the model, however, is limited by two experimental facts (which are deviations from the 'ideal case'):

First. During preparation, the aquifer material was crushed and oxidized ('pre-cooked'). Unavoidably, pores and pore fluids fill with fast-dissolved products that are pushed out by the first incoming flux. [Hence, the pyrite rate r_0 cannot be over-taken from literature data based on undisturbed systems; this rate was enhanced.]

Second. Due to the very high flow velocity (1 450 m/year !) the residence time, i.e. the contact time of the fluid with core material, is extremely short. The shorter the residence time the lower is the amount of dissolved products. That means, 'natural' mineral dissolution rates are too small in order to explain the high concentration maxima that are observed at breakthrough.

Both problems are treated by the dual porosity approach with an (empirical) exchange rate between mobile and stagnant water. Thereby, the reactive minerals within the stagnant zone are put into equilibrium (here thermodynamic equilibrium simulates an infinite fast kinetics or the pre-cooking effect).

The situation is quite different for the natural aquifer. Performing aquifer simulations we use literature data (for pyrite oxidation rates etc.).

2.6 Model Results – Parameter Variations

Based on the standard dataset defined in Sec. 2.4 several parameter variations are investigated. An overview of all variants is given in Tab. 2.3. It represents the extract of several hundred TRN calculations.

Tab. 2.3 Overview of performed model calculations (abbreviations: U-IX – uranyl ion-exchange species, U(VI)-secm – U(VI) secondary mineral)

Variant (Input Data)	Description	Changed Parameter	Standard Value
INP_0	standard dataset		
INP_00	only transport (no reactions)		
INP_N10	grid variation (cell number low)	N = 10	N = 20
INP_N40	grid variation (cell number high)	N = 40	N = 20
INP_DISP	with longitudinal dispersion	$\alpha_L = 5 \cdot 10^{-3}$ m	$\alpha_L = 0$
INP_ALPH	mobile/stagnant water exchange	$\alpha = 0.5$ h^{-1}	$\alpha = 1.1$ h^{-1}
INP_IX_0	no ion exchange	$C_{TOT} = 0$	$C_{TOT} = 13.5/\varepsilon$ meq/L
INP_IX_20	enhanced ion exchange capacity	$C_{TOT} = 20/\varepsilon$ meq/L	$C_{TOT} = 13.5/\varepsilon$ meq/L
INP_IX_STAG	ion exchange in	stagnant water	mobile water
INP_U_NO	no U retardation	no U(VI)-secm, no U-IX	with U(VI)-secm only
INP_U_ALL	enhanced U retardation	with U(VI)-secm and U-IX	with U(VI)-secm only
INP_U_IX_ONLY	U retardation by IX only	with U-IX, no U(VI)-secm	with U(VI)-secm only
INP_SEC_BECQ	change of U(VI) mineral	Becquerelite	Soddyite
INP_SEC_NO_FE	without Fe(III) mineral	–	Fe(OH)3(a)
INP_R_CALC_0	no calcite inventory	$m_0/V_{stgn} = 0$	$m_0/V_{stgn} = 40$ mM
INP_R_CALC_2	half calcite inventory	$m_0/V_{stgn} = 20$ mM	$m_0/V_{stgn} = 40$ mM
INP_R_CALC_SI_0	zero calcite saturation index	SI = 0	SI = 0.8
INP_R_CALC_SI_04	non-zero calcite saturation index	SI = 0.4	SI = 0.8
INP_R_COFF_0	no coffinite inventory	$m_0 = 0$	$m_0/V_{stgn} = 2$ mM
INP_R_PYR_0	no pyrite inventory	$m_0 = 0$	$m_0/V_{stgn} = 100$ mM
INP_R_PYR_INF	infinite pyrite inventory	$m_0 = \infty$	$m_0/V_{stgn} = 100$ mM
INP_R_PYR_2	enhanced pyrite dissolution	$r_0 = 2.0 \cdot 10^{-5}$ M/s	$r_0 = 1.6 \cdot 10^{-5}$ M/s
INP_PE_FREE	pe in stagnant water	pe develops freely	pe = 5

Grid Variation. The size of the cells Δx is determined by the cell number N. The finer the discretization the better is the numerical solution. Conversely, a high cell number enhances the computation time t_{PC} as well as the number of PHREEQC-calculations N_P. Three calculations are performed with the following parameters:

N = 10	$\Delta x = 0.10$ m	$\Delta t = 0.6$ h	($t_{PC} = 60$ s, $N_P = 3\,122$)
N = 20	$\Delta x = 0.05$ m	$\Delta t = 0.3$ h	($t_{PC} = 158$ s, $N_P = 12\,243$)
N = 40	$\Delta x = 0.025$ m	$\Delta t = 0.15$ h	($t_{PC} = 613$ s, $N_P = 47\,756$)

The computation time t_{PC} in the round brackets refers to a modeling timespan of 60 h. The results are shown in Fig. 2.10. It demonstrates that the standard dataset with N = 20 represents the optimum grid size regarding computational time and accuracy. A further doubling of N (which requires a 4-fold computer time) does not significantly improve the results.

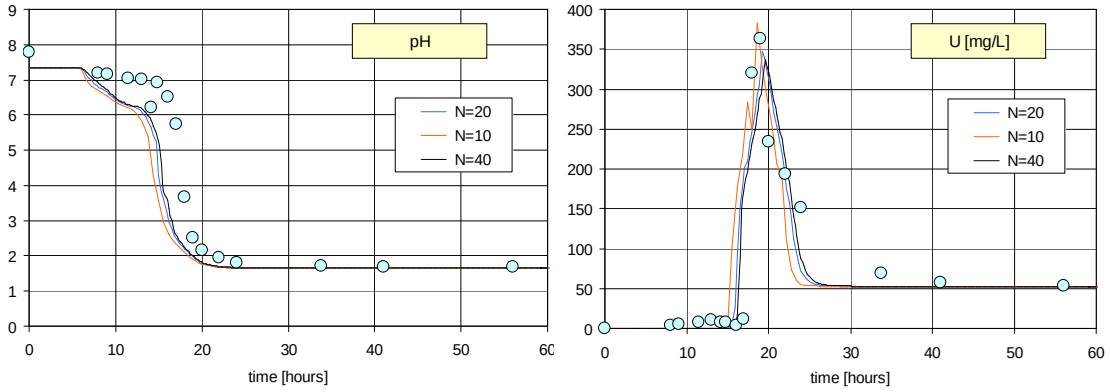

Fig. 2.10 Variation of cell number N

Dispersivity. The dispersion parameter for the column tests is assumed to be less than 10 % of the cell length. In order to demonstrate this effect we used the maximum value for the longitudinal dispersion, $\alpha_L = 5 \cdot 10^{-3}$ m (i.e. 10 % of $\Delta x = 5$ cm). As shown in Fig. 2.11, the inclusion of dispersion does not alter the results noticeable. This is a phenomenon of the dual porosity approach where the "smoothening" of curves is caused by the stagnant/mobile water exchange – see next item.

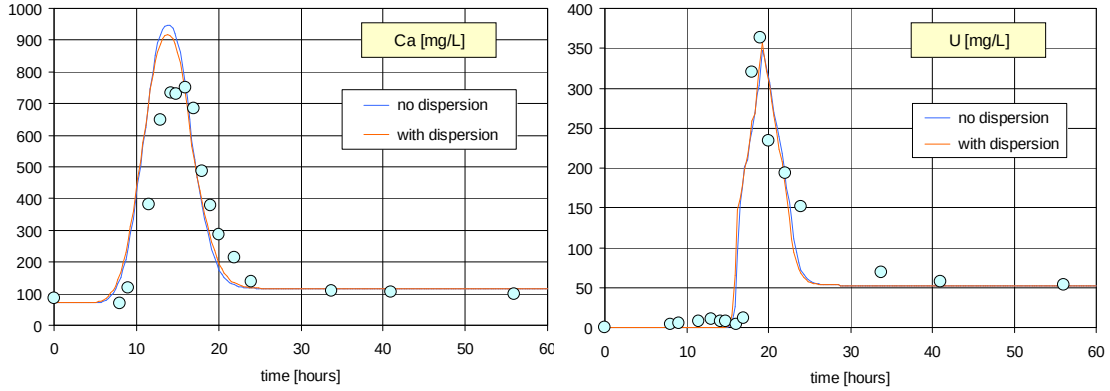

Fig. 2.11 Calculation without and with longitudinal dispersion

Dual-Porosity Mass Transfer. The transfer rate α between mobile and stagnant water was estimated using Eq. (2.16); it gives $\alpha = 1.1\ h^{-1}$. Fig. 2.12 represents two model calculations with

$\alpha = 0.5\ h^{-1}$
$\alpha = 1.1\ h^{-1}$ (standard dataset)

The smaller the transfer rate the higher is the retardation effect (that broadens the curves). Whereas $\alpha = 0.5\ h^{-1}$ fits the Ca curve well, it cannot describe the maxima for uranium (and the other elements). Therefore we chosen $\alpha = 1.1\ h^{-1}$ as the standard value.

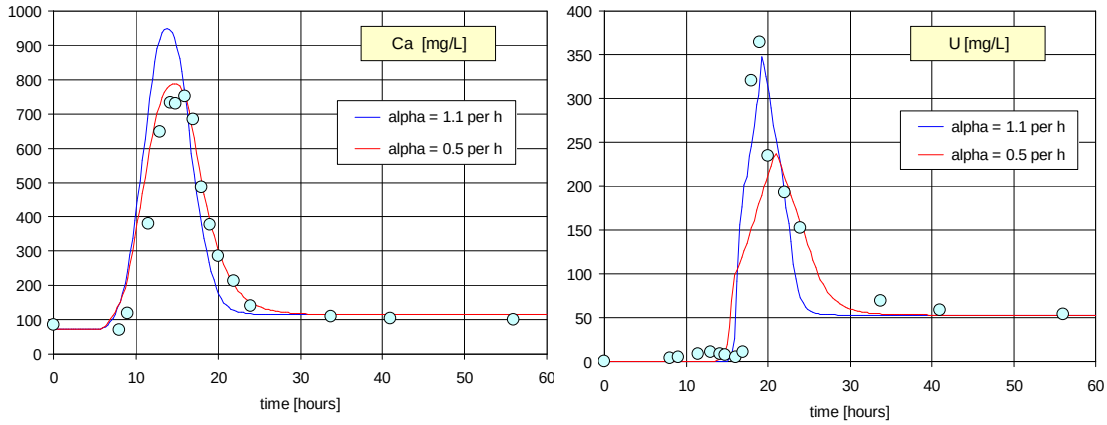

Fig. 2.12 Variation of the dual-porosity transfer rate α that controls the stagnant/mobile water exchange

Ion Exchange. Ion exchange on clay minerals plays a significant role. Here, we consider all species that are contained in the PHREEQC database *wateq4f*: H^+, K^+, Na^+, Ca^{2+}, Mg^{2+}, Fe^{2+}, and Al^{3+} (uranyl ion exchange is not considered here; it will be discussed separately). Calculations are performed for three total ion-exchange capacities:

$C_{TOT} = 0$ (no ion exchange)
$C_{TOT} = 13.5/\varepsilon$ meq/L (standard dataset)
$C_{TOT} = 20.0/\varepsilon$ meq/L

The results are shown in Fig. 2.13. Obviously, the exchange capacity increases the retardation. The best description for U (and for all other elements) was obtained for $C_{TOT} = 13.5/\varepsilon$ meq/L. In all cases ion exchange takes place in the mobile water phase (and not in the stagnant water).

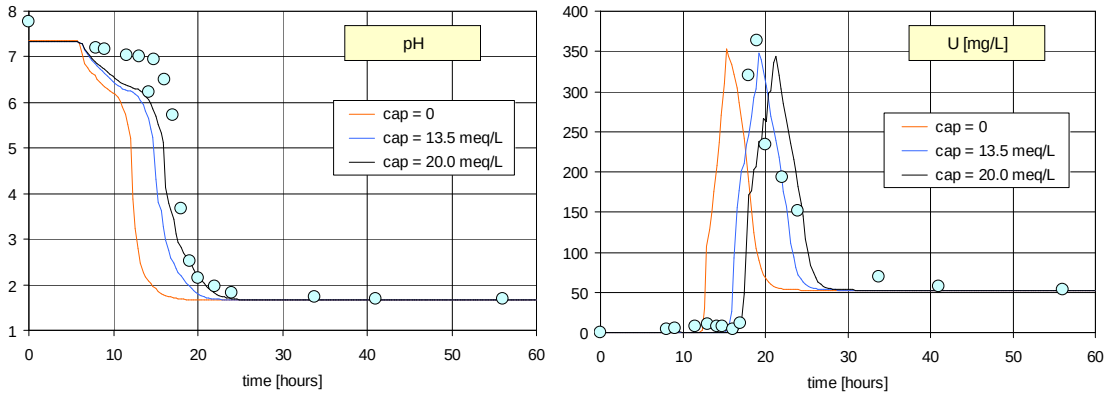

Fig. 2.13 Variation of the ion-exchange capacity (without

In addition, we proved the influence of the *location* where ion-exchange takes place (IX in mobile water or IX in stagnant water). The results are shown in Fig. 2.14. If ion exchange takes place in the stagnant water (black curve) rather then in mobile water (blue curve) retardation diminishes. Both curves have been calculated for $C_{TOT} = 13.5/\varepsilon$ meq/L with $\varepsilon = 0.30$ for mobile water (standard dataset) and $\varepsilon = 0.11$ for stagnant water.

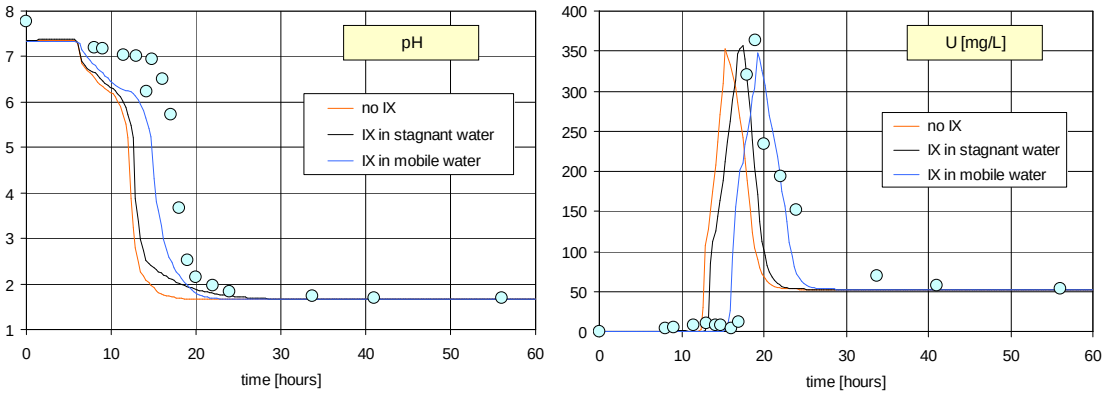

Fig. 2.14 Variation of ion-exchange options: (i) no IX, (ii) IX in stagnant water, and (iii) IX in mobile water

U Minerals. In the model, we distinguish between two mineral types: the *reactive* minerals in the stagnant water and the *secondary* minerals in the mobile water. In particular, the reactive U(IV) mineral coffinite acts as U source; the U(VI) minerals soddyite and/or becquerelite act as secondary minerals. The latter precipitate within the timespan 6 to 16 hours and, then, triggered by the decreasing pH, re-dissolve. In this way, the secondary minerals retard the U peak. In order to demonstrate the presence of both minerals several calculations are compared in Fig. 2.15:

- no Coffinite, no Soddyite (left diagram, green curve)
- no Coffinite, with Soddyite (left diagram, red curve)
- with Coffinite, no Soddyite (right diagram, green curve)
- with Coffinite, with Soddyite (both diagrams, blue curve)
- with Coffinite, with Becquerelite (right diagram, red curve)

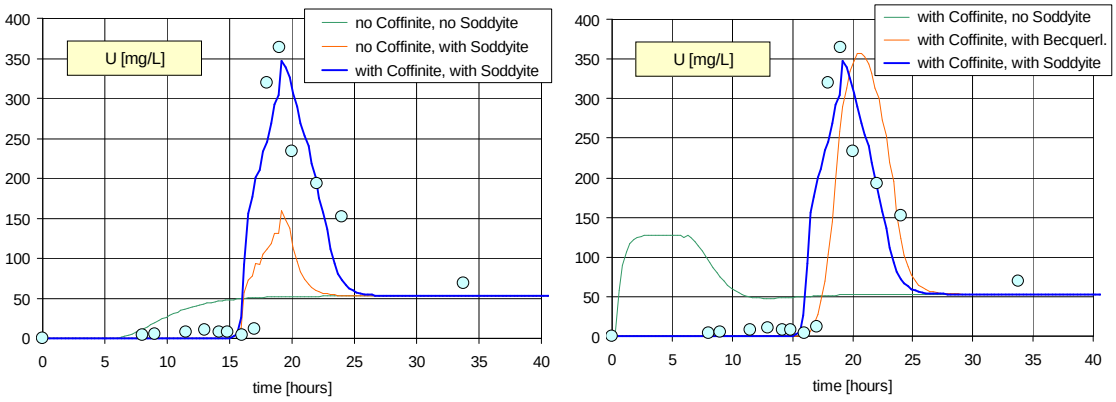

Fig. 2.15 Calculation without and with Coffinite as U source

The inclusion of coffinite *and* soddyite represents the standard dataset (blue curves). Almost the same description is obtained when soddyite is replaced by becquerelite. Otherwise, if both soddyite *and* becquerelite are put into equilibrium, the less soluble mineral becquerelite precipitates (and, again, we obtain the red curve in the right diagram).

Uranyl Ion Exchange. Until now we considered ion exchange *without* adsorption of uranyl ions (i.e. without the species UO_2X_2, UO_2OHX, and $U_3O_6(OH)_5X$). If we implement these species, uranyl ion exchange proves as an alternative process for U retardation. In sum, we have at least three possibilities for U retardation:

- precipitation and re-dissolution of U(VI) minerals (soddyite and/or becquerelite)
- uranyl ion exchange
- a combination of both processes

The three possibilities are demonstrated in Fig. 2.16. Please note, that the integral for all curves is the same (as required by mass balance). The blue curve represents our standard case.

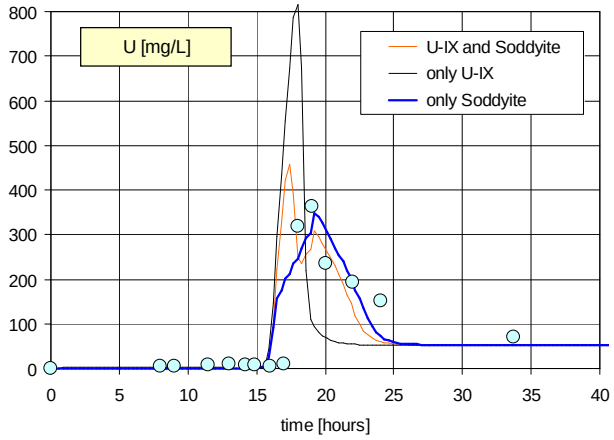

Fig. 2.16 Calculations with and without uranyl ion exchange

The species $U_3O_6(OH)_5X$ plays the dominant role among all three uranyl ion-exchange species defined above. The time-dependent behavior of $U_3O_6(OH)_5X$ in different cells of the column is depicted in Fig. 2.17. It illustrates the dynamics of uranyl adsorption within the column. In column cell 15, for example, the adsorption maximum is attained at t = 13.5 h.

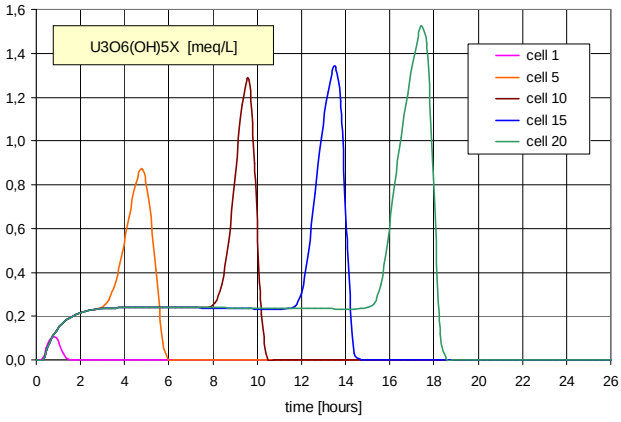

Fig. 2.17 Uranyl adsorption on ion-exchange sites in different cells as a function of time (here species $U_3O_6(OH)_5X$)

Fig. 2.18 shows the main cation distribution on the exchanger sites in cell 15. At the beginning, t = 0, we have neutral pH conditions and Ca occupies almost half of the total CEC. At t = 13.5 h uranyl reached its maximum adsorption (but a small part of the total capacity). Finally, at times t > 20 h acid conditions are established and most of the CEC is occupied by H^+.

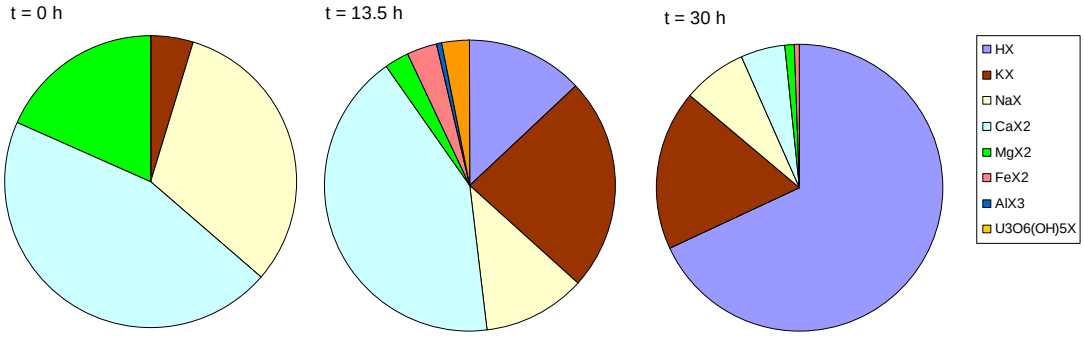

Fig. 2.18 Occupation of ion exchange sites at t = 0, 13.5 and 30 h (in column cell 15)

Iron. The iron chemistry is determined by the reactive Fe(II) mineral pyrite (as Fe source) and the secondary Fe(III) mineral Fe(OH)3 (which precipitates and re-dissolves). The experiments are only explainable if both minerals are present – see Fig. 2.19. The picture does not change if Fe(OH)3 is replaced by other Fe(III) minerals like schwertmannite.

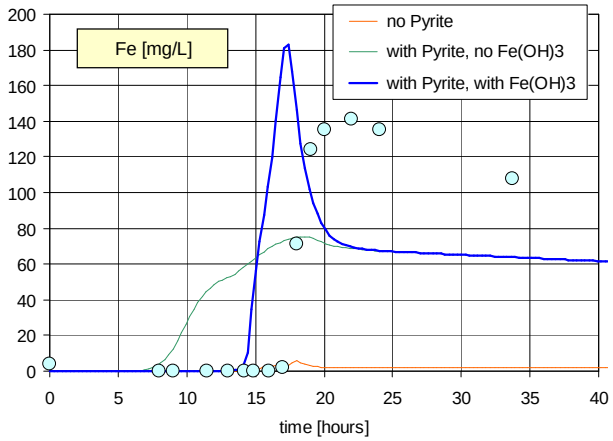

Fig. 2.19 Calculations with and without iron Fe(II) and Fe(III) minerals

The pyrite dissolution is described by the kinetic formula in Eq. (2.7) which contains two parameters: the rate r_0 and initial mass m_0. Fig. 2.20 illustrates the influence of both parameters on the iron breakthrough curve. The blue curve represents the standard dataset.

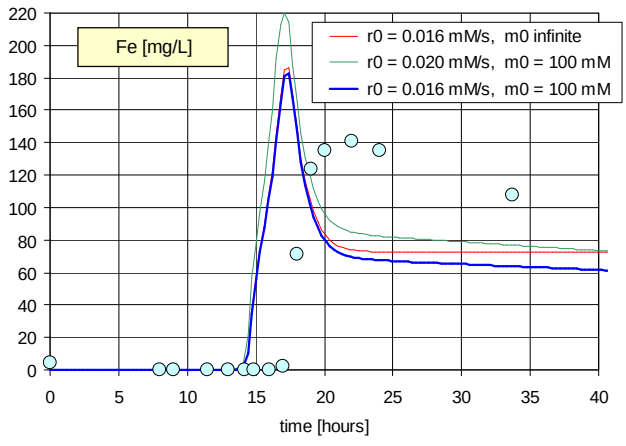

Fig. 2.20 Variation of pyrite kinetics

Calcite. The amount of calcite determines the pH behavior significantly. Fig. 2.21 and Fig. 2.22 illustrate the effect of the calcite amount (initial mass m_0) and calcite saturation index on pH, respectively. The blue curves represent the standard dataset.

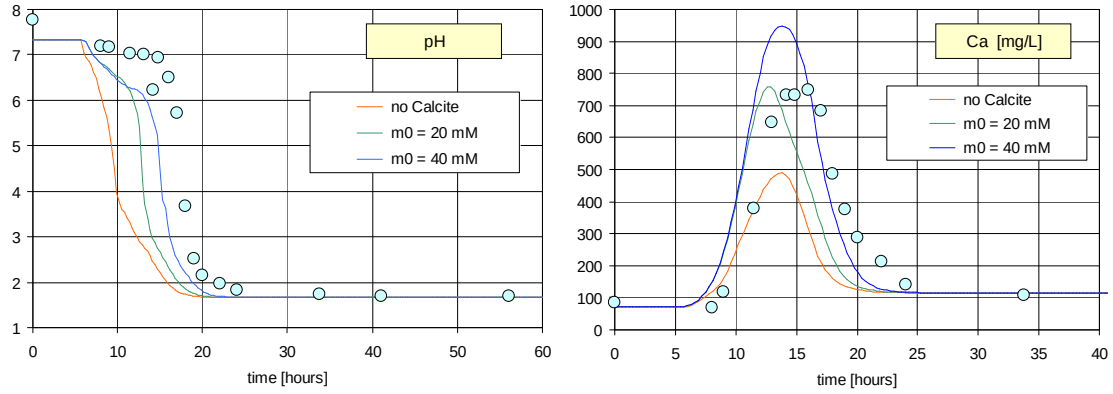

Fig. 2.21 Variation of the calcite inventory

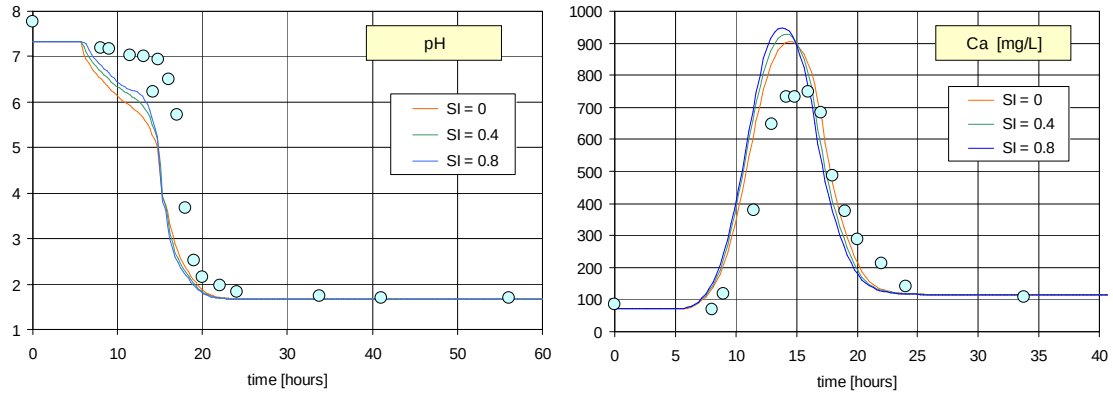

Fig. 2.22 Variation of the calcite saturation index

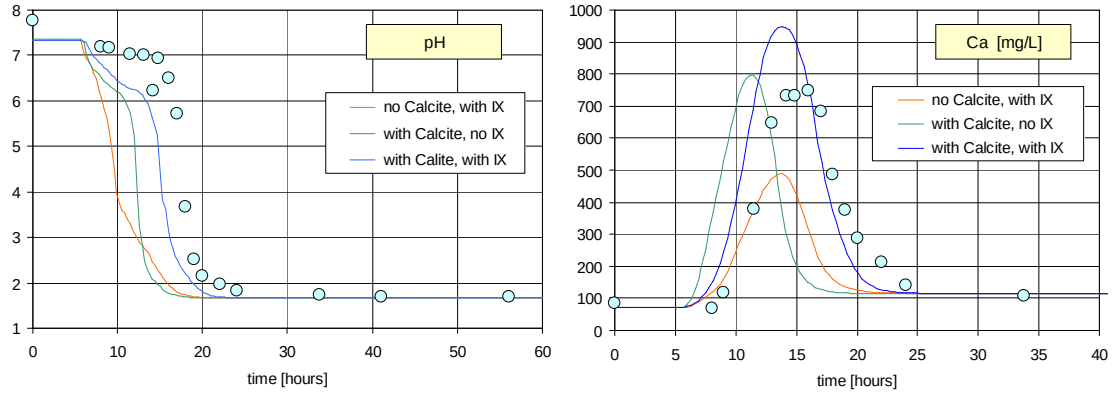

Fig. 2.23 Separate and combined effect of calcite dissolution and ion exchange on pH and Ca

In order to better understand the combined effect of calcite and ion exchange on pH buffering, we calculated both effects separately, i.e. calcite dissolution without IX and, vice versa, IX without calcite dissolution. The results are compared with the 'standard dataset' calculations in Fig. 2.23.

ORP. Within the dual-porosity approach mobile and stagnant waters behave quite different regarding ORP. The *stagnant* water is in direct contact with the reductive minerals pyrite and coffinite/uraninite and, thus, it has a lower pe than the mobile water (with pe ≈ 10). Two calculations have been performed:

Case (i) in the stagnant water the pe value is *not* fixed

As a result, the calculated pe in the stagnant water develops freely to approach pe ≈ 3.2. At these pH-pe conditions U(IV) precipitates (here in form of coffinite), and the U concentration in the effluent becomes extremely low, i.e. the measured U peak in the experiments cannot be described – see red curve in left diagram of Fig. 2.24. Additionally, the SI of pyrite reaches zero, i.e. pyrite dissolution stops, and thus the Fe concentrations drops below the measured data – see red curve in right diagram.

Case (ii) in the stagnant water the pe value *is fixed* to the measured pe = 5

In this case, due to the higher pe value, U does *not* precipitate as U(IV) mineral and remains mobile. Hence, the calculated U breakthrough curve is in accord with the experiments – see blue curve in Fig. 2.24. Also the Fe description improves. Thus, we apply case (ii) for the column tests (standard dataset).

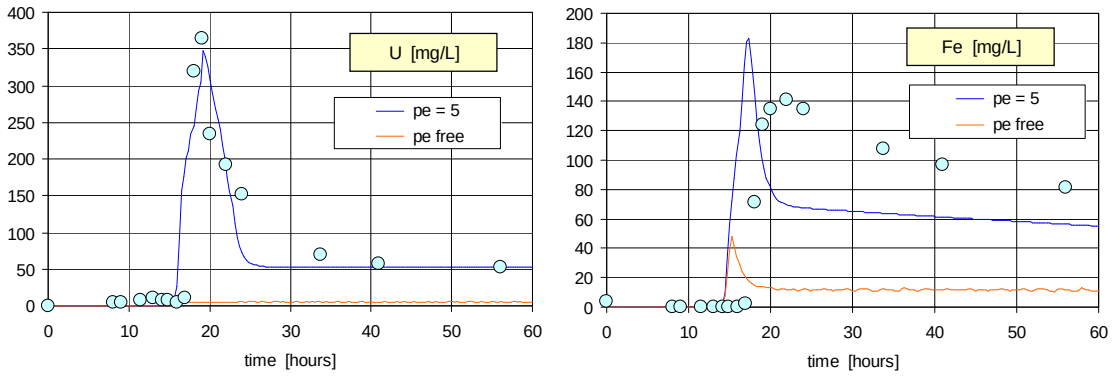

Fig. 2.24 Calculations with fixed pe = 5 and with free pe value

Nonetheless, pe-fixing is a 'direct intervention' and further investigations are necessary to improve this problem. There are several possibilities, for example:

- to implement additional (microbial) reactions and/or minerals for pe stabilization at the measured value
- to allow oversaturation of known U(IV) minerals or use other U(IV) minerals

As far as this problem is not solved appropriately we apply the straight pe handling in case (ii) for the column tests. For the aquifer simulations, however, the situation is different: under the lower ORP conditions U(IV) precipitation becomes more probable. The aquifer simulations in Chapter 4 are performed *without* pe-fixing.

3 BATCH TESTS

3.1 Experimental Setup and Core Analysis

The batch tests have been designed to provide additional and robust data to the geochemical modeling; they are complementary to the column tests (due to the higher residence time). The experimental set-up is simple: A suspension consisting of approximately 1 kg core material and 1 L synthetic mining fluid is stirred for 4 days,

core mass	m_{core}	= 1 kg
volume of solution	V_{sol}	= 1 L

The composition of the final solution (at t = 4 days) has been analyzed. The simple experimental design allows a greater number of tests so that the significance of the results increases.

Water Composition. Starting from FME groundwater, the synthetic mining fluids were made-up by adding H_2O_2, U_3O_8, and H_2SO_4 to achieve the desired ORP, U concentration, and pH value, respectively. Four different test fluids varying in the pH value are used (see Tab. 3.1). The charge balance of the solutions has been adjusted by the unknown Cl concentration.

Tab. 3.1 Synthetic fluid compositions (ΔIB denotes the ion/charge balance error)

Element	Unit	pH 1.7	pH 3	pH 4	pH 5
		raw data			
pH	-	1.7	3.0	4.0	5.0
ORP	mV-AgCl	560			
ORP	mV-SHE	770			
pE	-	13			
T	°C	25			
Ca	mg/L	21	21	21	21
Mg	mg/L	31	30	31	31
Na	mg/L	280	280	290	310
K	mg/L	14	13	13	13
Mn	mg/L	< 1			
SO_4	mg/L	1860	450	420	450
Fe	mg/L	< 1			
Al	mg/L	1.4	1.8	< 1	< 1
U	mg/L	48	46	42	32
Si	mg/L	8.5	7.6	7.6	7.6
ΔIB	%	16.68	35.54	35.56	33.42
Cl[1)]	mg/L	387	305	294	292
P[2)]	mg/L	< 1	< 1	1.6	1.4

[1)] Charge balance adjustment parameter
[2)] Element P has been neglected in the simulation since almost all measured values in the initial and resulting solutions are below the detection limit of 1 mg/L

Each solution was combined with three different core materials taken from 3 drill holes in the FME aquifer outside the ore body (ACK010, ACK024, ACK103). The tests have

been run in duplicate. Thus, the experimental program consists of $4 \times 3 \times 2 = 24$ solutions (12 test run combinations) and their analytical data.

The four synthetic solutions in Tab. 3.1 represent the *input* solutions for the modeling.

Core Material. Tab. 3.2 summarizes the elemental distribution within the core material. The first two cores (AKC010, AKC024) are fairly similar to each other (apart from a different Mn and U content). In contrast, the third core AK103 contains a much higher amount of Na, Mg, K, Ca, and Al, but a significant lower amount of Si and S.

Tab. 3.2 Composition of the 3 different core material

Sample name	Na (%)	Mg (%)	Al (%)	Si (%)	P (%)	S (%)	K (%)	Ca (%)	Mn (%)	Fe (%)	U (%)
AKC 010	0.020	0.006	1.856	41.48	0.011	1.024	0.143	0.045	0.022	2.199	0.003
	0.012	0.008	1.867	41.11	0.006	1.023	0.141	0.045	0.022	2.183	0.003
AKC 024	0.018	0.060	2.152	41.10	0.017	0.727	0.334	0.033	0.005	2.658	0.015
	0.017	0.057	2.148	41.25	0.017	0.651	0.335	0.033	0.006	2.679	0.016
AKC 103	0.140	0.306	6.244	35.26	0.018	0.166	1.699	0.113	0.003	1.751	0.004
	0.139	0.307	6.448	36.39	0.019	0.171	1.727	0.114	0.003	1.738	0.004

Obviously, a high Al content suggests a high amount of clay minerals. This assumption can be approved by the analysis of all available cores from the drill holes AKC026, AKC028 to AKC033, and AKC035. It shows that the Al content correlates with the amount of base cations (Na, K, Ca, Mg) and anti-correlates with Si – see left diagram in Fig. 3.1.

As shown in the right diagram of Fig. 3.1, Fe and S are correlated which indicates that pyrite is present. (A weak correlation could exist between Mn and S, too. However, the Mn content is near the detection limit and, therefore, the data are less significant.)

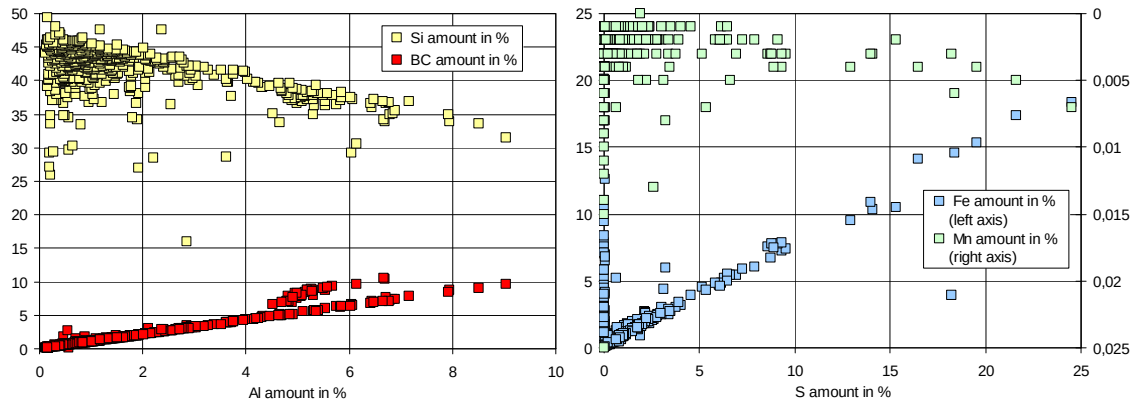

Fig. 3.1 Correlation of Si and base cations (BC) with Al (left) and correlation of Fe and Mn with S (right) in FME core material. (Note the reverted axis for Mn in the right diagram.)

The high amounts of Fe and Mn at low S occur at high clay contents. However, any dependence between clay minerals and sulfides cannot be derived since no correlation exists between Al and S in the cores. In fact, the weak anti-correlation between Si and S as well as between Si and C suggests a random distribution between clay minerals, quartz, sulfides, and carbonates (see left diagram in Fig. 3.2).

C and Ca correlate, whereby no significant correlation between C and Mg exists. Hence, calcite can be assumed to be the main carbonate mineral (see right diagram in Fig. 3.2).

Finally, no obvious correlations could be found between U content and other elements like S, Al, Si, and C.

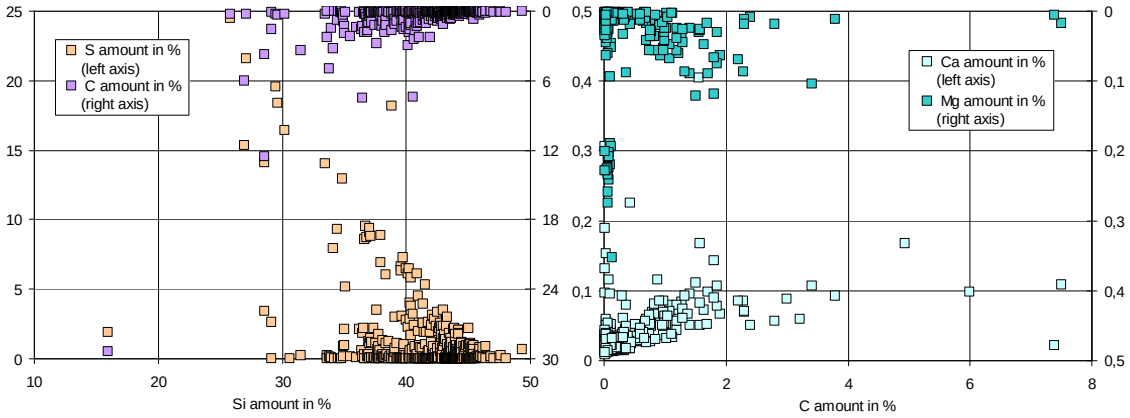

Fig. 3.2 Correlation of S and C with Si (left) and correlation between Ca and C amount (right) in FME core material. (Note the reverted axis for C in the left diagram, and for Mg in the right diagram.)

3.2 Experimental Results

The final compositions of all 24 solutions (after 4 days stirring) are summarized in Tab. 3.3 to Tab. 3.5 (for every core and every initial pH exists two runs; in total 24 runs). In all runs the pH and ORP are fairly stable to the end. Small variations in pH and ORP result from the contact with air which allows CO_2 and O_2 exchange as well as evaporation. The results of the duplicated runs are in agreement with each other. Problems aroused with the elemental analysis of the AKC103 solution at initial pH 3 (run 1) only; this data was inconsistent and has been neglected.

AKC010 & AKC024. In accord with the similar core compositions of AKC010 and AKC024 the results of the corresponding solutions are fairly similar, too. In all runs, independent of the initial pH, the final solutions attained pH ≈ 3 ... 4 and an ORP between 330 and 370 mV. In particular, with increasing initial pH the final pH increases from pH 2.9 to 3.5 (AKC010) and from pH 3.1 to pH 4.0 (AKC024). Therewith the final pH's for core AKC024 are slightly higher.

The other element concentrations behave similar in dependence of the pH value. There exist two exceptions, Mn and U, in accord with the differences in the core composition. The Mn content in AKC010 is an order of magnitude higher than for AKC024.

In contrast to Mn the U concentration in the final solution for AKC024 is higher than for AKC010 as expected from the core composition. However, it should be noted that the final U concentrations are lower than the U concentrations in the initial solutions (except from AKC024 with initial pH 1.7). This indicates a retardation mechanism (see Tab. 3.3 and Tab. 3.4).

Tab. 3.3 Composition of the solutions in contact with core AKC010 after 4 days stirring

Initial pH	pH	ORP	Al	Ca	Fe	K	Mg	Mn	Na	P	S	SO4	Si	U	HCO_3
			mg/L	mg/L	mg/L	mg/L	mg/L	mg/L	mg/L	mg/L	mg/L	mg/L	mg/L	mg/L	M
1.7	3.04	362	210	300	550	1.5	120	110	470	1.8	1420	4260	220	27	<0.01
	2.93	359	200	270	560	2.2	110	100	420	<1	1280	3840	180	24	
3	3.22	356	81	270	230	3.2	100	49	490	<1	860	2580	100	17	<0.01
	3.13	355	83	240	160	5.7	100	59	440	<1	810	2430	120	13	
4	3.40	339	80	280	170	14	110	90	480	1.2	890	2670	180	9.6	<0.01
	3.33	332	74	250	160	13	110	80	470	<1	830	2490	160	8.5	
5	3.46	354	68	260	92	12	100	78	470	<1	770	2310	160	9.1	<0.01
	3.27	342	71	240	130	10	100	71	480	<1	810	2430	140	10	

Tab. 3.4 Composition of the solutions in contact with core AKC024 after 4 days stirring

Initial pH	pH	ORP	Al	Ca	Fe	K	Mg	Mn	Na	P	S	SO4	Si	U	HCO_3
			mg/L	mg/L	mg/L	mg/L	mg/L	mg/L	mg/L	mg/L	mg/L	mg/L	mg/L	mg/L	M
1.7	3.12	369	240	220	230	74	120	9.5	460	<1	1150	3450	230	88	<0.01
	3.14	372	250	210	210	87	120	8	420	2	1390	4170	230	86	<0.01
3	3.69	338	56	210	21	62	100	6.5	480	<1	600	1800	120	21	<0.01
	3.78	339	48	180	18	60	91	6	430	<1	560	1680	100	16	<0.01
4	3.78	335	60	220	20	72	110	5.7	480	<1	640	1920	120	16	<0.01
	4.00	328	50	170	15	81	93	7	440	2	590	1770	130	10	<0.01
5	3.90	327	59	210	19	86	110	5.9	490	1.1	640	1920	130	12	<0.01
	3.99	329	57	180	19	100	99	8	460	1	670	2010	130	11	<0.01

Tab. 3.5 Composition of the solutions in contact with core AKC103 after 4 days stirring

Initial pH	pH	ORP	Al	Ca	Fe	K	Mg	Mn	Na	P	S	SO4	Si	U	HCO_3
			mg/L	mg/L	mg/L	mg/L	mg/L	mg/L	mg/L	mg/L	mg/L	mg/L	mg/L	mg/L	M
1.7	3.67	309	25	370	14	110	220	2.2	520	<1	910	2730	120	10	
	3.79	309	22	360	11	100	210	2	500	<1	850	2550	110	9	<0.01
3	7.15	218	420	270	2020	92	1010	340	770	400	5850	17550	15	90	
	7.15	218	390	270	2070	88	1010	350	760	400	5850	17550	15	120	
	6.86	218	3	97	<1	52	56	<1	410	<1	280	840	13	<1	<0.01
4	7.23	179	<1	91	1.5	57	51	<1	440	<1	320	960	12	<1	
	7.27	194	5	79	<1	42	46	<1	380	<1	250	750	9	<1	<0.01
5	7.47	200	<1	86	<1	47	47	<1	430	<1	300	900	10	<1	
	7.10	205	<1	86	<1	47	49	<1	400	<1	270	810	12	<1	<0.01

AKC103. In contrast to the first two cores the solutions in contact with AKC103 show a quite different behavior. Here, except for the run with initial pH 1.7, all final solutions are pH neutral.

The high concentrations of the base cations (Na, K, Mg, Ca) mirror the core composition of AKC103. Conversely, the S concentrations are much lower in comparison to the other core solutions. Similar to the other two cores the element concentrations reflect the expected pH dependence. Also the retention of U agrees with the results from the other cores (see Tab. 3.5).

3.3 Model Calculations

The batch test simulations are based on an *equilibrium* model. The assumption that the solutions after 4 days are in equilibrium is sustained by stable pH and ORP conditions (both parameters were measured during the batch tests).

We used the thermodynamic model PHREEQC and its database *wateq4f* for the calculation of:

- Ions speciation
- Mineral precipitation / dissolution
- Equilibrium with CO_2 in atmosphere (open system)
- Cation exchange

With respect to the air contact during the experiments the following conditions have been specified:

Dissolution of O_2: pe value was adopted to the pe in final solution
Dissolution of CO_2: equilibrium with partial pressure $p_{CO2} = 3.5 \cdot 10^{-4}$ atm

The initial solutions are equal for all three cores (see Tab. 3.1). These are taken as input waters.

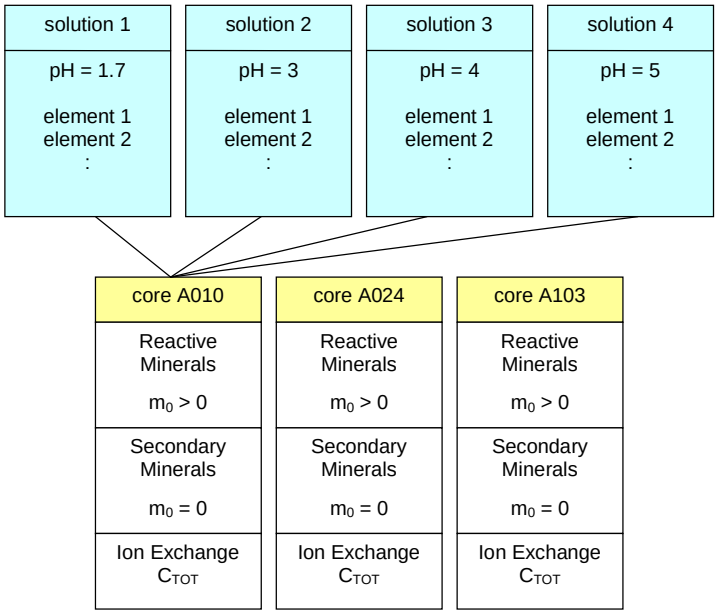

Fig. 3.3 Calculations are performed by combination of four aqueous solutions with three core inventories

In the model calculations four initial solutions (defined in Tab. 3.1) are combined with three core inventories composed of reactive and secondary minerals as well as ion exchangers (see Fig. 3.3). In total, $4 \times 3 = 12$ calculations are performed. Please note, the "model cores" A010, A024, and A103 contain the same elemental list; they differ by the values of m_0 and C_{TOT} only.

Minerals. The final solution is mainly influenced by mineral dissolution/precipitation and ion exchange. Great effort was undertaken to define a consistent set of minerals. Two kinds of minerals are considered:

- Reactive minerals (only dissolution)
- Secondary minerals (dissolution and precipitation)

Reactive minerals act as a source; secondary minerals act as a sink for elements. Reactive minerals require an initial mass m_0 (more precisely: the initial amount of moles per liter solution). This value is *less* or equal to the total mineral amount in the core (due to the limited availability). Therefore, the actual value for m_0 was treated as a free model parameter. Once a 'model core' was defined by the mineral set including m_0 it was used for all initial solutions (as depicted in Fig. 3.3).

Tab. 3.6 Initial mass m_0 per liter solution for reactive minerals

Reactive Minerals		core A010	core A024	core A103
		[mM]	[mM]	[mM]
Pyrite	FeS_2	13.3	9.2	4.2
MnS(Green)	MnS	1.9	0.19	0.08
Kmica	$KAl_3Si_3O_{10}(OH)_2$	2.5	4.8	6
Albite	$NaAlSi_3O_8$	7	7	6
Calcite	$CaCO_3$	8.2	7.2	15.7
Coffinite	$USiO_4$	0.03	0.40	0.04

The list of reactive minerals and their initial inventory m_0 are given in Tab. 3.6. On the other hand, the list of secondary minerals is in all cores the same. It contains Fe(III), U(VI) as well as clay minerals:

Ferrihydrite	$Fe(OH)_3$	
Jarosite	$K_{0.77}Na_{0.03}H_{0.2}Fe_3(SO_4)_2(OH)_6$	
Schwertmannite	$Fe_8O_8(OH)_{4.8}(SO_4)_{1.6}$	from [BCM94]
Soddyite	$(UO_2)_2SiO_4{:}2H_2O$	from [GL07]
Becquerelite	$Ca(UO_2)_6O_4(OH)_6{:}8H_2O$	from [GL08]
Kaolinite	$Al_2Si_2O_5(OH)_4$	
Diopside	$CaMgSi_2O_8$	

The choice of reactive minerals was guided by the analysis of the core composition in Sec. 3.1. In agreement with the good correlation of Fe and S pyrite (FeS_2) has been chosen as the main sulfate source. A second sulfate source is MnS. However, only core AKC010 consists of a significant amount of Mn. Irrespective of the weak correlation between Mn and S the higher S amount in the core and the lower final pH in the solutions suggest an extra sulfide (apart from pyrite).

As uranium source the U(IV) mineral coffinite was taken. [Calculations with uraninite as an alternative U(IV) mineral does not change the results.]

Calcite, as Ca source, is the only carbonate used in the mineral set. In reality the Ca source is divided in carbonates and clay minerals. However, in order to reduce the number of minerals a Ca-clay mineral, e.g. anorthite ($CaAl_2Si_2O_8$), has been neglected.

Clay minerals are not easy to model due to their highly varying stoichiometry and their incongruent dissolution behavior. The incongruent dissolution of clay minerals is seen by a reduction of base cations and an increase in Al and Si content.

Kaolinite can be considered as the final alteration product due to its thermodynamic stability. The dissolution of the lower stable clay minerals albite and K-mica leads to the precipitation of kaolinite. In this way the incongruent dissolution of the clay minerals is simulated. All final solutions are in equilibrium with kaolinite. Finally, diopside will be available as secondary Al-poor clay mineral.

Minerals	Ele-ment	AKC010		AKC024		AKC103	
		m_{minr} [g]	m_{inp} [g]	m_{minr} [g]	m_{inp} [g]	m_{minr} [g]	m_{inp} [g]
Pyrite	S	19.2	1.6	12.9	1.1	3.2	0.5
MnS	Mn	0.35	0.17	0.09	0.02	0.05	0.01
Calcite	Ca	1.12	1.22	0.82	1.12	2.83	2.76
Kmica	K	14.5	1.2	34.1	2.1	174	3.1
Albite	Na	1.8	1.8	2.0	2.8	15.9	4.6
Coffinite	U	0.04	0.01	0.21	0.13	0.06	0.01

Tab. 3.7 Mineral composition of the core as an upper limit for the model input

Tab. 3.7 compares the total mineral content in the core (m_{minr}) with the mineral mass used in the model calculations (m_{inp}). The latter quantity includes besides the initial mineral mass m_0 also the ion-exchange reservoir (the second element source). The m_{minr} values recalculated from the element composition in the core serve as an upper limit.

The amount m_{inp} is an outcome of the model calculations. It represents the reactive or available amount in core. Due to the stirring of the suspension for the duration of 4 days the contact time and contact area was high. Thus, the available amounts should be fairly near to the mineral content in the core.

The obtained amounts for Ca (Calcite) and Na (Albite) in core AKC010 and AKC024 are slightly above the initial amounts in core. However, especially for Na the mass balance does not fit at all for these cores. That means either the analyzing method of the core material underestimates the contents due to their small percentage or, more probably, due to evaporation the concentration in the solution increases.

Ion Exchange. The only input for the ion exchange model is the total ion exchange capacity C_{TOT}. This value depends on the clay content. The clay content was estimated from Al in the cores (assumption: all Al exists in the form of kaolinite). This assumption results in an upper limit (shown in 2nd column of Tab. 3.8). In the model calculations, however, we assume that only 50 % of the maximal content is available for ion exchange (see 3rd table column). From the latter value, using Eq. (2.14), C_{TOT} was calculated which enters the equilibrium model (see 4th table column).

	Clay Content from Al [g]	Clay Content in Simulation [g]	C_{TOT} [meq/L]
AKC010	90	50	25
AKC024	100	50	25
AKC103	300	150	75

Tab. 3.8 Clay content and cation exchange capacity in the cores

The ion exchange considered the cations H^+, Na^+, K^+, Ca^{2+}, Mg^{2+}, Mn^{2+}, Fe^{2+}, and Al^{3+}. For example, if 5 meq/L exchange sites (it corresponds to 1 % clay content) are put into equilibrium with the groundwater solution the following species distribution is obtained:

KX: 0.11 meq/L
NaX: 0.77 meq/L
CaX_2: 0.79 meq/L
MgX_2: 1.27 meq/L

In addition, three uranyl ion exchange species are implemented (see Sec. 2.3).

Model Results. The obtained results for all three cores are presented in Fig. 3.4 to Fig. 3.12. The diagrams include the measured data (blue dots), the initial solution data (yellow dots) and, most important, the calculated data for the final solutions (blue curves). All simulated data within one diagram are the outcome of the *same* mineral and IX inventory.

The model results (blue curves) match the observations nicely. Even the Fe concentrations, which are extremely sensitive to pH, could be captured quite well. However, the model overestimates the Si concentrations. This effect is probably caused by an *in*congruent dissolution of clay minerals (which is not included in the model yet).

The incongruent clay mineral dissolution occurs especially at neutral pH (see the final solutions of core AKC103 with neutral pH). In nature, during weathering clay minerals release K, Ca, Na, and Mg (without the complete dissolution of the mineral). This mechanism could not be simulated sufficiently with PHREEQC and the available database. In the present approach four minerals with fixed stoichiometry and log-k values are used: albite for Na, K-mica for K, diopside for Ca and Mg, and kaolinite. Therefore, the calculated concentration of the base ions does not fit the observations perfectly. In sum, despite the oversimplified clay mineral assembly the obtained results are still good.

Secondary Minerals	AKC010	AKC024	AKC103	
	all	all	pH_{ini} 1.7	pH_{ini} 3 - 5
Kmica				x
Diopside				x
Kaolinite	x	x	x	x
Jarosite	x	x	x	
Schwertmannite				x

Tab. 3.9 Secondary minerals that precipitate in the final solution

All secondary minerals that precipitate in the final solution are listed in Tab. 3.9. Interestingly, no U(VI) minerals precipitate at the low pH's. Therefore the U retention detected in the batch tests was described by uranyl ion exchange alone.

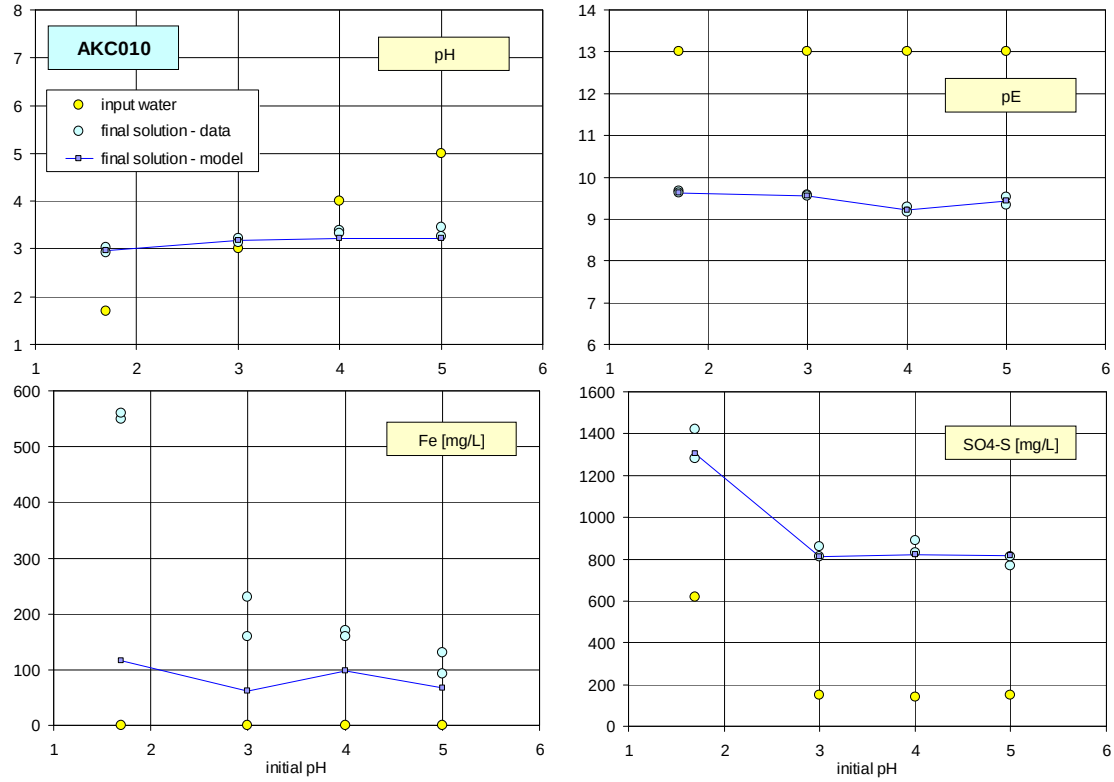

Fig. 3.4 Measured pH, pe, Fe, SO4-S compared with model calculations – core AKC010

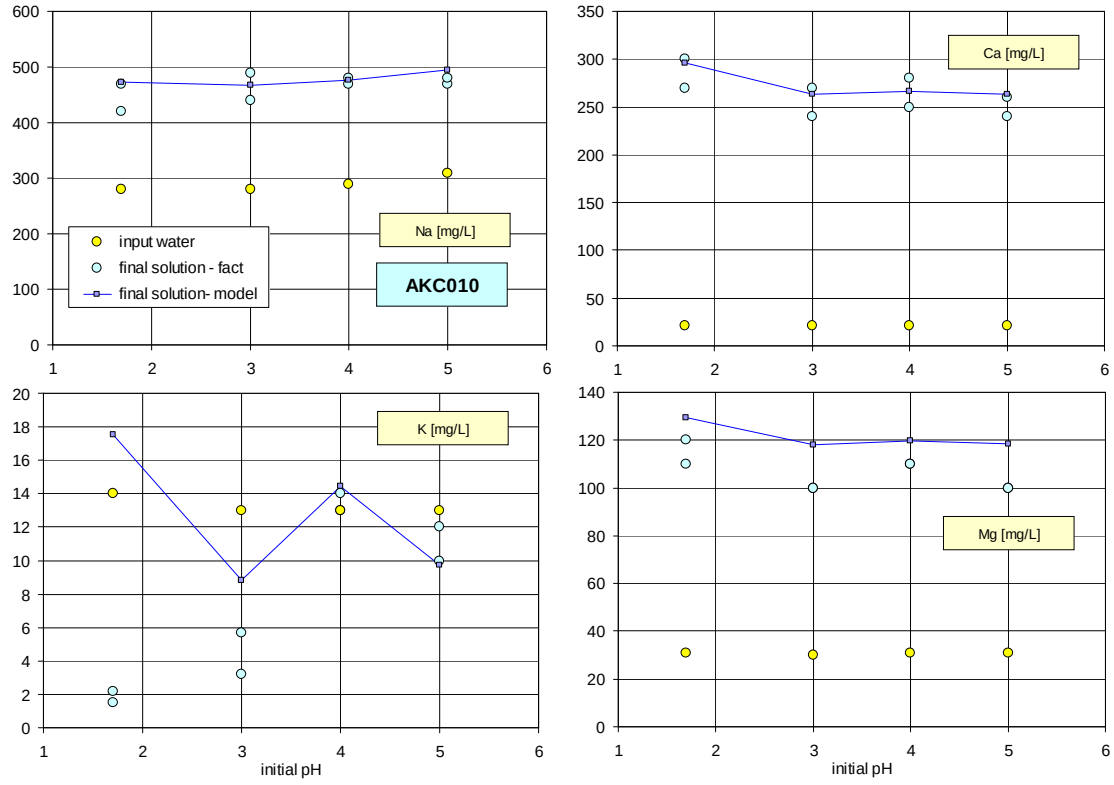

Fig. 3.5 Measured Na, Ca, K, Mg compared with model calculations – core AKC010

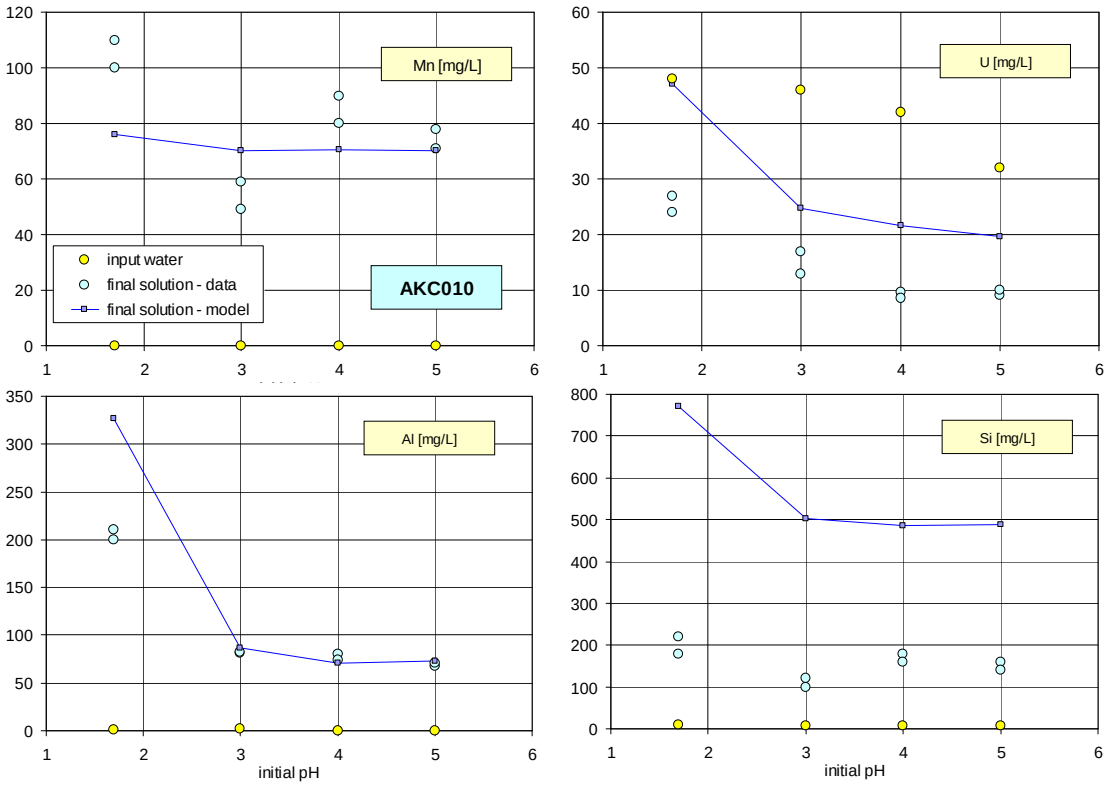

Fig. 3.6 Measured Mn, U, Al, Si compared with model calculations – core AKC010

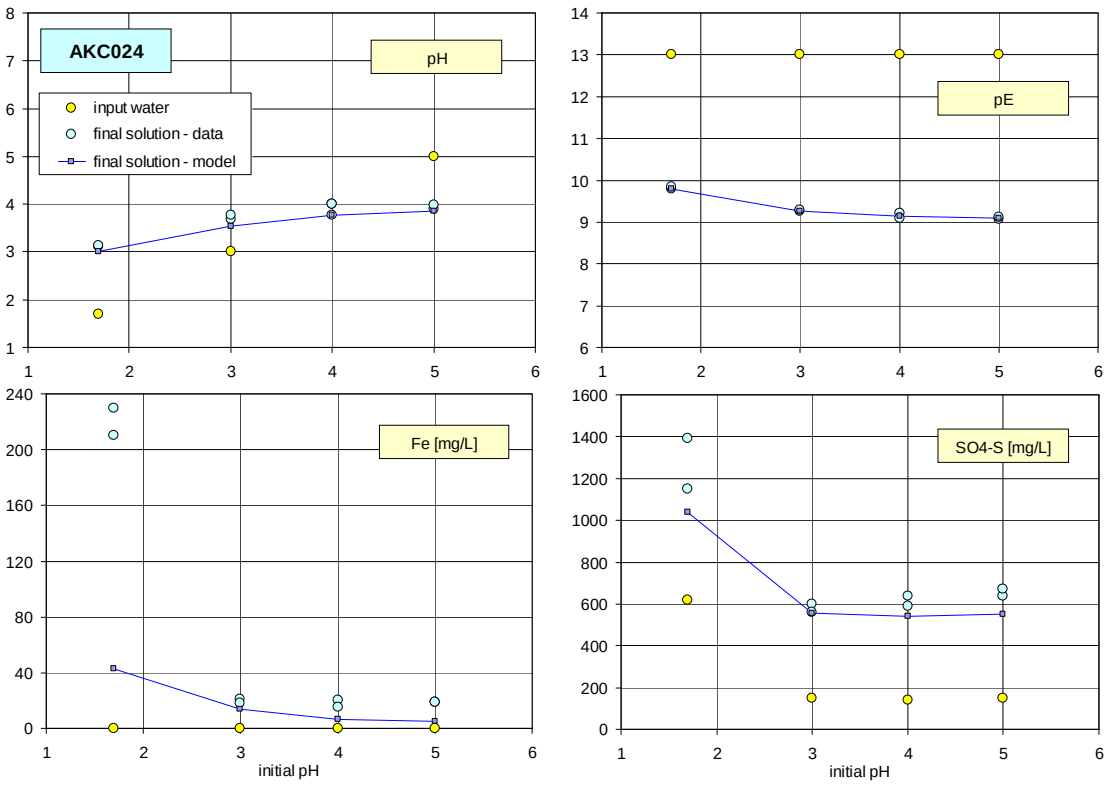

Fig. 3.7 Measured pH, pe, Fe, SO4-S compared with model calculations – core AKC024

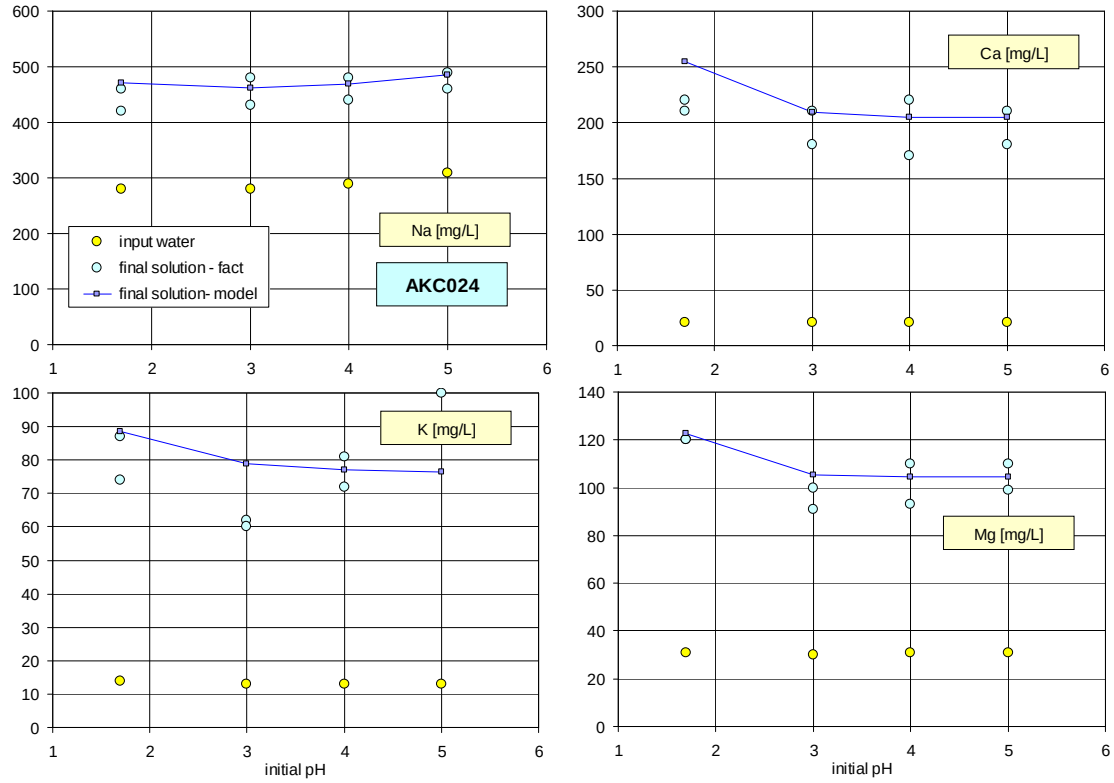

Fig. 3.8 Measured Na, Ca, K, Mg compared with model calculations – core AKC024

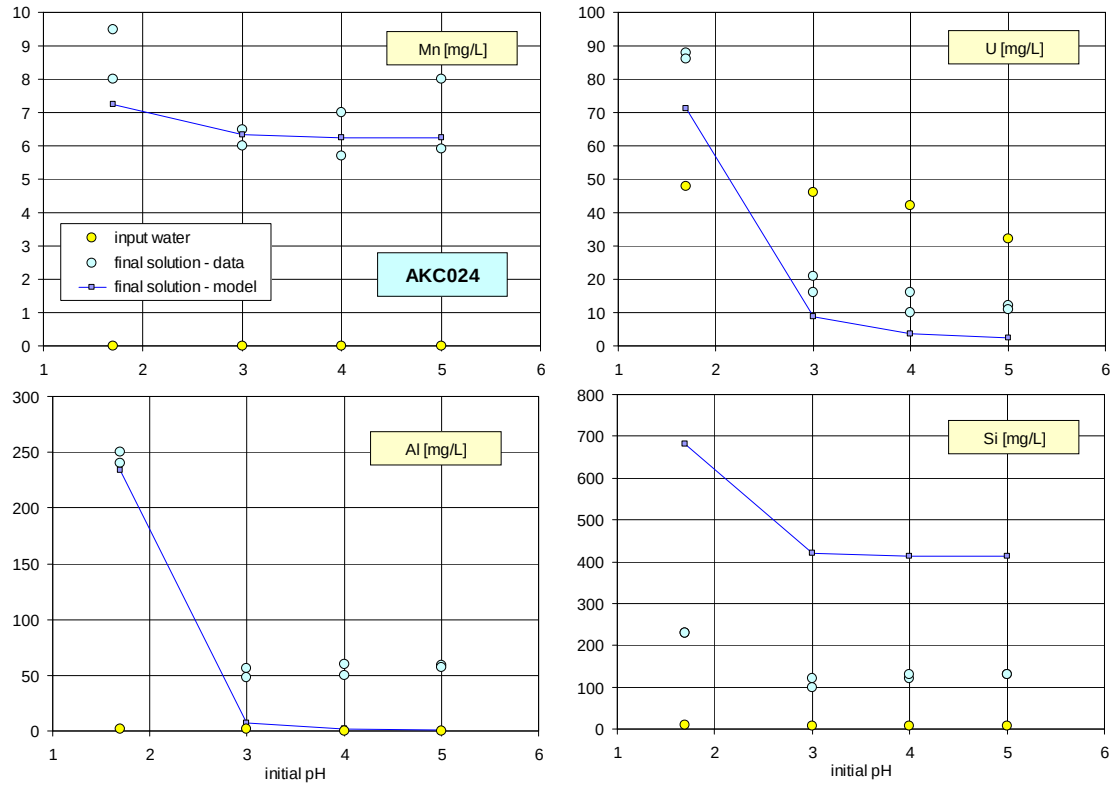

Fig. 3.9 Measured Mn, U, Al, Si compared with model calculations – core AKC024

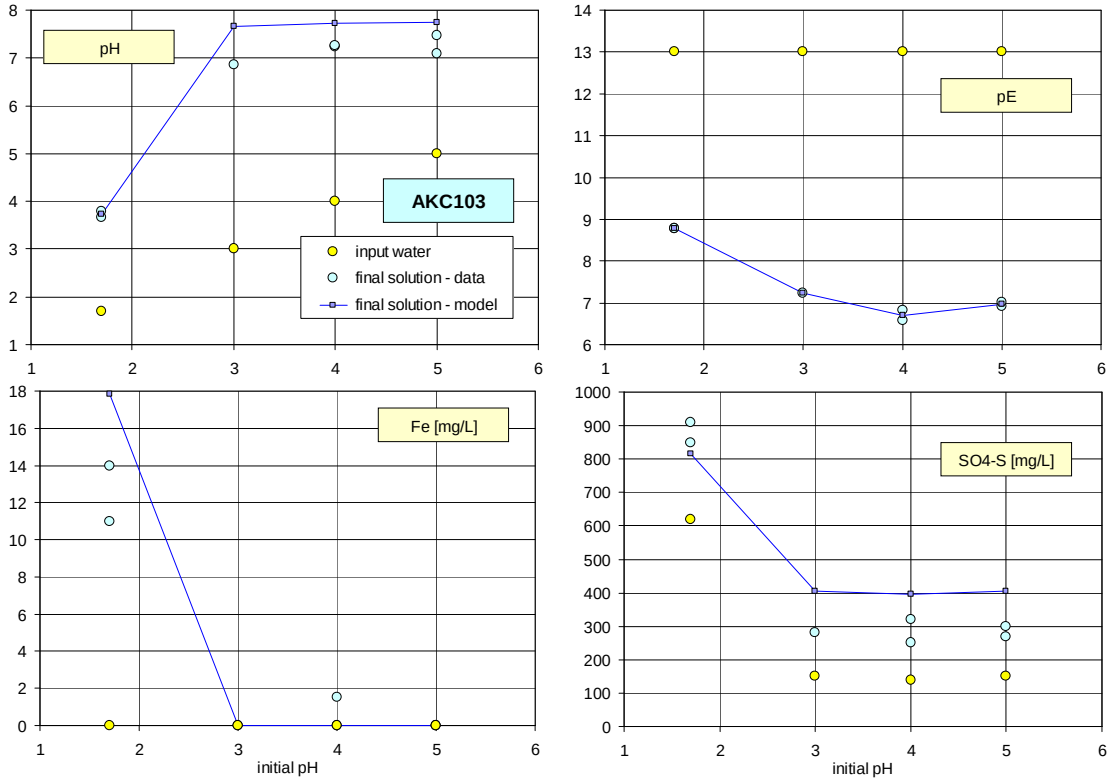

Fig. 3.10 Measured pH, pe, Fe, SO4-S compared with model calculations – core AKC103

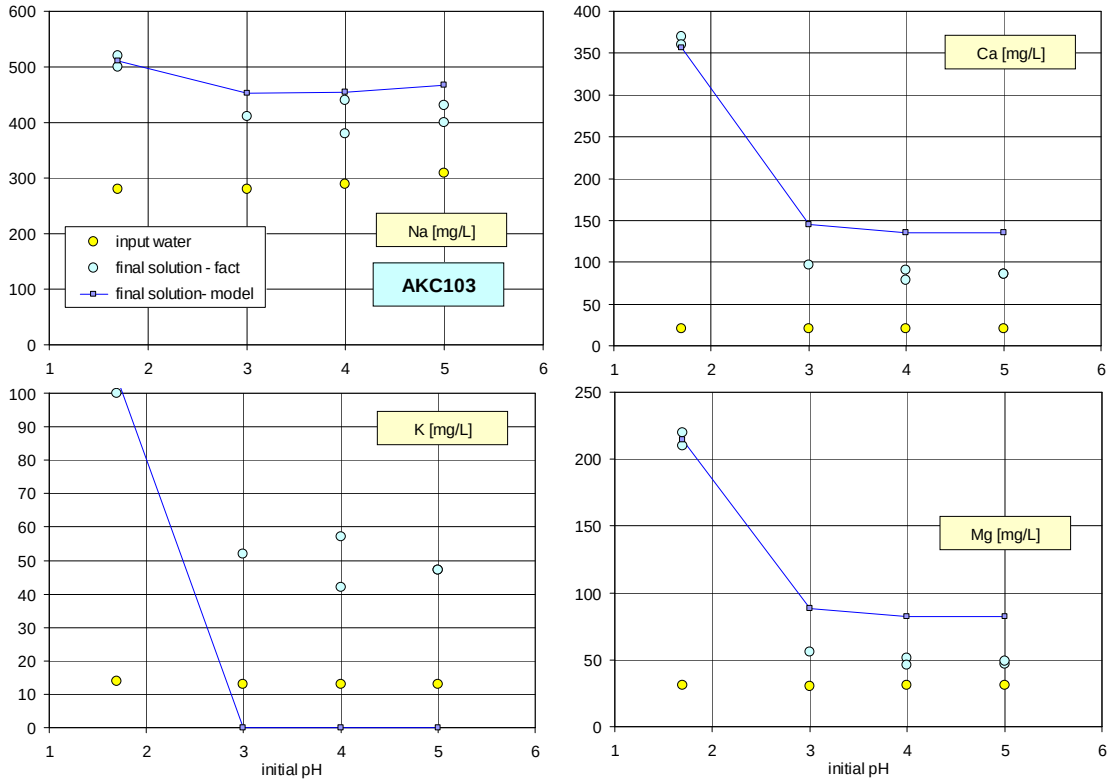

Fig. 3.11 Measured Na, Ca, K, Mg compared with model calculations – core AKC103

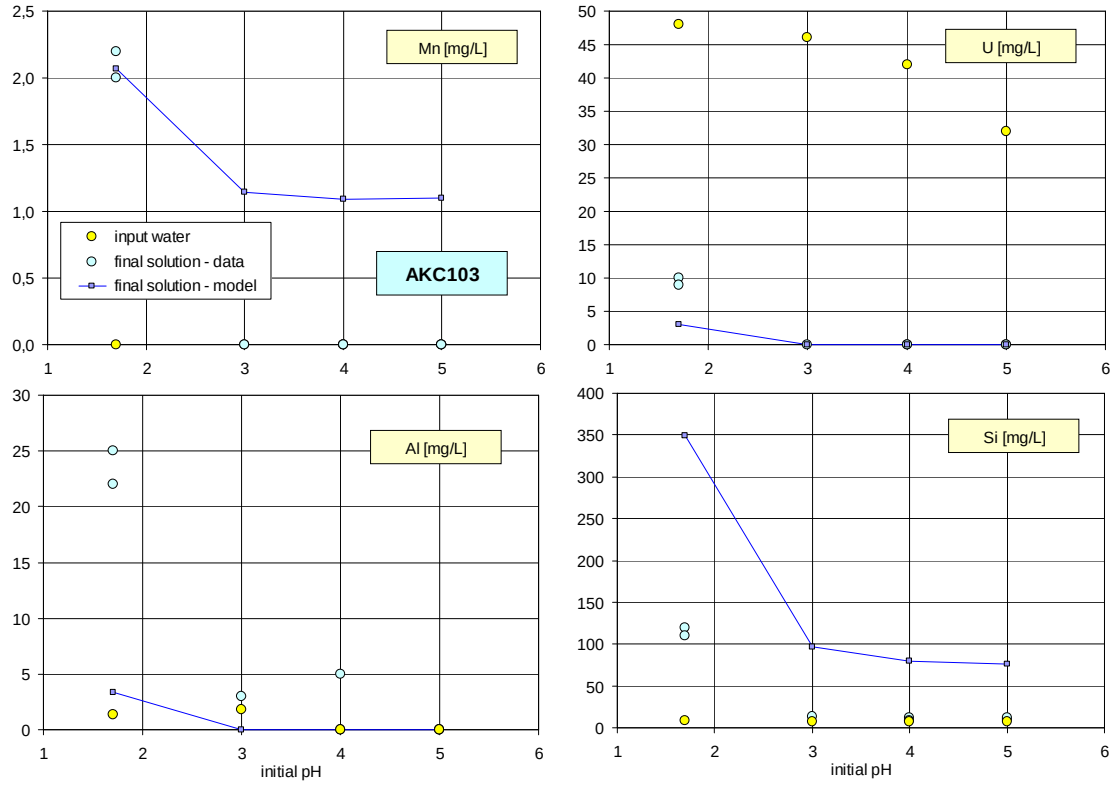

Fig. 3.12 Measured Mn, U, Al, Si compared with model calculations – core AKC103

4 AQUIFER SIMULATIONS

4.1 Definition of Scenarios

Fig. 4.1 shows the simplified structure of the FME aquifer in form of a flow path taken from [Bev08]. Here the groundwater enters the Ore Zone and flows via the FM Embayment into the Lake Frome Embayment (LFE). The flow velocity differs from zone to zone.

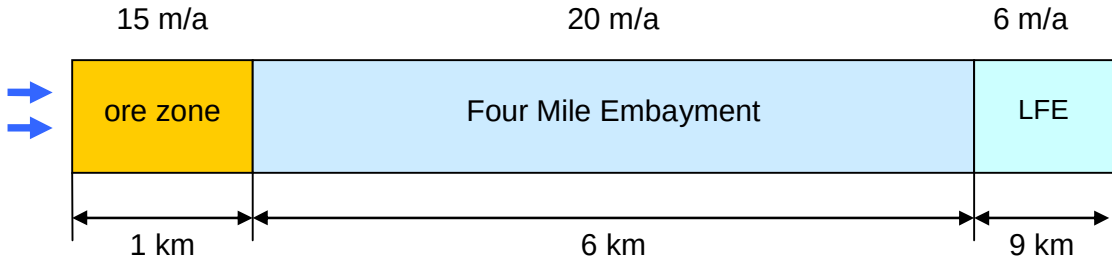

Fig. 4.1 Flow velocities within the FM aquifer taken from [Bev08] (LFE – Lake Frome Embayment)

In the following we consider a total timespan of 800 years and a model extension up to 7 000 meters including two compartments: the complete Ore Zone and the first half of the Four Mile Embayment. These are, in fact, the compartments where the principal geochemical processes take place.

The aquifer simulations depend on hydraulic and geochemical data. The hydraulic data are overtaken from the MODFLOW calculations in [Bev08]; the geochemical data has been upscaled from the column and batch tests described in Chapter 2 and 3.

Three aqueous solutions (input solutions) are considered:

- groundwater pH ≈ 7 ORP ≈ 0
- aggressive lixiviant pH = 1.7 ORP = 750 mV-SHE U = 52 ppm
- 1:1 diluted lixiviant pH = 2.0 ORP = 750 mV-SHE U = 26 ppm

Groundwater and aggressive lixiviant have been defined already for the column tests in Tab. 2.2 on page 18 (but now the lixiviant does not contain the KCl tracer). The third solution is generated by an 1:1 mix of lixiviant and groundwater (see Sec. 4.2). The complete elemental content for all three solutions is given in Tab. 4.1.

Within the dual porosity approach both compartments (ore zone and embayment) contain material in mobile and immobile form. By specifying the initial composition of mobile and immobile phase (at t = 0) we are able to define different scenarios. The FM Embayment is characterized by an initial state where both mobile and stagnant water pores are filled with groundwater. This assumption is unaltered in all scenarios. The situation is different for the ore zone where two distinct post-mining scenarios are considered: mobile and stagnant water pores are completely filled with aggressive lixiviant or with diluted lixiviant at t = 0. In both cases, the ion exchanger at t = 0 is put into equilibrium with lix or with diluted lix, respectively.

In this way, three base scenarios are specified (see Fig. 4.2):

Scenario 'Transport' (as demo for pure transport phenomena in Sec. 4.4)

Lix inflow (3 month) into the FM embayment followed by groundwater inflow

Scenario 'Worst Case' "The Extreme Post-Mining Case"

It starts after mining. The ore zone is completely filled with aggressive lixiviant (in both mobile and stagnant zones). Inflowing groundwater transports the contaminants into the FM embayment.

Scenario 'Real Case' "Post-Mining Case"

It starts after mining and considers the fact that, during mining/leaching, there is an ongoing transversal dilution in the ore zone. As a result, the initial solution (inside the ore zone) for the post-mining simulations is not *lix* with pH = 1.7 (as in the 'Worst Case'), but a diluted lixiviant *lix_R* (with pH = 2.0). Inflowing groundwater transports the contaminants into the FM embayment.

The first scenario with the 'short pulse' lix inflow represents a sound basis for discussions of dispersion and dual-porosity phenomena in Sec. 4.4. The focus is then shifted to the Post-Mining Scenarios. Thereby, from all thinkable configurations scenario 'Worst Case' is the most hazardous case (only theoretical possible). The much more realistic case ('Real Case') will be explained and generated in Sec. 4.2.

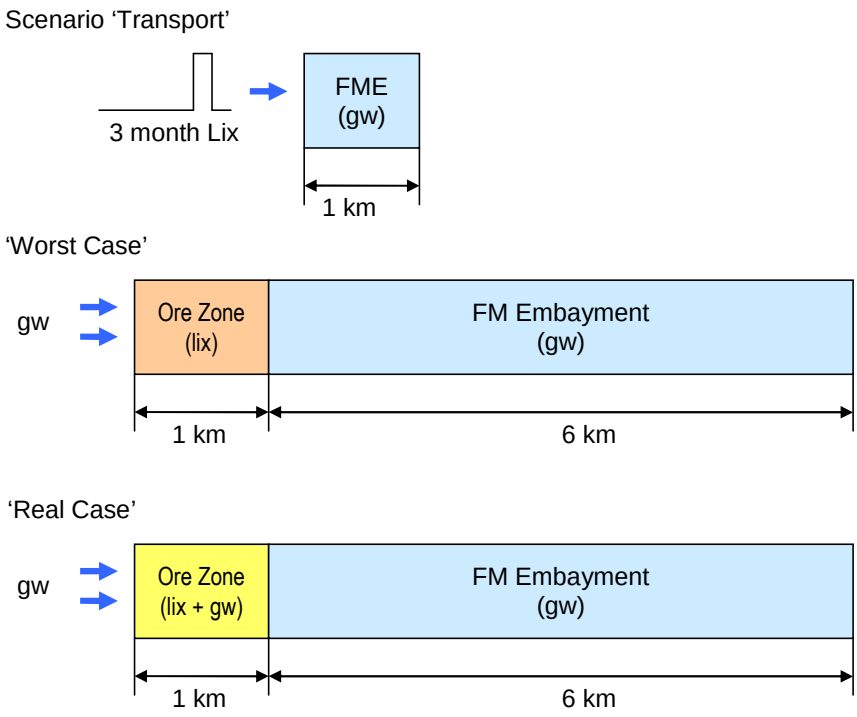

Fig. 4.2 Three scenarios for geochemical aquifer simulations (gw – groundwater, FME – Four Mile Embayment)

The model space 'Flow Path' shown in the above pictures is embedded in the FM aquifer of 70 m thickness – see Fig. 4.3. The thickness of the 'Flow Path' is determined by the vertical extension of the ore zone (thickness 5 to 10 m).

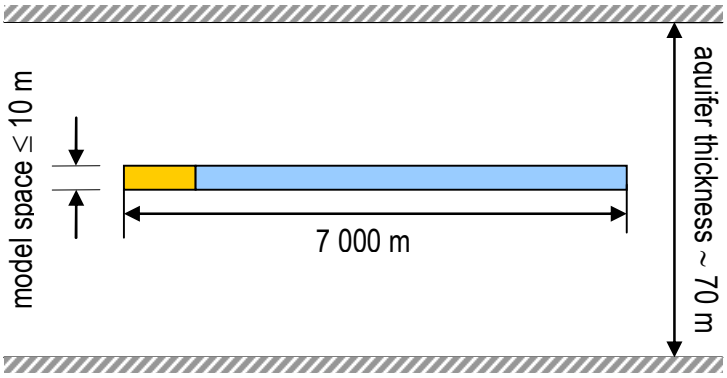

Fig. 4.3 Model space 'Flow Path' embedded in the FM aquifer (non-scale division)

4.2 Generation of the 'Real Case'

The "Real Case" considers the fact that, during mining/leaching, there is an ongoing transversal dilution in the ore zone. As a result, the initial solution (inside the ore zone) for the post-mining simulations is not *lix* with pH = 1.7 (as in the "Worst Case"), but a diluted solution *lix_R* (with pH = 2.0). The aim is now to generate the solution *lix_R*.

As shown in Fig. 4.4, the ore zone (thickness 5 to 10 m) is embedded in the aquifer (thickness 70 m). Due to the water movement caused by continuous injection and extraction there is a transversal dispersion that mixes groundwater and lixiviant.

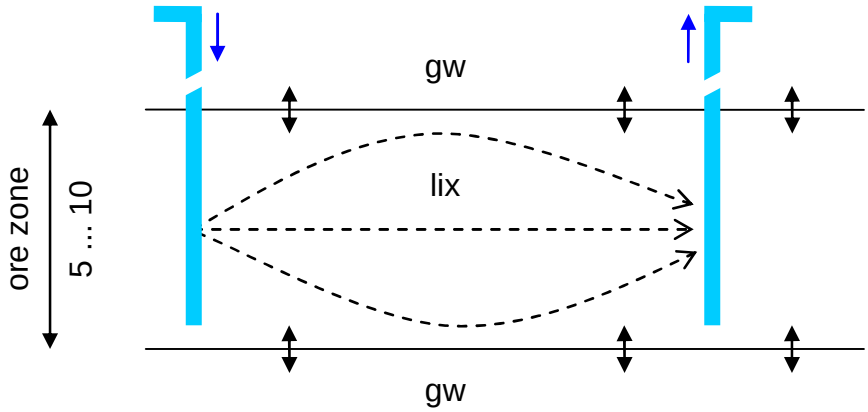

Fig. 4.4 The ore zone embedded in the aquifer with injection and extraction well for the lixiviant

At the beginning, the ore zone is filled with lix (pH = 1.7) whereas the aquifer above and below the ore zone contains groundwater (pH = 7). The mixing factor is then defined by

$$\text{mix} = \frac{\text{groundwater}}{\text{lixiviant}} = 2 \cdot \frac{\Delta z}{Z_{ore}} \qquad (4.1)$$

Here, Δz symbolize the penetration depth of groundwater into the ore zone caused by transversal dispersion; Z_{ore} is the thickness of the ore zone, and the factor 2 describes the fact that groundwater penetrates from both sides above and below.

The penetration depth is given by

$$\Delta z = \sqrt{\alpha_T v_T T_{leach}} \tag{4.2}$$

where α_T denotes the transversal dispersivity, v_T the transversal flow velocity, and T_{leach} the total leaching time.

The *maximum* value of the transversal velocity can be estimated from the total amount of water that is pumped through the aquifer per year, Q_{leach}, and the mining area A_{ore}:

$$v_{T,max} = \frac{Q_{leach}}{A_{ore}} = \frac{10\ \text{Mio m}^3/\text{a}}{1\,\text{km} \times 1\,\text{km}} = 10\,\frac{\text{m}}{\text{a}} \tag{4.3}$$

In order to calculate the mix factor in Eq. (4.1), the following parameters will be used

thickness of ore zone	Z_{ore}	= 10 m	(worst case)
transversal dispersivity	α_T	= 1 m	(worst case)
transversal velocity	v_T	= 2.5 m	(worst case, 25 % of $v_{T,max}$)
mining/leaching period	T_{leach}	= 10 a	(order of magnitude)

This leads to

$$\text{mix} = \frac{2}{10\ \text{m}} \sqrt{1\,\text{m} \cdot 2.5\,\tfrac{\text{m}}{\text{a}} \cdot 10\,\text{a}} = 1 \quad \Leftrightarrow \quad \boxed{\text{gw : lix = 1 : 1}} \tag{4.4}$$

Tab. 4.1 Model input for ground water and lixiviant

		groundwater (cell.sol)	lixiviant (lix.sol)	mix water1:1 (lix_R.sol)
pH	-	7.33	1.67	2.01
pE	-	1.0	12.5	12.5
T	°C	35	35	35
Ca	mg/L	84.4	115	100
Mg	mg/L	30.1	26.6	28.3
Na	mg/L	876	718	797
K	mg/L	44.3	60.2	52.3
SO4-S	mg/L	203	851	527
HCO3	mM	5	<0.01	2.5
Cl	mg/L	1 001	1 001	1 001
Fe	mg/L	<0.01	1.73	0.87
Al	mg/L	1.67	4.76	3.21
U	mg/L	0.001	52.9	26.5
Si	mg/L	16.0	28.3	22.1
DO	mM	0	0.1	0.05

In this way, the initial solution for the "Real Case" can be easily generated by 1 : 1 mixing of lixiviant and groundwater (using PHREEQC). The resulting solution *lix_R* with pH = 2 is presented in Tab. 4.1.

4.3 Input Data & Parameter Upscaling

The input data for the aquifer simulations results from two sources: the hydrogeologic model [Bev08] and the column/batch results of the previous chapters.

Hydraulic Data. From the hydrogeologic model we use:

flow velocity:	15 m/a	(ore zone)
	20 m/a	(embayment)
effective porosity:	0.30	
longitudinal dispersivity:	10 m	

For variation of these parameters we refer to [Bev08]. The effective porosity $\varepsilon_F = 0.30$ coincides with the column test values (total porosity $\varepsilon_T = \varepsilon_{eff} + \varepsilon_{res} = 0.30 + 0.11$).

Upscaling α. The dual-porosity mass transfer rate α is only meaningful in context with flow velocity v. For example, the 'high-velocity' column value $\alpha = 1.1\ h^{-1}$ overpredicts the 'low-velocity' aquifer case by far. Unfortunately, the empirical van Genuchten's approach in Eq. (2.16) does not contain any dependence on v or residence time Δt. To overcome this problem we assume a fixed relation between α and Δt for the upscaling:

(4.5) $$\alpha = \frac{1}{3 \cdot \Delta t}$$ for columns *and* aquifer

From this simple relation we get:

column tests:	$\Delta t = 0.3$ h	$\alpha = 1.1\ h^{-1}$
aquifer:	$\Delta t = 3$ month	$\alpha = 1.5 \cdot 10^{-4}\ h^{-1}$
aquifer:	$\Delta t = 6$ month	$\alpha = 7.5 \cdot 10^{-5}\ h^{-1}$

All hydraulic parameters used in the aquifer simulations are summarized in Tab. 4.2. This table also contains the column data input for comparison. Please note the huge differences between the aquifer and column simulations.

Tab. 4.2 Hydraulic parameters for aquifer simulations (in comparison with column data)

Parameter		Columns	Transport Scenario	Post Mining Scenarios	
			embayment	ore zone	embayment
L	total length [m]	1	1 000	1 000	6 000
N	number of cells	20	200	133	600
Δx	cell length [m]	0.05	5	7.5	10
Δt	time step	0.3 h	2 190 h = 3 month	4 380 h = 6 month	
T	simulation time	200 × Δt = 60 h	400 × Δt = 100 a	1 600 × Δt = 800 a	
v	flow velocity [m/a]	1 460	20	15	20
α_L	longitud. dispersivity [m]	$\leq 1 \cdot 10^{-3}$	10	10	10
α	mass transfer rate [h^{-1}]	1.1	$1.5 \cdot 10^{-4}$	$7.5 \cdot 10^{-5}$	
ε_T	total porosity	0.41	0.41	0.41	
ε_{eff}	effective porosity	0.30	0.30	0.30	

Geochemical Data. The geochemical parameters for the aquifer are based on the column dataset in Sec. 2.4. The upscaling, however, requires some modifications.

Pyrite Oxidation. During filling the columns the core material was crushed and an oxidation process takes place. This 'pre-cooking' was described by enhancing the pyrite rate from the original value $r_0 = 6.5 \cdot 10^{-11}$ M/s [WR94] (valid for undisturbed systems) to $r_0 = 1.6 \cdot 10^{-5}$ M/s (adjusted for the disturbed column system). The aquifer simulations are performed with the value $r_0 = 6.5 \cdot 10^{-11}$ M/s from literature.

U(IV) Precipitation. In addition to the U(IV) minerals coffinite and uraninite(c) used for the column simulations we include the amorphous U(IV) mineral *$UO_2(a)$*. The latter has a much higher solubility and does not precipitate at pH-pe conditions at which coffinite or uraninite(c) precipitate. Thus, in the spirit of very *conservative* assumptions, we exclude the precipitation of coffinite/uraninite at all and allow the precipitation of UO_2(a) only.

Kaolinite. Due to the high flow velocity in the columns the residence time, i.e. the contact time of the fluid with core material, is very short (which diminishes the amount of dissolved minerals significantly). Therefore, we reduced the amount of soluble kaolinite to $m_0/V_{stgn} = 1.2$ mM. In the aquifer (high residence time) there is no such constraint, and a larger amount of $m_0/V_{stgn} = 550$ mM (that corresponds to 1 % clay content) could be assumed. [Please note, that the secondary mineral kaolinite is controlled by thermodynamics, so the dissolved amount is much less than the input m_0 irrespective if we assume 1 % or 2 % clay content.]

Redox Potential. The redox potential within the aquifer is definitely *less* than in the column tests (performed under non-reducing conditions) which was fixed at pe = 5. Thus, in the aquifer simulations the initial ORP of groundwater is set equal to pe = 1.0 (see Tab. 4.1). During the calculations, for t > 0, the pe is *not* fixed; it develops freely with regard to the actual chemical conditions.

Tab. 4.3 Geochemical parameters for aquifer simulations (in comparison with column data)

Parameter			Columns	FM Aquifer		
				Ore Zone		FM Embayment
				Worst Case	Real Case	
	solution in mobile zone		gw	lix	lix_R	gw
	solution in stagnant zone		gw	lix	lix_R	gw
	IX in equilibrium with		gw	lix	lix_R	gw
C_{TOT}	total IX capacity [meq/L]		13.5	13.5	13.5	13.5
reactive minerals	Calcite	m_0/V_{stgn} [mM]	40	0	0	40
	Kaolinite	m_0/V_{stgn} [mM]	1.2	0	0	550
	U(IV)	m_0/V_{stgn} [mM]	2	0	0	2
	Pyrite	m_0/V_{stgn} [mM]	110	0	0	110
		r_0 in M/s	$1.6 \cdot 10^{-5}$	0	0	$6.5 \cdot 10^{-11}$
second. miner.	Fe(III)		$Fe(OH)_3$	$Fe(OH)_3$	$Fe(OH)_3$	$Fe(OH)_3$
	U(VI)		Soddyite	Soddyite	Soddyite	Soddyite
	U(IV)		Coffinite	UO_2(am)	UO_2(am)	UO_2(am)
pe	in stagnant zone		5			≤ 1

Uranyl Ion Exchange. As shown in the batch test with aquifer material there is – irrespective of the relatively small clay mineral content – an U(VI) adsorption on-ion exchanger sites. This reversible process is included in the calculations.

Tab. 4.3 gives an overview about all geochemical parameters used in the aquifer simulations (in comparison with the column dataset). [The advantage of using m_0/V_{stagn} rather than m_0 is that the former quantity is independent of the cell size.] The SI for Calcite is set to zero.

Dilution. Since the model space 'Flow Path' is embedded within a huge groundwater basin (see Fig. 4.3), there is an ongoing dilution caused by transversal dispersion. In particular, we use

transverse dispersivity in vertical direction $\alpha_{TV} = 1.0$ m
transverse dispersivity in horizontal direction $\alpha_{TH} = 0$

Tab. 4.4 Parameters for horizontal dispersion used in MODFLOW and TRN

Parameter	MODFLOW	TRN
vertical (transversal) dispersivity α_{TV}	2.13 m	1.0 m
vertical to horizontal permeability ratio	1 : 30	1 : 30

Of course, these parameters are not well known. Therefore, the following assumptions are made:

(i) The MODFLOW-dispersivity in Tab. 4.4 is diminished by a factor of two: $\alpha_T = 2.1 \Rightarrow 1.0$ m (worst case).

(ii) TRN considers only the *vertical* dispersion (in z-direction), but neglects the transversal dispersion in horizontal direction (worst case).

(ii) The thickness of the simulated aquifer zone 'Flow Path' is $\Delta z = 10$ m with respect to the maximum thickness of the ore zone (worst case).

(iv) The flow path is surrounded by an "infinite" groundwater reservoir (i.e. the water composition *outside* the column cells does not change during dispersion). Possible inaccuracies would be compensated by (i) to (iii).

Within the numerical model the mix factor for the transversal dispersion (between each cell and the groundwater basin) is similar to the mix factor for the longitudinal dispersion (between two adjacent cells):

(4.6) $$mix_L = \frac{\alpha_L}{\Delta x}$$

(4.7) $$mix_T = \frac{v_T}{v} \cdot \frac{\alpha_{TV}}{\Delta z}$$

The ratio v_T/v is equivalent to the ratio of vertical to horizontal permeability, i.e. 1:30 as shown in Tab. 4.4.

In particular, for a cell geometry with $\Delta x = 10$ m and $\Delta z = 10$ m we get:

(4.8) $\quad mix_L = 1.0$

(4.9) $\quad mix_T = 3.3 \cdot 10^{-3}$

It shows that the dilution effect caused by transversal dispersion is 2.5 orders of magnitude smaller than that of the longitudinal dispersion.

4.4 Transport without Reactions

In order to demonstrate the effect of dispersion and/or mobile-immobile mass transfer we consider the scenario depicted in Fig. 4.5. Four different calculations are performed:

ADV	without dispersion and dual porosity	$\alpha_L = 0$	$\alpha = 0$
DUAL	with dual porosity, but without dispersion	$\alpha_L = 0$	$\alpha = 7.5 \cdot 10^{-5}\ h^{-1}$
DISP	with dispersion, but without dual porosity	$\alpha_L = 10$ m	$\alpha = 0$
DISP + DUAL	with dispersion and with dual porosity	$\alpha_L = 2.5$ m	$\alpha = 7.5 \cdot 10^{-5}\ h^{-1}$

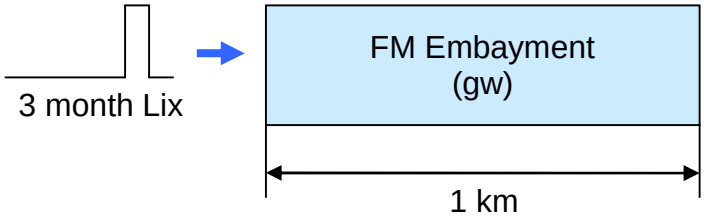

Fig. 4.5 Lix inflow (3 month) into the FM embayment followed by groundwater inflow

The start conditions are all the same: Lix (with 850 mg/L SO_4-S) enters the Four Mile Embayment for 3 month in form of a 'short pulse'. The path length is 1 000 m; the embayment is filled with groundwater. In this example *all* reactions are ignored, i.e. there is no mineral dissolution/precipitation, no ion exchange.

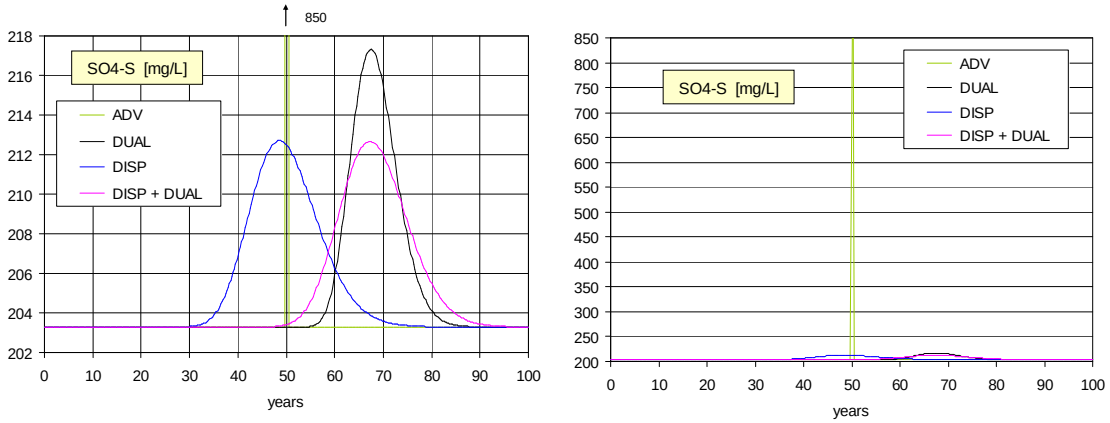

Fig. 4.6 Breakthrough of SO_4 at x = 1 000 m for different transport scenarios. (Left and right diagrams differ only in the scale of the y-axis.)

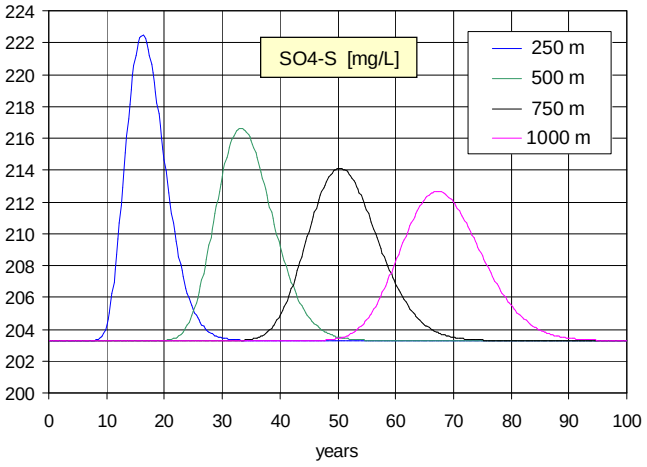

Fig. 4.7 Breakthrough of sulfate at different x positions (Scenario 'DISP + DUAL')

The results are shown in Fig. 4.6 and Fig. 4.7. The left and right diagrams of Fig. 4.6 differ by the scale of y-axis only. In full agreement with mass conservation all four curves own the same integral (i.e. the same area below the curves).

In Fig. 4.6, the green curve depicts the pure advection case (ADV) where the initial 3-month pulse passes unaltered through the aquifer; after 50 years it reaches 1 000 m (in full agreement with the flow velocity 20 m/a). If dispersion is included (DISP), the curve broadens but the centroid moves with the advection peak. Remarkable, after 1 000 m the peak reduces from 850 mg/L to 213 mg/L (i.e. only 10 mg/L above the background).

In contrast to the dispersion, the dual-porosity approach broadens *and* retards the curves (DUAL). Finally, the pink curve shows the cumulative effect (DISP + DUAL). In practice, the additional broadening within the dual porosity approach can be re-adjusted by a smaller dispersivity $\alpha_L = 2.5$ m (instead of 10 m). Please note, by the re-normalization we obtain nearly the same width and shape of the curves:

$\alpha_L = 10$ m (blue curve) $\Leftrightarrow$ $\alpha_L = 2.5$ m + dual porosity (pink curve)

Thus, in order to simulate $\alpha_L = 10$ m as listed in Tab. 4.2 we use $\alpha_L = 2.5$ m within the dual-porosity approach.

4.5 Post Mining Scenarios – Worst and Real Case

This Section summarizes the main results of the post-mining scenarios: 'Worst Case' and 'Real Case' with and without dilution (caused by transversal dispersion). There are 4 scenarios defined in Tab. 4.5; the most probable and most improbable cases are the following:

most improbable case: W_noDILU
most probable case: R_DILU

Tab. 4.5 Definition of four post-mining scenarios

Scenario		transversal dilution	solution in ore zone	solution pH in ore zone
W_noDILU	worst case	no	lix	1.7
W_DILU	worst case + dilution	yes	lix	1.7
R_noDILU	real case	no	lix_R	2.0
R_DILU	real case + dilution	yes	lix_R	2.0

The complete results are presented in Appendix D. For each scenario there are diagrams for SO_4, U, Fe, Al, Ca, Mg, Na, K, and pH as well as for all ion-exchanger species. The diagrams depict the concentration pattern along the flow path through the ore zone (x = 0 to 1 km) and FM embayment (x = 1 to 7 km) at different times (t = 0, 100, 200, 300, 400, 500 and 800 years).

The chemical elements travel at different velocities. Sulfate is neither affected by ion exchange nor by precipitation/re-dissolution, thus, it moves fast and unretarded (the same holds for chloride). All other elements (including pH) are retarded more or less strongly.

The behavior of Ca, Mg, K, Na becomes clear if we look on the cation distribution on the ion-exchanger sites. These diagrams show the adsorbed species that sum up to the total capacity $C_{TOT} = 13.5/\varepsilon = 45$ meq/L. Remarkable is the H^+ ion adsorption and how it passes gradually from the ore zone into the embayment thereby loosing weight. On the other hand, the invasion of aluminum is caused by silicate mineral dissolution (kaolinite). Due to the low ORP, uranyl adsorption is marginally and therefore not visible in the diagrams.

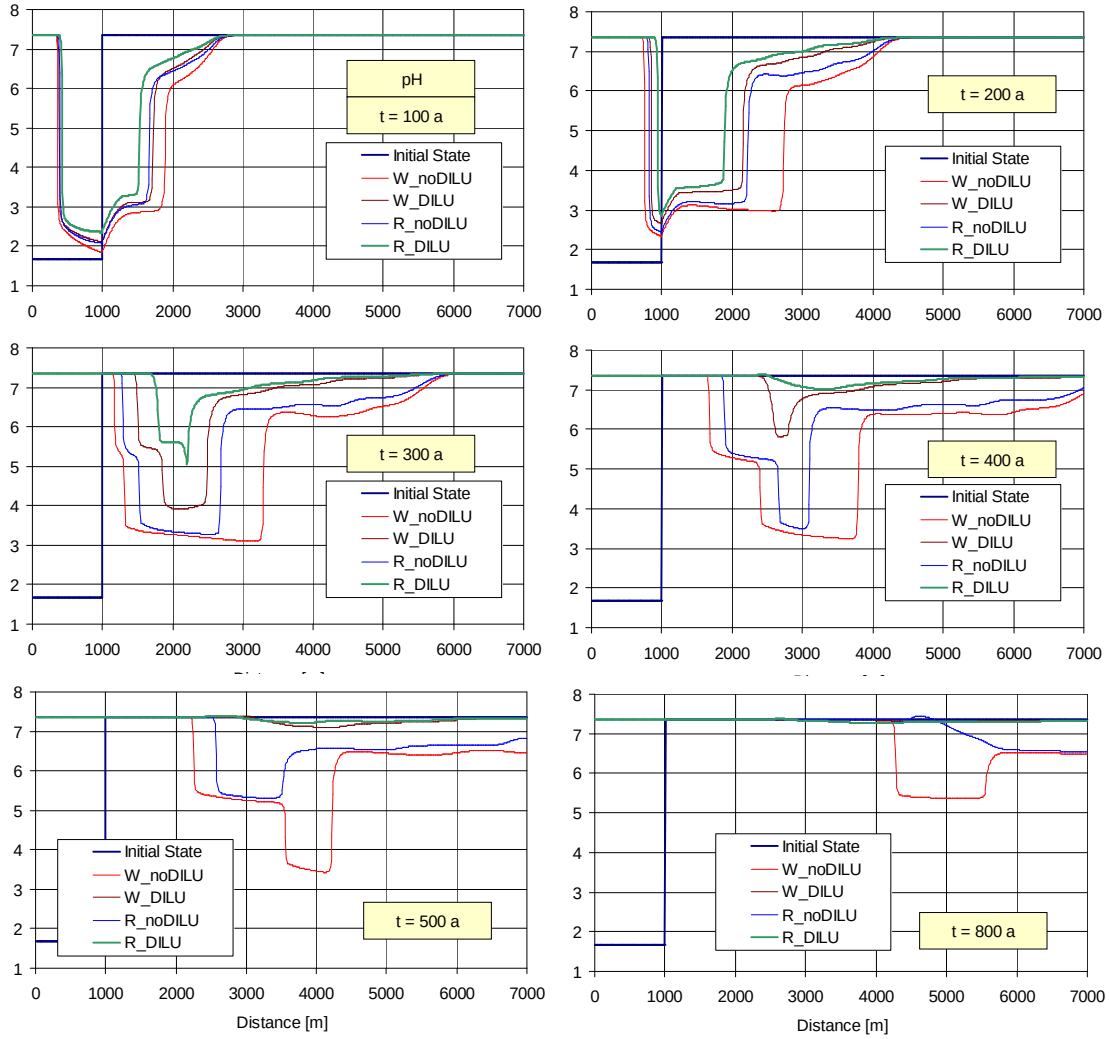

Fig. 4.8 pH as a function of distance x – comparison of different scenarios

A direct comparison of all four scenarios is presented for pH, uranium, and sulfate in Fig. 4.8 to Fig. 4.10. Here the most probable case is represented by the green curve. In all cases, the *acid* front (with pH < 6) as well as uranium never leaves the FM Embayment; their influence is confined within a maximum range of 3 to 4 km apart from the ore zone.

[*Remark.* The blue curves labeled 'Initial State' represent the pH and concentrations for the Worst Case.]

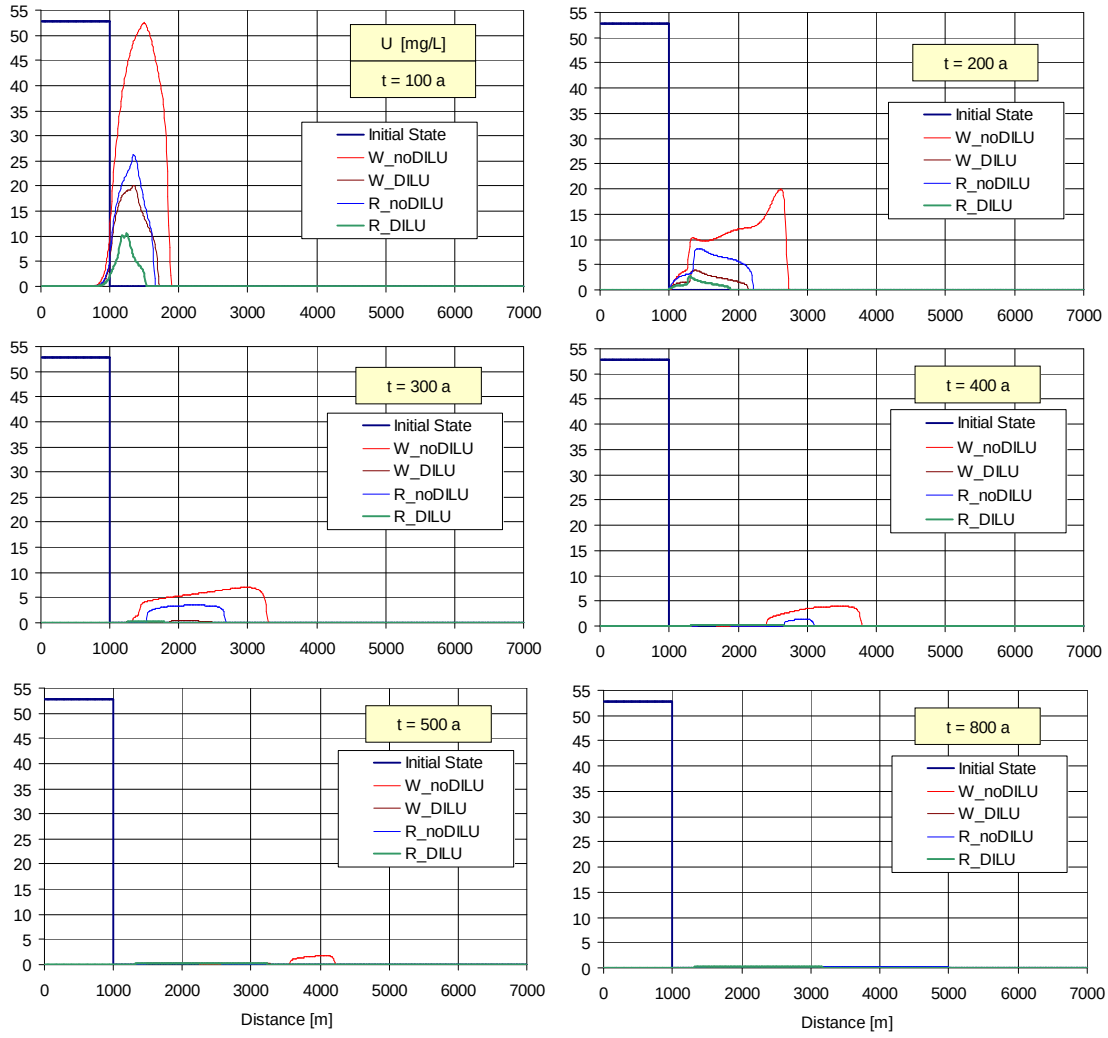

Fig. 4.9 Uranium [mg/L] as a function of distance x – comparison of different scenarios

There is a principal difference between the behavior of uranium and sulfate in Fig. 4.9 and Fig. 4.10. Sulfate is only influenced by dispersion and dilution (except a tiny gain due to pyrite oxidation); uranium is affected by dispersion, dilution, *and* U(IV) precipitation in form of amorphous UO_2 (depending on the actual pH-pe conditions). The effect of uranyl ion-exchange is small (due to the low ORP).

More details to the U geochemistry are given in Sec. 4.6. There it will be shown that the curves in Fig. 4.9 are based on conservative assumptions.

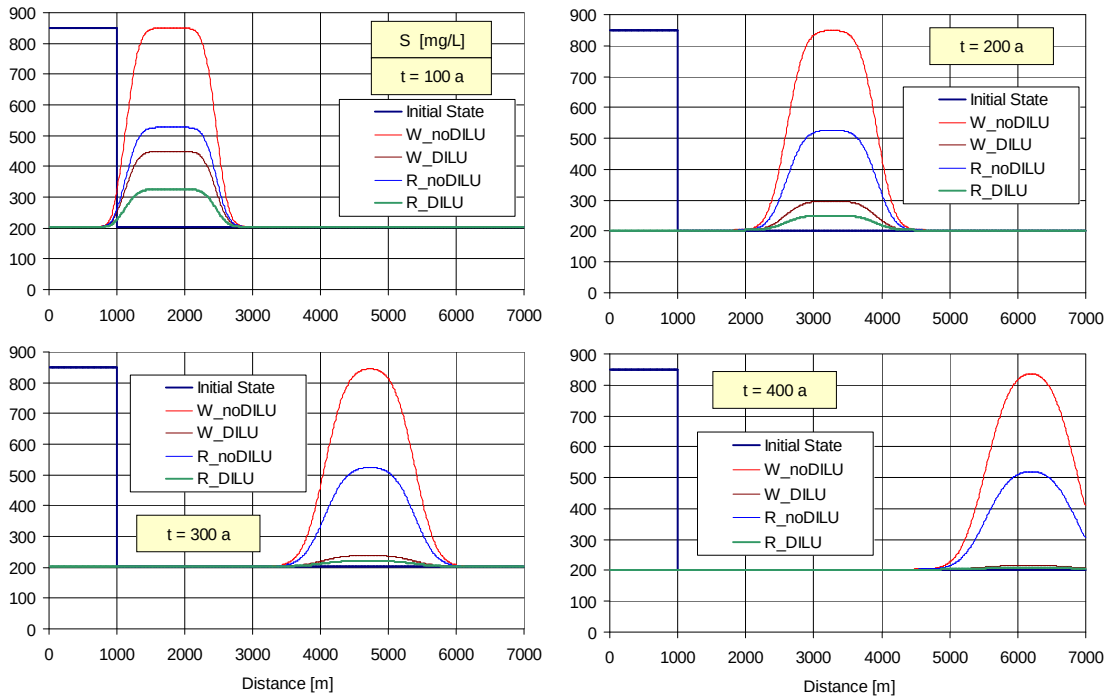

Fig. 4.10 SO_4-S [mg/L] as a function of distance x – comparison of different scenarios

4.6 Uranium Geochemistry

The fate of uranium strongly depends on the ORP. However, our knowledge of the real redox conditions inside the aquifer is limited due to several reasons: (i) The measurement and interpretation of ORP is a complex task [EPA02]; (ii) natural systems are hardly in redox equilibrium; (iii) redox processes are mediated by microorganisms. Finally, in the lab tests we obtained information about the U(VI) precipitation but not about U(IV) (because they are performed under non-reducing conditions).

In order to investigate the influence of the ORP on the U chemistry three different cases have been studied:

(i) definite ORP conditions (pe fixed at 1.0 or at -0.5)
(ii) with the U(IV) minerals: coffinite/uraninite and amorphous UO_2(a)
(iii) only with amorphous UO_2(a); no coffinite/uraninite precipitation

In case (ii) and (iii) the pe value is not fixed; it develops freely.

(i) The U chemistry was studied under *definite* ORP conditions, i.e. the pe value for the stagnant water was fixed to pe = 1 (i.e. the observed groundwater ORP in the aquifer) and to pe = -0.5. The results are displayed in Fig. 4.11. In both cases there exist a concentration peak at the boarder line between ore zone and embayment (at x = 1 km), but downstream this location (at x > 1 km) the picture differs. In the case of pe = 1 uranium precipitates as U(VI) mineral ‘soddyite’; in case of pe = -0.5 as U(IV) mineral ‘coffinite’.

In fact, for pe = 1 the main geochemistry is quite similar to that of the column tests: Fe and U precipitate as Fe(III) and U(VI) minerals and re-dissolve (thereby producing concentration peaks).

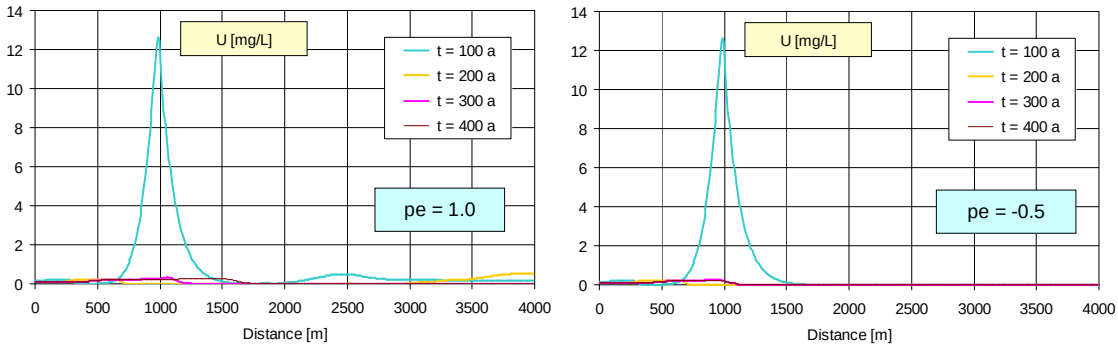

Fig. 4.11 U concentration as a function of distance x – Scenario 'Worst Case' without dilution (W_noDILU) for fixed pe values

Please note that the concentration peaks in Fig. 4.11 are much lower than in Fig. 4.9 at t = 100 a.

In conclusion, whereas for pe ≥ 1 the geochemistry behaves similar to the column tests (uranium precipitates or adsorbs in U(VI) form), the situation changes for pe ≤ -0.5 where uranium precipitates as U(IV) mineral (uraninite or coffinite). This is schematically depicted in Fig. 4.12. Between pe = -0.5 and 1 there is a 'gray' zone where the system behaves instable. Ironically, the measured ORP, which is near zero, indicates that the aquifer is in such an 'unstable' state.

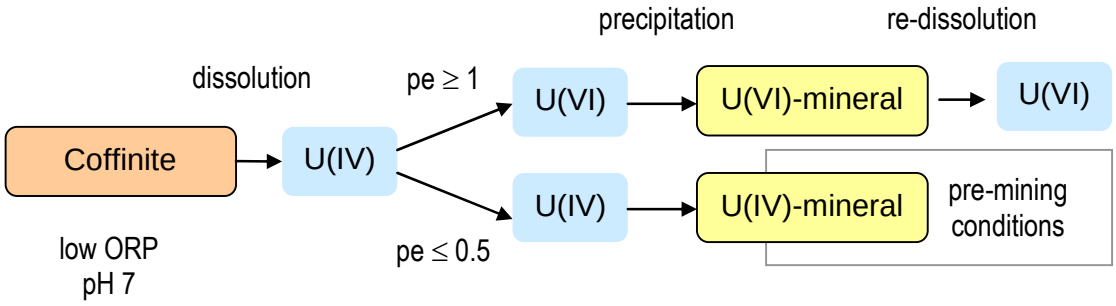

Fig. 4.12 Two different pathways of U precipitation

(ii) In case (i) above the ORP is fixed to definite pe values which maintain the measured ORP inside the aquifer. Now, we consider the case where the pe is *not* fixed but evolves freely. Then, due to the dissolution of reductive minerals (pyrite and coffinite) the ORP drops below pe = -1. Consequently, the dissolved U(VI) contained in the lixiviant transforms into the U(IV) form and precipitates immediately as coffinite or uraninite (irrespective if UO_2(am) is included in the calculations or not). This results from thermody-

namics whereby crystalline minerals are more stable than amorphous minerals. Thus, for the very worst case W_noDILU we obtain the result shown in Fig. 4.13. For the 'Real Case' nearby all dissolved uranium precipitates.

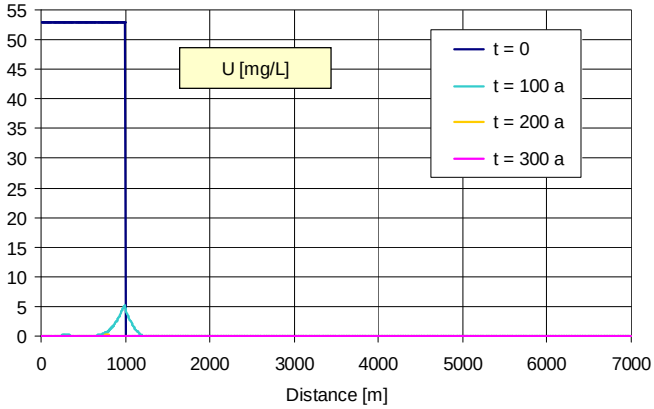

Fig. 4.13 U concentration as a function of distance x – Scenario 'Worst Case' without dilution (W_noDILU) for non-fixed pe value (U precipitates as coffinite)

(iii) The optimistic picture of case (ii) where nearby all U is mobilized in form of coffinite changes if we switch-off the precipitation of coffinite/uraninite. In this case only amorphous UO_2(a) precipitates which, however, has a higher solubility than coffinite/uraninite. For example, the log k values of both UO_2 modifications differ significantly:

Uraninite(c)	$UO_2 + 4\ H^+ = U^{+4} + 2H_2O$	log_k = -4.8
UO2(a)	$UO_2 + 4\ H^+ = U^{+4} + 2H_2O$	log_k = 0.1

Afterwards, during mineral aging the amorphous phase converts into more stable (crystalline) phases. In the end, pre-mining conditions are established where U(IV) is deposited as coffinite/uraninite. This case is considered in Sec. 4.5 and Appendix D.

There is no clear dividing line between case (ii), i.e. U precipitates as coffinite, and case (iii), i.e. U precipitates as amorphous UO_2. Thus, the calculations shown in Fig. 4.9 represent a *pessimistic* view (in contrast to the optimistic description in Fig. 4.13). The reality lies between both cases.

5 SUMMARY

The geochemical modeling within Heathgate's Natural Attenuation Project consists of two parts:

Part I:	Interpretation of Column and Batch Tests	(Chapter 2 and 3)
Part II:	Reactive Transport Simulations in FME aquifer	(Chapter 4)

Part I lays the foundations for the subsequent aquifer studies in Part II. The main goal is to understand the *principal* geochemical processes that determine the fate of uranium and other pollutants. By focusing on the *main* phenomena, we avoid interpreting (and misinterpreting) effects of higher order.

During this study, a reactive transport model was provided by UIT to describe the column tests and the geochemistry in the FM aquifer. It combines transport (advection & dispersion) with geochemistry (thermodynamics & kinetics). The chemical equilibrium module is based on PHREEQC. A detailed model/program description is given at the end of this report (Appendix A and B).

5.1 Part I – Lab Test Simulations

First. Batch and column tests are complementary. The large residence time (contact time with core material) during the batch tests allows an equilibrium approach using PHREEQC. On the other hand, the column tests, with a small residence time, are modeled with the reactive transport model TRN.

	Batch Tests	Column Tests
Residence Time	large (4 days)	small (<< 1 h)
Model	Equilibrium Model	Reactive Transport
Program	PHREEQC	TRN (incl. PHREEQC)
Results	Chapter 3	Chapter 2

All batch and column simulations are based on the *same* fundamental assumptions and model parameters (including the thermodynamic database *wateq4f*). This was achieved in a long run of single calculations and by a permanent cross-checking of the input datasets for batch and column tests.

Second. The model simulations for both batch and columns are in good agreement with the observations. They are based on a dataset with *minimum* assumptions and parameters. This makes the approach straightforward and transparent. The obtained dataset provides a firm platform for the prediction of geochemical processes in the FM aquifer (see Part II).

Third. The main geochemical transformations within the columns can be summarized as follows (see Figure below): The aggressive lixiviant enters the stagnant water zone and dissolves the *reductive* minerals pyrite and coffinite. Due to the contact with the O_2-rich mobile phase the released Fe(II) and U(IV) species are oxidized and precipitate as Fe(III) and U(VI) minerals. As a result Fe and U are immobilized, and both elements disappear in the column outflow. The immobilization occurs as far as pH > 3 ... 4. If pH drops below 3 (due to the ongoing lix inflow), the precipitation stops and all accumulated Fe(III) and U(VI) minerals re-dissolve (which generate the concentration peaks). The greater the pH buffer the more the peaks are retarded. The pH is buffered by both ion exchange and calcite dissolution.

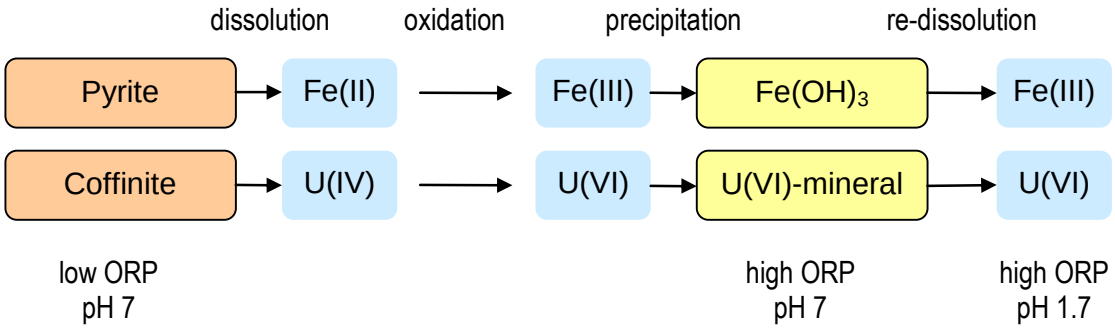

Fourth. The batch and column tests show explicitly a retardation of pH and uranium. Uranium retardation/immobilization is caused by:

- precipitation of U(VI) minerals
- uranyl ion exchange at clay minerals
- a combination of both processes

Both effects are reversible. There are several candidates for U(VI) precipitation: Becquerelite, Soddyite etc.

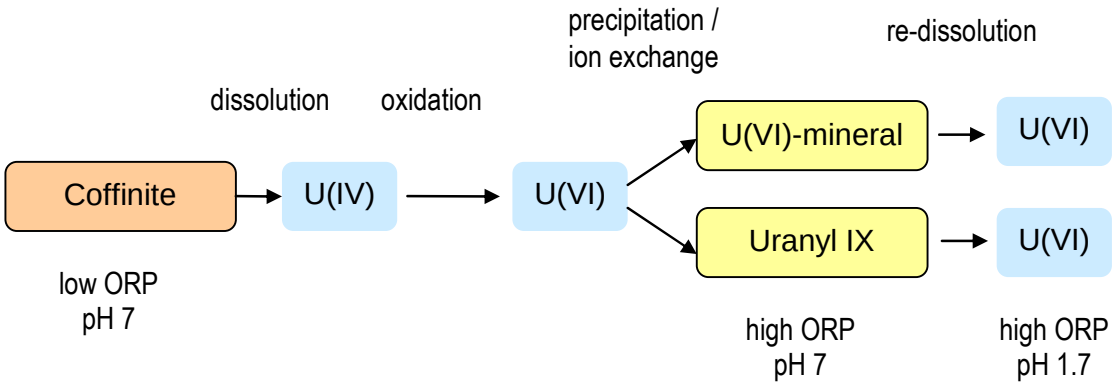

5.2 Part II – FME Aquifer Simulations

First. The aquifer simulations rest on two pillars: (i) the hydraulic parameters overtaken from the hydrogeological model [Bev08], and (ii) the geochemical data overtaken from the column and batch tests in Chapter 2 and 3. The upscaling procedure is described in Sec. 4.3 (using an optimum spatial-time discretization). The 'great step' from columns to the aquifer is characterized by a significant changeover:

Length:	1 m	⇒	7 000 m
Time:	60 h	⇒	800 years
PHREEQC calls:	12 000	⇒	5 Mio
Runtime:	160 sec	⇒	14 hours

Second. The study of post-mining scenarios represents the central part of the report. The model configuration is as follows: After mining/leaching, groundwater flows into the ore zone and pushes the dissolved inventory and contaminants from the ore zone into the clean FM Embayment. At the beginning (initial state t = 0), mobile and stagnant pores of the ore zone are filled

- with aggressive lixiviant (pH = 1.7, U = 50 ppm) 'Worst Case' or
- with diluted lixiviant (pH = 2.0, U = 25 ppm) 'Real Case'

In addition, there is an ongoing dilution along the flow path caused by transversal dispersion. Based on these assumptions four calculations are performed:

W_noDILU	Worst Case	without Dilution
W_DILU	Worst Case	with Dilution
R_noDILU	Real Case	without Dilution
R_DILU	Real Case	with Dilution

Thereby, W_noDILU represent the most improbable and R_DILU the most probable case. The results are discussed in Sec. 4.5.

In all cases, the *acid* front (with pH < 6) as well as uranium never leaves the FM Embayment; their influence is confined within a maximum range of 3 to 4 km away from the ore zone.

Third. The uranium geochemistry strongly depends on ORP. In contrast to the lab tests, which have been performed and modeled under *non*-reducing conditions ($pe \approx 5$), reducing conditions definitely exist in the aquifer ($pe \leq 1$). Thus, the aquifer simulations are performed at lower pe values. In particular, due to the dissolution of *reducing* minerals (pyrite and coffinite) pe drops below zero.

As shown in Sec. 4.6, the amount of dissolved uranium also depends on the type of U(IV) mineral that precipitate: coffinite/uraninite or amorphous UO_2. Amorphous UO_2 precipitates if and only if coffinite/uraninite is excluded. Due to the higher solubility of amorphous UO_2 the dissolved U in the aquifer is much higher. In all scenario calcula-

tions we applied the *conservative* assumption of amorphous UO_2 precipitation (rather than coffinite precipitation).

Fourth. The impact of an uncontrolled flow through fractured rocks is discussed in Appendix E. This impact is small and can be neglected.

Fifth. U.S.G.S. performed in 2007 a similar study for groundwater restoration after leaching. Our study is based on their experiences; we refined their model and applied it to a real case. A comparison of both approaches is given in Tab. 5.1.

Tab. 5.1 Model comparison with the U.S.G.S study from 2007 [DC07]

	U.S.G.S report [DC07]	present report
ISL chemistry	alkaline leaching	acid leaching
Model	1D reactive transport	1D reactive transport
Program	PHREEQC	TRN (incl. PHREEQC)
Approach	thermodynamic	thermodynamic + kinetic
Dual Porosity	yes	yes
Scenarios	post mining	post mining
Model Space	ore zone (100 m)	ore zone (1000 m) plus embayment (7000 m)
Number of Cells	5	733
Time step Δt	20 years	0.5 years
Forecast	$\leq$ 400 years	800 years
Lab Tests	none	batch and column tests

Sixth. The instrument and methodology developed in this study enables us to describe geochemical processes in the FM aquifer. On this fundament in combination with extended knowledge about the real aquifer conditions (observations, experimental data) new investigations can be done easily and the forecast can be refined.

6 REFERENCES

[AN07] ANSTO Minerals, Report (Draft), Characterisation of Four Mile PROJECT AREA Cores, Nov. 2007

[AN08] ANSTO Minerals, Preliminary data to column experiments for Four Miles, 2008 (unpublished)

[AP93] Appelo C.A.J., D. Postma: Geochemistry, Groundwater and Pollution, A.A. Balkema, Rotterdam 1993

[AS02] Ander, L., B. Smith: The health hazards of depleted uranium munitions, part II. Annexe F, The Royal Society, March 2002

[Bro01] Brooks, S.C.: Waste characteristics of the former S-3 ponds and outline of uranium chemistry relevant to Nabir Field Research Center studies, Report to U.S. DOE, 2001

[BSH03] Bostick, W.D., R.J. Stevenson, L.A. Harris, D. Peery, J.R. Hall, J.L. Shoemaker, R.J. Jarabek, E.B. Munday: Use of apatite for chemical stabilization of subsurface contaminants, Report to U.S. DOE, 2003

[BST96] Bingham, J.M., U. Schwertmann, S.J. Traina, R.L. Winland, M. Wolf: Schwertmannite and the chemical modelling of iron in acid sulfate waters, Geochimica Cosmochimica Acta, 60, 2111-2121 (1996)

[CBL04] Chrisholm-Brause, C.J., J.M. Berg, K.M. Little, R.A. Matzner, D.E. Morris: Uranyl sorption by smectites: spectroscopic assessment of thermodynamic modeling, Journal of Colloid and Interface Science, 277, 366-382 (2004)

[DC07] Davis, J.A., G.P. Curtis: Consideration of geochemical Issues in Groundwater Restoration at Uranium In-Situ Leach Mining Facilities, NUREG/CR-C870, U.S.G.S. Jan. 2007

[DS97] Domenico P.A., F.W. Schwartz: Physical and Chemical Hydrogeology, John Wiley & Sons, Inc. New York 1997

[EPA02] Workshop on Monitoring Oxidation-Reduction Processes for Ground-Water Restoration, Dallas, Texas – April 2000, EPA/600/R-02/002 Jan 2002

[GL07] Gorman-Lewis, D.J., L. Mazeina, B. Fein Jeremy, J. Szymanowski, P.C. Burns, A. Navrotsky, J. Chem. Thermodyn. 39 (2007) 568–575

[GL08] Gorman-Lewis, D.J., Jeremy B. Fein, P.C. Burns , J.E.S. Szymanowski, J. Converse, J. Chem. Thermodyn. 40 (2008) 980–990

[HGR08] Beverly Mine Report: Flow and solute transport modelling of migration of mining fluids from the proposed Four Mile East mining zone, B. Jeuken, Heathgate Resources, Sep 2008

[HRD02] Hennig C., T. Reich, R. Dähn, A.M. Scheidegger: Structure of uranium sorption complexes at montmorillonite edge sites, Radiochim. Acta, 90, 653-657 (2002)

[KXP04] Krestou, A., A. Xenidis, D. Panias: Mechanism of aqueous uranium(VI) uptake by hydroxyapatite, Minerals Engineering, 17, 373-381 (2004)

[MSO07] Manaka, M., Y. Seki, K. Okuzawa, H. Kamioka, Y. Watanabe: Natural attenuation of dissolved uranium within a small stream of central Japan, Limnology, 8, 143-153 (2007)

[MZS95] McKinley, J.P., J.M. Zachara, S.C. Smith, G.D. Turner: The influence of uranyl hydrolysis and multiple site-binding reactions on adsorption of U(VI) to montmorillonite, Clays and Clay Minerals, 43, 586-598 (1995)

[Num03] Press W.H., S.A. Teukolsky, W.T. Vetterling, B.P. Flannery: Numerical Recipies in C++ – The Art of Scientific Computing, Second Edition, Cambridge University Press, 2003

[PA99] Parkhurst David L, C.A.J Appelo: User's guide to PHREEQC (version 2) – a computer program for speciation, batch-reaction, one-dimensional transport, and inverse geochemical calculations, Water-Resources Investigation Report 99-4259, Denver, Colorado 1999

[SS92] Scheffer, F., P. Schachtschabel: Lehrbuch der Bodenkunde, 13. Edition, Stuttgart, Enke Verlag, 1992

[VG85] Van Genuchgten, M.Th.: A general approach for modeling solute transport in structured soils, IAH Memoirs, v. 17, 513-526, 1985

[WR94] Williamson, M.A., J.D. Rimstidt: The kinetics and electrochemical rate-determining step of aqueous pyrite oxidation, Geochimica et Cosmochimica Acta, v. 58, 5443-5454, 1994

Appendix

A REACTIVE TRANSPORT – MAIN EQUATIONS

A.1 Definition of the System

A.1.1 Aqueous and Mineral Phases

The reactive transport model combines transport with reactions (chemical equilibrium and kinetics). The reaction module describes the mass transfer of species i between several phases:

(A.1)	mobile water:	$m_i^W = c_i^W \cdot V_W$
(A.2)	stagnant water:	$m_i^P = c_i^P \cdot V_P$
(A.3)	secondary minerals:	m_i^S
(A.4)	ion exchange:	m_i^Y
(A.5)	primary minerals:	m_i^R

Here, m_i denotes the mass (amount in moles), c_i the concentration (in mol/L), and V the water volume.

The distinction between two water phases (mobile and stagnant) is a key feature of the so-called 'dual-porosity approach'. The mass transfer between all phases is depicted in Fig. A.1. (For orientation, Fig. A.2 shows the stagnant and mobile water phases between mineral grains.)

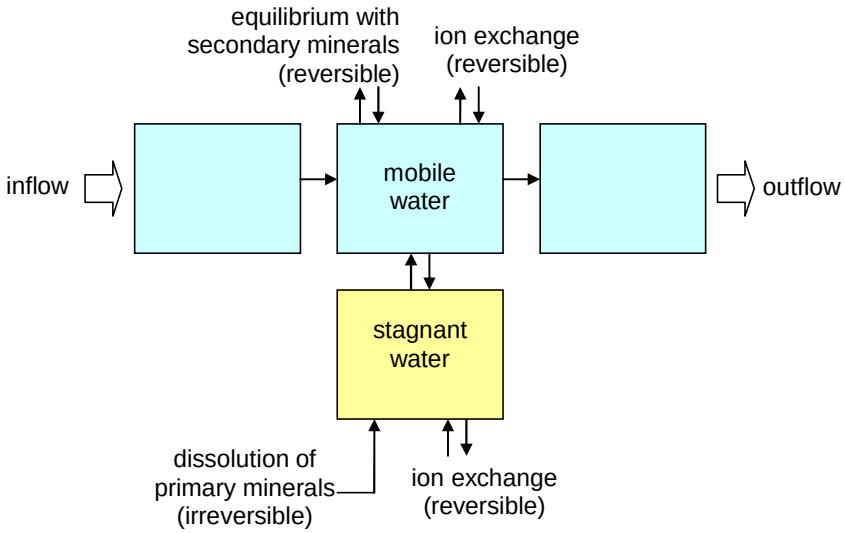

Fig. A.1 Interplay of all processes within one cell of a 1D-column (dual porosity approach)

The reversible reactions (mineral phase equilibrium and ion exchange) are calculated by the thermodynamical code PHREEQC [PA99]; irreversible reactions (mineral dissolution) are based on a kinetic approach.

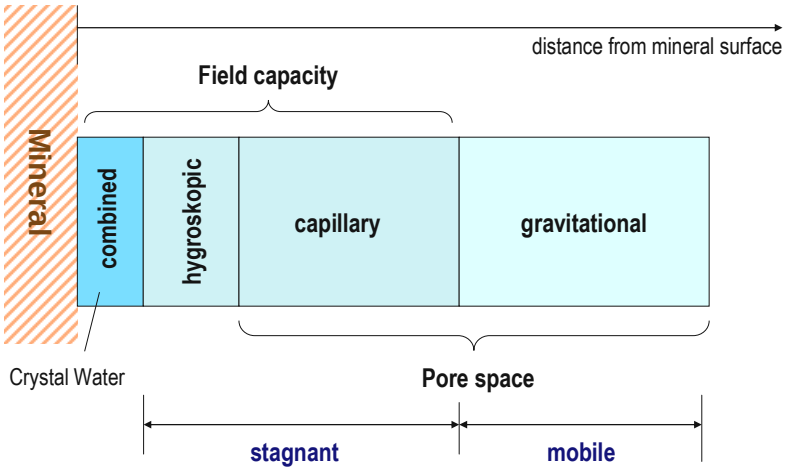

Fig. A.2 Stagnant and mobile water phases between mineral grains

A.1.2 Main Equations

Dual Porosity. The complete system for the dual-porosity approach is described by a set of differential equations (stoichiometric coefficients are not written):

(A.6) $$\frac{\partial m_i^W}{\partial t} = -v\frac{\partial m_i^W}{\partial x} + D_L\frac{\partial^2 m_i^W}{\partial x^2} + \alpha V_P(c_i^P - c_i^W) - J_{W\leftrightarrow S}$$

(A.7) $$\frac{dm_i^P}{dt} = -\alpha V_P(c_i^P - c_i^W) - J_{P\leftrightarrow Y} + J_{reac}$$

(A.8) $$\frac{dm_i^S}{dt} = J_{W\leftrightarrow S} \qquad \text{(thermodynamic model)}$$

(A.9) $$\frac{dm_i^X}{dt} = J_{P\leftrightarrow Y} \qquad \text{(thermodynamic model)}$$

(A.10) $$\frac{dm_i^R}{dt} = -J_{reac} \qquad \text{(kinetic model)}$$

To keep the notation simple all stoichiometric coefficients are omitted here. The first two terms in Eq. (A.6) describe advection (with velocity v) and dispersion (with the longitudinal dispersion coefficient D_L). The exchange between both water phases is controlled by the rate α (third term). The 'rates' $J_{w\leftrightarrow S}$ and $J_{w\leftrightarrow S}$ symbolize the precipitation/dissolution of secondary minerals and the ion exchange; both are calculated by PHREEQC. Finally, for the primary mineral dissolution rate J_{reac} several kinetic approaches are possible, for example:

(A.11) $$J_{reac} = r\cdot\left(\frac{m}{m_0}\right) \qquad \text{(first-order kinetics)}$$

(A.12) $$J_{reac} = r\cdot\left(\frac{m}{m_0}\right)\cdot\left(1-10^{SI}\right)$$

(A.13) $$J_{reac} = r \cdot \left(\frac{m}{m_0}\right) \cdot 10^{-b \cdot pH} \cdot \left(1 - 10^{SI}\right) \qquad \text{(mixed-order kinetics)}$$

Single Porosity. In case of the single-porosity approach the above set of differential equations reduces to:

(A.14) $$\frac{\partial m_i^W}{\partial t} = -v\frac{\partial m_i^W}{\partial x} + D_L \frac{\partial^2 m_i^W}{\partial x^2} - J_{W\leftrightarrow S} - J_{W\leftrightarrow X} + J_{reac}$$

(A.15) $$\frac{dm_i^S}{dt} = J_{W\leftrightarrow S} \qquad \text{(thermodynamic model)}$$

(A.16) $$\frac{dm_i^X}{dt} = J_{W\leftrightarrow Y} \qquad \text{(thermodynamic model)}$$

(A.17) $$\frac{dm_i^R}{dt} = -J_{reac} \qquad \text{(kinetic model)}$$

A.2 Transport Phenomena

A.2.1 Advection in a Homogeneous System

For systems with fluid motion, mass transport is due to both advection and hydrodynamic dispersion, which are described by the first two terms in Eq. (A.6). The advection-dispersion equation,

(A.18) $$\frac{\partial c_i}{\partial t} = -v\frac{\partial c_i}{\partial x} + D_L \frac{\partial^2 c_i}{\partial x^2}$$

is the workhorse for modelling studies in groundwater contamination [DS97].

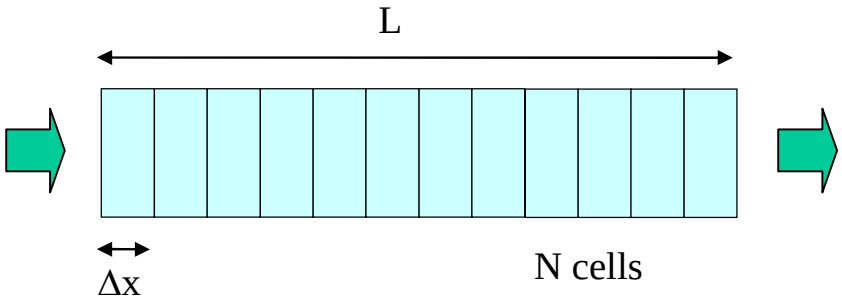

Fig. A.3 Discretization of an homogeneous 1D-system into N cells

Homogeneous System. To discuss the advection we consider a homogeneous 1D-system of total length L, cross section A, and porosity ε. According to a spatial discretization the system will be decomposed into N cells of equidistant length Δx (see Fig. A.3), whereas

(A.19) $$\Delta x = \frac{L}{N} \qquad \text{(cell length)}$$

In the homogeneous system all cells have the same pore volume

(A.20) $$\Delta V_{pore} = \varepsilon A \cdot \Delta x$$

Given the volumetric flow Q as the constant inflow rate, the timestep width can be determined by

(A.21) $$\Delta t = \frac{\Delta V_{pore}}{Q} = \frac{\varepsilon A\, \Delta x}{Q}$$

The relation between pore velocity v and inflow rate Q is given as

(A.22) $$v = \frac{Q}{\varepsilon A} = \frac{\Delta x}{\Delta t}$$

Using this relationship between time and distance discretization, $\Delta t = \Delta x/v$, numerical dispersion is minimized [AP93]. This is a great advantage of the applied procedure. Thus, in case of pure advection we simply move along, pouring at every time step concentrations from one cell into the next one. Fronts move neatly and remain sharp. Such sharpness is blurred when front transfer and grid boundaries do not correspond (i.e. when $\Delta t \neq \Delta x/v$). In this case the mixing of old and new concentrations in a cell leads to gradual smoothening of transitions (which is called *numerical* dispersion). In conclusion, applying rigorously Eq. (A.22) our model becomes free of numerical dispersion. (A quite similar approach is used in the advection procedure of PHREEQC [PA99].)

A.2.2 Advection in a Heterogeneous System

In practice, the mass transport takes place in heterogeneous systems where the water flow transverse several layers (for example a passage from sandy aquifers to dense sediments or such like). To account for this situation the system will be decomposed in several homogeneous 1D-compartments (layers). Each compartment K is again divided into N_K cells. For example, Fig. A.4 shows an inhomogeneous system decomposed in three homogeneous compartments (layers). The number of layers in the model is unlimited.

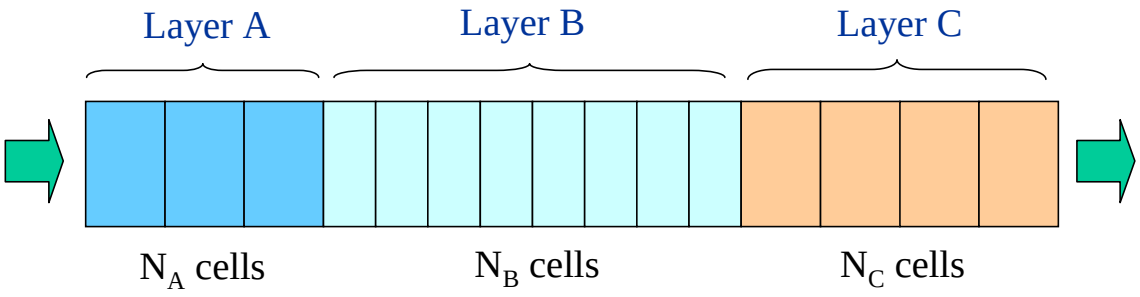

Fig. A.4 Decomposition of an inhomogeneous system into three homogeneous compartments (layers)

To employ the advantages of the model described in Sec. A.2.1 (i.e. a model without numerical dispersion), the cell structure of the compartments should fulfill the condition that all cells in the system have the same pore volume:

(A.23) $$\Delta V_P = \text{ const } = \varepsilon_A A\, \Delta x_A = \varepsilon_B A\, \Delta x_B = ...$$

Thus, given a constant inflow rate Q, at every time step

(A.24) $$\Delta t = \frac{\Delta V_P}{Q} = \frac{\varepsilon A_K \Delta x_K}{Q} = \text{const} \qquad \text{(for all layers K)}$$

the pore volume ΔV_P of cell n is shifted entirely to the next cell n+1. A consequence of Eq. (A.23) is that due to the different porosities ε, cells of different layers have different cell lengths Δx. Further on, whereas Q is constant in the whole system the pore velocity v differs from layer to layer:

(A.25) $$v_K = \frac{Q}{\varepsilon_K A} = \frac{\Delta x_K}{\Delta t} \neq \text{const}$$

The total number of cells of an heterogeneous system is

(A.26) $$N = N_A + N_B + ... = \frac{L_A}{\Delta x_A} + \frac{L_B}{\Delta x_B} + ...$$

A.2.3 Dispersion

The coefficient of hydrodynamic dispersion, D_L, incorporates the combined effects of diffusion and mechanical dispersion

(A.27) $$D_L = D_e + \alpha_L v$$

Dispersivity α_L represents the spreading of a solute over a given length of flow, and therefore, it has the unit of length. If we have no water flow, v = 0, mechanical dispersion vanishes, i.e., the hydrodynamic dispersion reduces to diffusion, $D_L = D_e$.

The process of molecular diffusion is slower in porous media than in open water because ions must follow more tortuous flow path [DS97]. To account for this an effective molecular diffusion coefficient is used

(A.28) $$D_e = wD = \frac{D}{\tau} \qquad \text{with} \qquad w = 0.01 ... 0.5$$

Here, the meaning of the symbols is:

D_L	hydrodynamic dispersion coefficient	$[L^2/T]$
D_e	effective diffusion coefficient	$[L^2/T]$

D	molecular diffusion coefficient	$[L^2/T]$
α_L	longitudinal dispersivity	[L]
w	empirical coefficient	[1]
τ	tortuousity	[1]

The usual assumption is that the pore velocity v and the dispersion coefficient are equal for all solute species, so that c can be the total dissolved concentration for an element, including all redox species.

Numerics. Numerical instabilities (oscillations) in the calculation of dispersion are eliminated with the constraint [PA99]:

$$\Delta t_D \le \frac{\Delta x}{3D_L} \qquad \text{(dispersion time step)} \tag{A.29}$$

This quantity should be compared with the advection time step defined in Sec. A.2.1:

$$\Delta t = \frac{\Delta x}{v} \qquad \text{(advection time step)} \tag{A.30}$$

The meaning of Eq. (A.29) is explained easily: Dispersive transport is essentially mixing of cells. The restriction is that never more is mixed out of a cell than stays behind. Thus, if Δt_D is n_D times smaller than Δt, i.e.

$$\Delta t_D = \frac{\Delta t}{n_D} \tag{A.31}$$

Then, the model will perform automatically n mixes at every time step Δt.

A.2.4 Numerical Model versus Analytical Solution

We consider the general expression of a transport equation with retardation (due to sorption) and first-order kinetics

$$R\frac{\partial c}{\partial t} = -v\frac{\partial c}{\partial x} + D\frac{\partial^2 c}{\partial x^2} - \lambda c \tag{A.32}$$

where the retardation factor is defined as

$$R = 1 + \frac{\rho_b}{\varepsilon} K_d \tag{A.33}$$

The initial and boundary conditions are given by

$$\begin{aligned} c &= 0 \quad \text{for} \quad t = 0, \quad x > 0 \\ c &= c_0 \quad \text{for} \quad x = 0, \quad t > 0 \\ c &= 0 \quad \text{for} \quad x = \infty, \quad t > 0 \end{aligned} \tag{A.34}$$

The initial condition (first line) states that at all points have at time t = 0 zero concentration. The first boundary condition (second line) states that at x = 0, for all time t, the concentration is c_0 (that is, a continuous source). The analytical solution is:

$$c(x,t) = \frac{c_0}{2}\left\{ \exp\frac{x(v-w)}{2D}\cdot \operatorname{erfc}\frac{Rx-wt}{\sqrt{4DRt}} + \exp\frac{x(v+w)}{2D}\cdot \operatorname{erfc}\frac{Rx+wt}{\sqrt{4DRt}}\right\} \quad \text{(A.35)}$$

with the abbreviation

$$w = \sqrt{v^2 + 4DR\lambda} \quad \text{(A.36)}$$

and the complementary error function

$$\operatorname{erfc} x = \frac{2}{\sqrt{\pi}} \int_x^\infty \exp(-t^2)\, dt \quad \text{(A.37)}$$

If there is no retardation, R = 0, and no degradation, λ = 0, we have w = v. In this special case Eq. (A.35) reduces to the so-called Ogata-Banks equation:

$$c(x,t) = \frac{c_0}{2}\left\{ \operatorname{erfc}\frac{x-vt}{\sqrt{4Dt}} + \exp\frac{xv}{D}\cdot \operatorname{erfc}\frac{x+vt}{\sqrt{4Dt}}\right\} \quad \text{(A.38)}$$

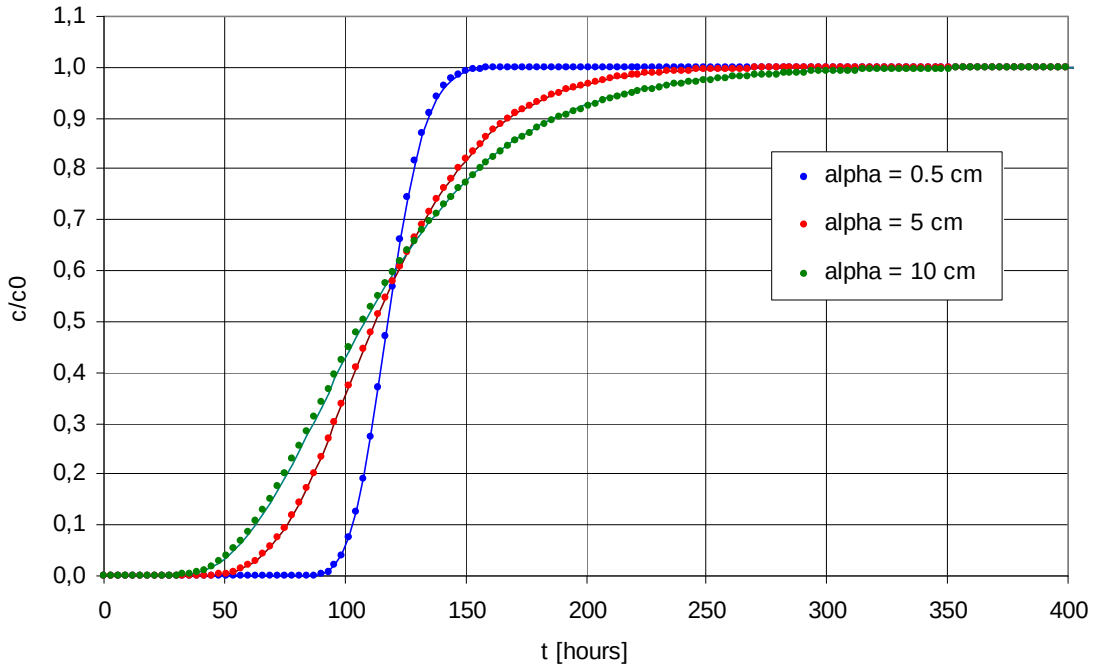

Fig. A.5 Comparison of the numerical model (circles) with analytical solutions (lines) for three dispersivities α_L

Numerical Test. An analytical solution of the ADR equation exists only for some special cases (like homogeneous flow tube, no higher order kinetics etc.), and where the initial and boundary conditions defined in Eq. (A.34) are valid. In the following, we consider 3 special cases of an 1-dimensional plug flow:

A	transport with small dispersion	α_L = 0.005 m
B	transport with medium dispersion	α_L = 0.05 m
C	transport with large dispersion	α_L = 0.10 m

The size of the flow tube and all other parameters are the same for all 3 cases:

total length	L = 1.0 m
number of cells	N = 40
cell length	$\Delta x = L/N$ = 0.025 m
porosity	ε = 0.2
flow velocity	v = 0.2 m/day
time step	$\Delta t = \Delta x/v$ = 3 h

For example, if the flow tube or column has a diameter of d = 42 mm, the cross section area is $A = (\pi/4)d^2 = 1.38 \cdot 10^{-3}$ m^2. This correspond to a

total pore volume	$V_P = \varepsilon AL$	$= 2.76 \cdot 10^{-5}$ m^3
pore volume of a cell	$\Delta V_P = V_P/N$	$= 0.69 \cdot 10^{-6}$ m^3
volumetric flux	$Q = \Delta V_P/\Delta t$	= 0.23 mL/h

The time span for a total pore volume exchange is $T_P = V_P/Q$ = 120 h. The simulation time will be t_E = 400 h which correspond to 3.33 pore volume exchanges.

The comparison between the numerical model (described below) and the analytical solution, i.e. Eq. (A.35), is shown in Fig. A.5. In all 3 cases the numerical model fits the exact solution.

A.3 Operator Splitting Method

Translating the reactive transport phenomena into equations is half the art; solving them the other. As mentioned above, the partial differential equations (PDE) introduced in Sec. A.1.2 can not be solved analytically. Numerical methods like ‘operator splitting’ [Num03] are appropriate.

The structure of the basic advection-dispersion-reaction equation (ADR) can be written in the operator form

$$\frac{\partial c}{\partial t} = \Phi\, c \qquad \text{with} \qquad \Phi = \Phi_{adv} + \Phi_{disp} + \Phi_{reac} \tag{A.39}$$

Here, the operator Φ is a sum of three parts (advection, dispersion, reaction). According to [Num03] these partial differential equations will be solved using the operator splitting method (also known as the method of fractional steps).

For each part we use a special differencing scheme ($\tilde{\Phi}_{adv}, \tilde{\Phi}_{disp}, \tilde{\Phi}_{reac}$), for updating the variable c from time step n to time step n+1, valid if the piece of the operator were the only one on the right-hand side of Eq. (A.39). Symbolically, we have the following sequence of updatings:

$$\left.\begin{aligned} c^{n+1/3} &= \tilde{\Phi}_{adv}(c^{n}, \Delta t) && \text{(A.40)} \\ c^{n+2/3} &= \tilde{\Phi}_{disp}(c^{n+1/3}, \Delta t) && \text{(A.41)} \\ c^{n+3/3} &= \tilde{\Phi}_{sorp}(c^{n+2/3}, \Delta t) && \text{(A.42)} \end{aligned}\right\} \; c^{n} \rightarrow c^{n+1}$$

With each time step, first advective transport is calculated, followed by dispersive transport and reactions. Equilibrium controlled chemical reactions are calculated by calling PHREEQC (this code is incorporated as a subroutine in the model).

B PROGRAM DESCRIPTION

B.1 Short Overview

The mathematical and numerical model defined in the previous Chapters was the basis for the programming. The software was written in the object oriented programming (OOP) language C++. The program consists of a clearly arranged user interface (see Fig. B.1) as well as visualization tools which present all results in form of diagrams and tables (see Fig. B.3). During runtime the dynamics can be observed by online graphics (see Fig. B.2).

Software Design. In the philosophy of OOP, the model was build with a modular design that consists of a main program and "packages". The packages are groups of independent subroutines that carry out specific simulation tasks such as transport, dispersion, sorption, kinetics, and chemical equilibrium calculations with PHREEQC. This modular design is useful in several ways. It provides a logical basis for organizing the actual code with similar program elements or functions grouped together. Such a structure facilitates the integration of new packages to enhance the code's capabilities.

Code Capabilities. There are several issues in which the program differs from other existing reactive transport models. One of them is the special treatment of transport phenomena (advection without numerical dispersion, dispersion with interlacing time steps etc.).

Another advantage is the direct link between transport and hydrochemistry due to the inclusion of PHREEQC code with its huge thermodynamic database. This allows the consistent calculation of pH, of CO_2 equilibrium with HCO_3^- and CO_3^{-2} and, especially, the tricky redox reactions. In general, PHREEQC allows much more:

- the number of anions and cations in aqueous solutions is unlimited
- the number of mineral phases is unlimited (in any case we can extend the database)
- complexation and speciation using activity models (DEBEY-HÜCKEL etc.)
- equilibrium with mineral phases (precipitation and dissolution)
- equilibrium with gas phases (open and closed systems)
- ion exchange

Finally, the numerical model will be embedded in a comfortable graphical user interface (GUI). The model data (input and output) will be displayed in various diagrams and tables. The offline graphic allows the direct comparison of different runs (scenarios).

Mass Balance. During computation mass balance is checked in each timestep.

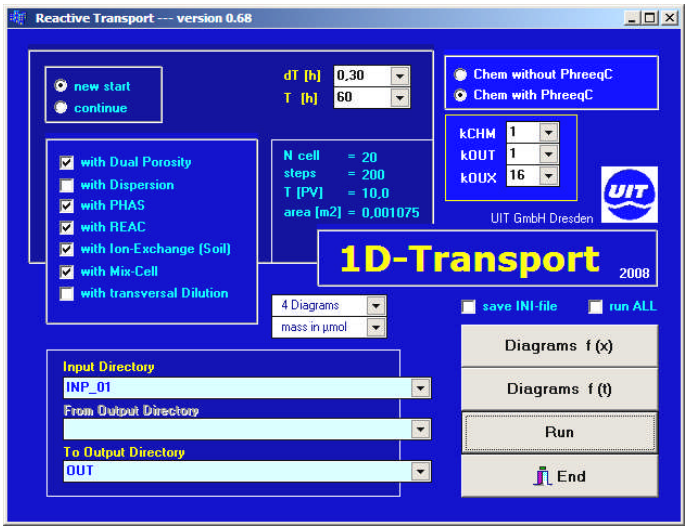

Fig. B.1 Start window of the Reactive Transport Model

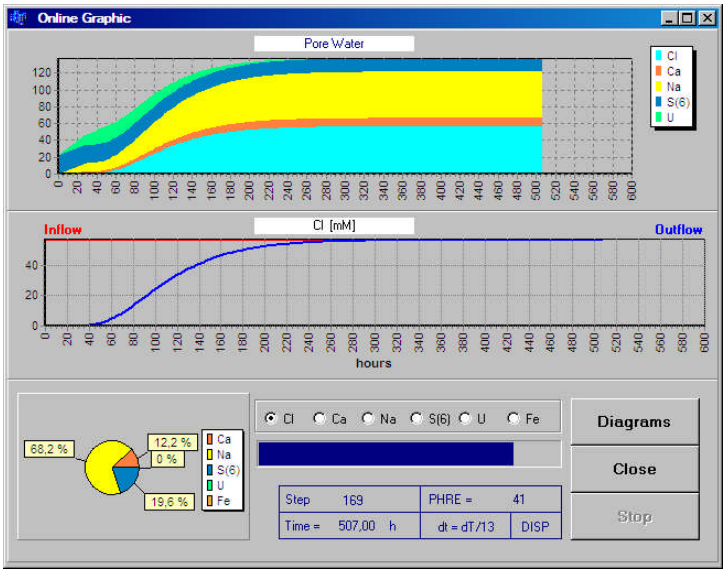

Fig. B.2 Online-graphic showing the inflow and outflow concentrations

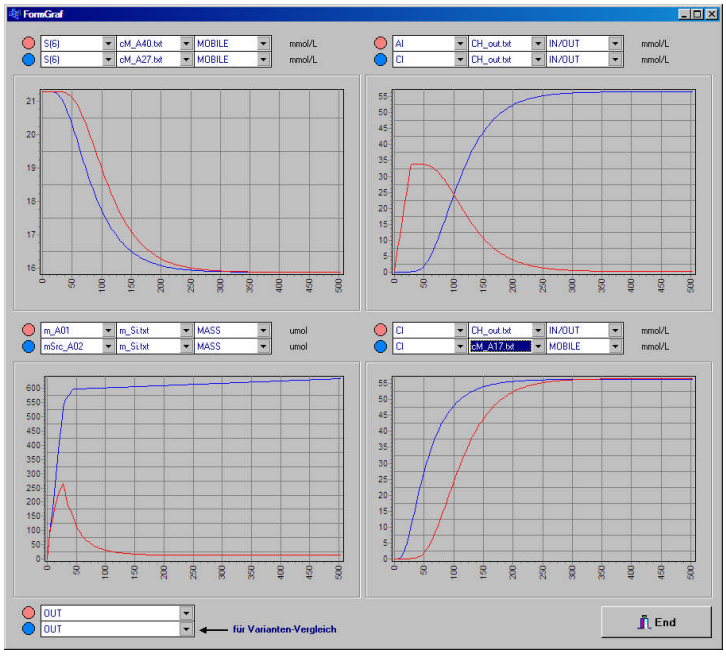

Fig. B.3 The complete output is visualized in diagrams

B.2 General File Structure

B.2.1 Root Directory and Executable Code

The root directory contains the executable code, several dynamical link libraries (dll's) and packages (bpl's). The main files to run

`trn.exe`	executable code
`start.dat`	text file containing the initial input-directory paths
`p211.dll`	dynamical link library that includes PHREEQC
`wateq4f.dat`	thermodynamic database for PHREEQC

After program installation, the first run creates other auxiliary files within the root directory (for diagnostic purposes only – see Sect. B.2.2). These files will be automatically overwritten when a new calculation starts.

Input Directory. The directory INPUT contains the input data for one or more scenarios. The complete data and input files necessary for one calculation (scenario) are stored in a single subdirectory, for example:

INP_01	(for scenario 1)
INP_A3	(for scenario A3)
INP_TEST_03	(for test calculation 03)

The name of the input directory should begin with the characters '`INP_`'; all subsequent characters are arbitrary. The general structure of an input directory is described in Sec. B.2.3.

Output Directory. The complete output of one calculation/scenario will be written into one separate directory, for example:

OUT_01_var_C
OUT_A3
OUT_TEST_03_CC …

You can choose any name for the output directory. It should begin with the characters '`OUT_`'; all subsequent characters are arbitrary. The general structure of the output directory is described in Sec. B.4.

B.2.2 Files in the Root Directory

There are several files in the root directory. Most of them are files that are created during a program run (so called tmp-files). The only text files that are necessary to start the program are `start.dat` and `wateq4f.dat`.

start.dat. The text file `start.dat` is used for presetting the input and output directories at program start. It contains two lines. The first line which begins with the keyword `DIR_INP` defines the input directory; the second line which begins with the keyword

DIR_OUT defines the output directory. The chosen directories should be set in quotation marks. For example:

```
DIR_INP   "INP_02"
DIR_OUT   "OUT"
```

The user can *change* the pre-selected input and/or output directory also in the main window of the graphical user-interface (GUI).

Temporary Files. During the calculation several temporary files are written into the root directory. These files are used for checking the program and input data files. Some of these files are:

para.tmp	contains the global and control parameters defined in trn.ini
resul.tmp	contains all information to continue calculations after an interrupt
phre	actual PHREEQC input file (is overwritten in each PHREEQC call)
phre.txt	actual PHREEQC output file (is overwritten in each PHREEQC call)
*.phr	PHREEQC input files selected with PHRE_SHOW in trn.ini

All temporary files will be automatically deleted when a new computation starts.

B.2.3 Input Directory INP_*

All relevant information to run the reactive transport is contained in one input directory INP_* (located in the INPUT directory). In general, several such input directories (for each scenario one) can exist. The directory INP_* contains one subdirectory CHM and 8 text files:

CHM	subdirectory for aqueous solutions and kinetic data	
trn.ini	defines the global parameters	see Sec. B.3.1
box.dat	defines cell data	see Sec. B.3.2
qIn.dat	defines inflow solutions	see Sec. B.3.3
elem.dat	defines chemical elements	see Sec. B.3.4
ions.dat	defines ions and complexes	see Sec. B.3.4
secm.dat	defines secondary minerals	see Sec. B.3.4
exch.dat	defines ion-exchange species	see Sec. B.3.4
reac.dat	defines reactive materials	see Sec. B.3.4

The subdirectory CHM contains files which define the aqueous solutions of pore and inflow waters as well as kinetic data files. At least there are four files in subdirectory CHM, for example:

cell.sol	defines the mobile water solution at t = 0	see Sec. B.3.5
celW.sol	defines the pore water solution at t = 0	see Sec. B.3.5
inp.sol	defines the inflow water solution	see Sec. B.3.5
pMin.dat	defines reaction rates and kinetic data	see Sec. B.3.6

In general, for any cell a separate mobile or pore water: `cell_A.sol`, `cell_B.sol` etc can be assigned. The assignment between cell number and pore water composition is defined in file `box.dat` (see Sec. B.3.2).

Similarly, the inflow water composition can change from time step to time step. The assignment between a given time period and an inflow water composition is defined in file `qIn.dat` (see Sec. B.3.3).

B.3 Input Data

B.3.1 Global Data in `trn.ini`

Global parameters are defined in the ini-File `trn.ini`. Within the file each line begins with a keyword followed by one parameter:

`BOXN`	total number of cells	N	
`DELT`	time step	Δt	in h
`T_END`	simulation time	T_E	in h
`AREA`	cross section area of flow tube	A	in m^2
`DBL_POR`	0 – single-porosity / 1 – dual porosity		
`DISP`	0 – without dispersion (pure advection) / 1 – with dispersion		
`REAC`	0 – without kinetics / 1 – with kinetics		
`PHAS`	0 – without mineral equilibrium / 1 – with mineral equilibrium		
`EXCH`	0 – without ion exchange / 1 – with ion exchange		
`EXCH_TYP`	0 – resin / 1 – soil		
`ICHM`	0 – without PHREEQC / 1 – with PHREEQC		
`DISP_PHRE`	0 – without PHREEQC / 1 – with PHREEQC for dispersion routine		
`KCHM`	increment factor for PHREEQC-calculations		
`KOUT`	increment factor for Output in `cM_*.txt` and `cP_*.txt`		
`KOUX`	increment factor for Output in profile directories (`PROF_M`, `PROF_P`)		
`MIX_VOL`	volume of upstream mix cell	V_{mix}	in m^3
`MIX_SOL`	initial water in upstream mix cell (file name)		
`CTOT`	total ion-exchange capacity	c_{tot}	in meq/L
`CHRG`	parameter for charge-balance adjustment for t > 0	(default: pH)	
`CHRG_IN`	parameter for charge-balance adjustment for t = 0	(default: pH)	
`UNIT`	concentration units (-2 – mg/L / 2 – mmol/L)	(default: 2)	
`PE_MIN`	parameter to fix minimum pe-value: pe_min = par – pH		
`PE_MAX`	parameter to fix maximum pe-value: pe_max = par		
`PE_FIX`	1 – without pe changes during reactions (simulates pe buffer)		
`PHRE_SHOW`	time step for PHREEQC-input check (copy of file `phre`)		
`ELEM_NB`	number of elements for mass balance		
`ELEM_01`	name of first mass balance element		
...			
`ELEM_08`	name of last mass balance element (if `ELEM_NB` = 8)		
`PRN_MASS_UNIT`	units of mass balance element (1 – mol, 2 – mmol, 3 – µmol)		
`PRN_MASS_EBOX`	number of cells in mass balance output		
`PRN_MASS_FULL`	type of mass output (0 – standard, 1 – for each dispersion step)		

If a keyword is absent in the list, the corresponding parameters automatically are set equal to zero by the program. The line sequence in the file is arbitrary. Comments can be included behind a "//"-sign.

Example for file `trn.ini`:

```
BOXN              20
DELT              0.4
T_END             60
AREA              0.001075
DBL_POR           0
DISP              1
REAC              1
PHAS              1
EXCH              1
EXCH_TYP          1                 // 0-resin, 1-soil
ICHM              0
KCHM              1
KOUT              1
KOUX              16
MIX_VOL           1     0.0002      // on/off  in m3
MIX_SOL           ini_col2.sol
CTOT              14.28             // in meq/L
CHRG              pH
CHRG_IN           Cl
UNIT              2                 // -2 mg/L , +2 mmol/L
PE_MIN            1     7           // pe_Min = par - pH
PE_MAX            1     10
PE_FIX            1
DISP_PHRE         1
PRN_MASS_UNIT     3
PRN_MASS_EBOX     3                 // number of boxes
PRN_MASS_FULL     0                 // 1 = output per disp-step
ELMB_NB           8
ELMB_01           U
ELMB_02           Si
ELMB_03           Ca
ELMB_04           Al
ELMB_05           Na
ELMB_06           Fe
ELMB_07           S(6)
ELMB_08           Cl
PHRE_SHOW         1                 // -1 no output
```

Most of these inputs (keywords) can be changed within the GUI (main window).

During the calculation the complete list of all keywords is stored in the temporary file `para.tmp` (in the root directory).

B.3.2 Input File box.dat

All information about cell geometry, transport phenomena and other cell characteristics are contained in the file box.dat. The text file has a fixed table structure were the first line (header line) defines the parameters in the columns. Thus, starting with line 2, each line represents one section (homogenous layer). The columns (parameters) are:

box	number of first cell in the section (first section begins with 1, second section with N_1+1, third section with N_2+1, etc.)		
name	name of section (for example A, B, C or other)	character string	
dx	cell length	Δx	in m
eps	porosity for the mobile phase	ε	in m^3/m^3
epsP	porosity for the stagnant phase	ε_P	in m^3/m^3
diffu	effective diffusion coefficient	D_e	in m^2/s
disp	longitudinal dispersivity	α_L	in m
alpha	exchange rate between mobile and stagnant water	α	in 1/h
cell	file name for initial mobile water		*.sol
pore	file name for initial pore water		*.sol
REAC	file name for kinetic data and reaction rates		*.dat

The last three parameters cell, pore and REAC define files that are stored in a special subdirectory called CHM.

Example. We consider a 3-section (3-layer) configuration of length 80 m with N = 40 cells (the total number of cells is defined by BOXN in trn.ini). The layers differ only in the primary-mineral inventory defined in the reaction files pMinA.dat, pMinB.dat, and pMinC.dat as well as in the pore water compositions (all other geometry and hydraulic parameters are the same). The sections have a length of 1 m, 5 m, and 2 m. The corresponding input data are:

box	name	dx	eps	epsP	diffu	disp	alpha	cell	pore	REAC
1	A	0.2	0.25	0.3	0	0.05	0.03	cellA.sol	celP_A.sol	pMinA.dat
11	B	0.2	0.25	0.3	0	0.05	0.03	cellB.sol	celP_B.sol	pMinB.dat
31	C	0.2	0.25	0.3	0	0.05	0.03	cellC.sol	celP_C.sol	pMinC.dat

In case of DUAL = 0, i.e. single-porosity approach (rather than dual porosity) the input data for epsP and pore are ignored.

Data Check. After the input file box.dat is read, the program writes the input data (together with other calculated quantities) into the text file box.txt in the output directory. In this way, the user can check these data. Below two header lines, the table contains N lines, i.e. for each cell n from 1 to N one line. The header lines define the parameters in the columns and their units:

name	cell name		
area	cross section area of flow tube (defined in trn.ini)	A	in m^2
dx	cell length	Δx	in m
x	distance of the cell midpoint from zero	x_n	in m

`eps`	porosity	ε	in m^3/m^3
`epsP`	porosity	ε_P	in m^3/m^3
`volW`	volume of mobile water	$\Delta V_W = \varepsilon\ A\ \Delta x$	in m^3
`volP`	volume of stagnant pore water	$\Delta V_P = \varepsilon_P\ A\ \Delta x$	in m^3
`diffu`	effective diffusion coefficient	D_e	in m^2/s
`disp`	longitudinal dispersivity	α_L	in m
`mixA`	dispersion mix-factor with cell n–1:	$mix_A = D_L/(v\Delta x) = \alpha_L/\Delta x$	unitless
`mixB`	dispersion mix-factor with cell n+1:	$mix_B = D_L/(v\Delta x) = \alpha_L/\Delta x$	unitless
`nD`	number of dispersion steps n_D within one advection step	$(\Delta t \rightarrow \Delta t/n_D)$	
`alpha`	exchange rate between mobile and stagnant water	α	in 1/h
`cTOT`	total ion-exchange capacity	c_{tot}	in meq/L
`cTOT/pore`	total ion-exchange capacity per liter pore water		in meq/L
`nmCH`	file name for mobile water solution		
`nmCP`	file name for stagnant pore water solution		
`reac`	file name for kinetic/reaction data		

B.3.3 Input File `qIn.dat` (Inflow Water Composition)

The aqueous solution of the inflow water is defined in file `qIn.dat`. Besides a *constant* (time-independent) inflow water composition the program allows also calculations with changing inflow water compositions, i.e. where the inflow concentrations differ in several time periods.

The structure of the file is simple: any time period between t_0 and t_1 is represented by a single line:

`Box`	name of the first cell (= inflow cell)	character string
`Typ`	= 0 (this parameter should not be changed)	
`t0`	begin of time period (measured from t = 0)	t_0 in hours
`q0`	= 1 inflow scaling at t_0 (this parameter should not be changed)	
`t1`	end of time period (measured from t = 0)	t_1 in hours
`q1`	= 1 inflow scaling at t_1 (this parameter should not be changed)	
`nmCX`	file name for aqueous inflow solution	character string

The first line is always a header line. To define a *constant* inflow water composition a single data line is sufficient, with $t_0 = 0$ and $t_1 > t_E$ (in this case t_1 can be put equal to any high number, for example: $t_1 = 10^6$ h). Otherwise, additional lines should be included (for every time period one line).

Example for file `qIn.dat` (non-constant inflow conditions):

```
Box   Typ   t0    q0    t1    q1    nmCX
A01   0     0     1.0   200   1.0   inp.sol
A01   0     200   1.0   400   1.0   inp2.sol
A01   0     400   1.0   600   1.0   inp.sol
A01   0     600   1.0   800   1.0   inp2.sol
A01   0     800   1.0   9999  1.0   inp3.sol
```

A line can be cancelled by setting the characters "//" in front of the line.

B.3.4 Definition of Species

The input dataset contains 5 specification files (`elem.dat`, `ions.dat`, `secm.dat`, `exch.dat`, `reac.dat`) which define the corresponding species: elements, ions, secondary phase minerals, ion-exchange species, and reactants (primary minerals). In these files a given species can be included or excluded from the calculations by setting 1 or 0 after the corresponding chemical symbol. The number of elements, species and phases is, in principle, unlimited.

The order of the species within the specification files defines also the sequence of the chemical species in the output tables.

Example for file `elem.dat`:

```
BDAT  wateq4f.dat
Ca    1
Mg    1
Na    1
K     1
Fe(2) 1
Fe(3) 1
Fe    1
Al    1
Mn    1
U     1
S(6)  1
Cl    1
C(4)  1
Si    1
```

Remark. The first line in `elem.dat` contains the keyword `BDAT` which defines the thermodynamic PHREEQC-database, here `wateq4f.dat`. This database file should exist in the root directory; otherwise the calculation will not start.

Example for file `ions.dat`:

```
CO2         0
HCO3-       0
CO3-2       0
SO4-2       1
HSO4-       1
```

Remark: In contrast to all other specification files the ion's list does not influence the calculation at all; the file `ions.dat` defines only the output, i.e. which ions will be explicitly shown in the output files (provided it is switched on by 1). During the calculations *all* ions and ion-complexes defined in `wateq4f.dat` are considered (their number is in the order of 10^2).

Example for file `secm.dat` (here comments are included behind the # sign):

```
Gypsum           1     # CaSO4:2H2O
Calcite          1     # CaCO3
Fe(OH)3(a)       1     # Fe(OH)3
Al(OH)3(a)       1     # Al(OH)3
Celestite        1     # SrSO4
Silicagel        1     # SiO2
```

Example for file `exch.dat` (the second parameter defines the log k value; the soil exchanger is abbreviated by the upper-case letter Y)

```
HY          1     1.0
KY          1     0.7
NaY         1     0.0
CaY2        1     0.8
MgY2        1     0.6
FeY2        1     0.44
AlY3        1     0.36
```

Example for file `reac.dat` (this file defines both primary minerals and other reactive compounds):

```
Coffinite         1
Greenalite        1
Kaolinite         1
Dolomite          1
Alunite           1
Halite            1
Gypsum            1
Diopside          1
Anorthite         1
Pyrite            1
Kmica             1
Adularia          1
O2                1
FeCl3             1
H2SO4             1
HCl               0
NaOH              0
```

B.3.5 Aqueous Solution Files (`*.sol`)

Hydrochemical data which define the aqueous solutions, the amount of secondary minerals as well as the ion-exchange distribution are stored in special data files with extension `*.sol` (one file for one water composition located in subdirectory `CHM`). The syntax is similar to the syntax of PHREEQC. Each file consists of the following data blocks:

```
SOLUTION  1
 units    mol/kgw
...
...       } data for aqueous species
...
EQULIBRIUM_PHASES   1
...
...       } data for secondary mineral phases
...
EXCHANGE  1
...
...       } data for ion exchange species
...
END
```

The `SOLUTION` data block is obligatory; the other two data blocks for the secondary mineral phases and ion-exchange species are optionally. The inclusion of the latter two

blocks depends on the chosen option: single or dual porosity (see Tab. B.1). For the single porosity approach (DUAL = 0) only *one* sol-file is required for a cell; the file name is defined in `box.dat` (see Sec. B.3.2).

Tab. B.1 Input data that enter the sol-files depend on the single and dual porosity approach

	single porosity DUAL = 0	dual porosity DUAL = 1
mobile phase (cell)	• aqueous species • secondary minerals (optional) • ion-exchangers (optional)	• aqueous species • secondary minerals (optional)
stagnant phase (pore)	–	• aqueous species • ion exchangers (optional)

Aqueous Solution. Each data line consists of three parts:

parameter name numerical data # "comment"

Here, the comment is optional and starts with the #-sign. The `SOLUTION` block contains the following parameters (each line begins with the parameter name):

`temp`	temperature of the solution	in °C
`pH`	pH value	
`pe`	pe value	
`element_1`	concentration	in mol/L
`element_2`	concentration	in mol/L
`element_3`	concentration	in mol/L
... etc.		

The line order is arbitrary; the parameter name is case sensitive. In principle, the number of elements is arbitrary, but, into the calculation enter only those elements that are explicitly defined in `elem.dat` (with switch-on value '1' after the element name). In contrast to `elem.dat` the file `ions.dat` has no impact on the PHREEQC calculations.

The only condition all parameters should satisfy is *charge conservation* (number of anions = number of cations). Anyway, the read subroutine of the program checks the input solution and, if there is no charge balance, the solution will be adjusted by modification of the element parameter defined by `CHRG_IN` in `trn.ini`.

Secondary Minerals. With help of the data block `EQULIBRIUM_PHASES` an initial inventory of secondary minerals is added to the cells (in mol per liter pore water). If there is at t = 0 no such inventory, the `EQULIBRIUM_PHASES` block can be skipped. This data block (present or not) does not influence the secondary mineral precipitation which will be always calculated if the key-parameter `PHAS = 1` in `trn.ini` is set.

The syntax is in full accord with PHREEQC syntax:

phase name 0 amount in mol per liter pore water (at t = 0)

Here, the second parameter defines the saturation index, SI = 0. Phase names that are not defined in file `secm.dat` will be ignored. After the data is read into the program the input solution will be equilibrated with the mineral phases (thereby they can dissolve or precipitate).

Ion-Exchange. In case of ion-exchange calculations (switch on by key-parameter `EXCH = 1` in `trn.ini`), the `EXCHANGE` data block should contain at least one ion-exchange species. The syntax is

species name amount in mol per liter pore water (at t = 0)

Species that are not defined in file `exch.dat` will be ignored. The soil exchanger is abbreviated by the upper-case letter Y.

After the data is read into the program the input solution will be equilibrated with the ion exchanger. Thereby the total exchange capacity will normalized to `CTOT`/pore per liter pore volume. In particular,

(B.1)	`CTOT/eps`	for `DUAL = 0`	(single porosity)
(B.2)	`CTOT/epsP`	for `DUAL = 1`	(dual porosity)

The parameters `CTOT`, `eps` and `epsP` are defined in `trn.ini`.

Example. The file `cell.sol` for a calculation with secondary minerals and ion exchangers (single-porosity approach) is specified by

```
SOLUTION    1
      units mol/kgw
      temp  35
      pH    8.707
      pE    5.855
      Na    0.04341
      Ca    0.001238
      Mg    0.001555
      K     0.001003
      Al    0.000001
      Fe(3) 0.0
      S(6)  0.00584
      U     0.0
      Si    0.000266
      Cl    0.03827
EQUILIBRIUM_PHASES  1
      Gypsum      0     0.002
EXCHANGE  1
      HY    0.02
      KY    0.98
END
```

Here, the number in the brackets right to the element symbol in the `SOLUTION` block denotes the oxidation number. In this example we have 0.002 mol gypsum per liter pore water at t = 0.

Remark. Before the calculation starts the input solution `cell.sol` will be set into phase and ion-exchange equilibrium. Hence, the equilibrated solution at t = 0 in most cases differ (slightly) from the input solution.

B.3.6 Dissolution Rates and Kinetic Data

Reaction rates and kinetic data are stored in special files `reac.dat` or `pMin.dat` or others (located in the subdirectory `CHM`). The files contain 1 header line and an arbitrary number of lines (for each reactant 1 line) that contain the reactant name followed by 4 parameters:

`name`	name of reactant		character string
`type`	type of kinetic approach		integer
`m0`	initial inventory at t = 0	m_0	in mol
`r`	reaction rate constant	r	in mol/s
`par`	additional parameter	b	unitless

Optionally, at the line's end comments can be included behind '`//`'. The file mainly contains primary minerals, but, also other reactants like (NaOH, HCl, etc.) are allowed. The line sequence is arbitrary.

The initial mass at t = 0 is m_0 in mol. During the dissolution process the mass m diminishes according to the law

(B.3) $$\frac{dm}{dt} = -\text{rate} \qquad \text{with initial condition:} \qquad m(t=0) = m_0$$

Here the 'rate' expression depends on `type` parameter:

(B.4) `type` = 0: $\text{rate} = 0$ (no reaction)

(B.5) `type` = 1: $\text{rate} = r$ for m > 0 (zero-order kinetics)

(B.6) `type` = 2: $$\text{rate} = r \cdot \left(\frac{m}{m_0}\right)$$ (first-order kinetics)

(B.7) `type` = 3: $$\text{rate} = r \cdot \left(\frac{m}{m_0}\right) \cdot \left(1 - 10^{SI}\right)$$ for SI < 0, otherwise 0

(B.8) `type` = 4: $$\text{rate} = r \cdot \left(\frac{m}{m_0}\right) \cdot \exp\left\{ b\,(2 - pH) \right\}$$

(B.9) `type` = 5: $$\text{rate} = r \cdot \left(\frac{m}{m_0}\right) \cdot 10^{-b \cdot pH} \cdot \left(1 - 10^{SI}\right)$$ (mixed-order kinetics)

(B.10) `type` = 6: $$\text{rate} = r \cdot \left(\frac{m}{m_0}\right) \cdot 10^{b \cdot (pe - 13)}$$

The reactants and primary minerals should be included in the definition file `reac.dat`, otherwise the reaction will be ignored. Obviously, the reaction process for a reactant or primary mineral can be switched off either by setting `type` = 0 or by `m0` = 0, respectively.

Example for file `pMin.dat`:

```
name        type  m0_mol/L    r_mol/L/s    par2  // comment
Coffinite   1     0.19        1.2e-8       0.2   // USiO4
Greenalite  1     0.5         1.0e-9       0.2   // Fe3Si2O5(OH)4
Diopside    5     1.0         1.0e-9       0.2   // CaMgSi2O6
Anorthite   5     1.0         5.0e-9       0.5   // CaAl2SiO8
Kmica       0     1.0         1.0e-9       0.2   // KAl3Si3O10(OH)2
Adularia    5     1.0         1.0e-9       0.2   // KAlSi3O8
Kaolinite   5     1.0         1.0e-9       0.5   // Al2Si2O5(OH)4
Pyrite      5     1.0         1.0e-9       0.2   // FeS2
Alunite     5     1.0         1.0e-9       0.2   // KAl3(SO4)2(OH)6
```

B.4 Output Data

After computation, the complete set of output files are stored in a directory defined by the keyword `OUT_DIR` in `start.dat`. (The user can also change the directory name in the main window.)

B.4.1 General Notation

The main information is stored in form of species concentrations. To distinguish the corresponding output files, the files of the mobile phase (dissolved pore water concentration) and the stagnant phase (sorbed species concentrations) are marked by characters “M” and “P” in the file name:

M	– *m*obile solution	c_i (x,t)
P	– stagnant *p*hase	c_i^S (x,t)

where i denotes the species index. In total, we have for types of chemical output files:

- tables of spatial distribution (x variable, t = const) for mobile solutions
- tables of spatial distribution (x variable, t = const) for stagnant phase
- tables of temporal distribution (x = const, t variable) for mobile solutions
- tables of temporal distribution (x = const, t variable) for stagnant phase

Every file represents a table with the following structure (here only symbolically):

for temporal distribution

	c_1	c_2	c_3
t_0			
t_1			
t_2			

$t_k = t_0 + k\Delta t$
with k = time step

for spatial distribution

	c_1	c_2	c_3
x_1			
x_2			
x_3			

$x_n = ½\ \Delta x + (n\text{-}1)\ \Delta x$
with n = cell number

The meaning of the columns and rows of the table are:

columns	chemical species concentrations
lines	variable t (for temporal distribution) or x (for spatial distribution)

The file notation is as follows: Whereas the *variable* parameter, t or x, is included in the tables, the *fixed* parameter, x or t, is included in the file name. Thus, *temporal*-distribution files are labeled by the cell number (cell name):

`cM_cell_1.txt`	mobile solution in first cell	(n = 1)
`cM_cell_2.txt`	mobile solution in second cell	(n = 2)
...		

and (only for `DUAL = 1`)

`cP_cell_1.txt`	stagnant phase in first cell	(n = 1)
`cP_cell_2.txt`	stagnant phase in second cell	(n = 2)
...		

Otherwise, *spatial*-distribution files are labeled with the time parameter:

`000000.txt`	concentrations at initial time t_0	
`0000t1.txt`	concentrations at t_1	(in minutes)
`...`		
`0000tE.txt`	concentrations at end time t_E	(in minutes)

The spatial-distribution files for the mobile solution (stagnant phase) are stored in subdirectory `PROF_M` (`PROF_P`).

B.4.2 Structure of Output Directory

The output directory OUT has the following structure:

`PROF_M`	subdirectory for *spatial* distribution files (mobile solution)	
`PROF_P`	subdirectory for *spatial* distribution files (stagnant phase)	
`cM_cell_1.txt`	*temporal* distribution file for cell n = 1	(mobile solution)
`cM_cell_2.txt`	*temporal* distribution file for cell n = 2	(mobile solution)
...		
`cM_cell_N.txt`	*temporal* distribution file for last cell	(mobile solution)
`cP_cell_1.txt`	*temporal* distribution file for cell n = 1	(stagnant phase)
`cP_cell_2.txt`	*temporal* distribution file for cell n = 2	(stagnant phase)
...		
`cP_cell_N.txt`	*temporal* distribution file for last cell	(stagnant phase)
`CH_inp.txt`	aqueous *inflow* solution	
`CH_out.txt`	aqueous *outflow* solution	
`inSOL.txt`	initial aqueous solutions (pore water in all cells)	

The number of temporal-distribution files equals the total cell number; the number of spatial-distribution files is equal to the total number of time steps. Because the number of time steps can be very large, the user can regulate the output sequence of the spatial-distribution files by setting the parameter KOUX in `trn.ini`:

KOUX = 1	output for each time step
KOUX = 2	output for every second time step
KOUX = n	output for after each n-th time step

The file `CH_inp.txt` contains the inflow solution defined in `qIn.dat` (see Sec. B.3.3). The file `CH_out.txt` contains the outflow solution which is equal to the pore water solution of the last cell, i.e. equal to `cM_cell_N.txt`.

In addition, there are also files that describe both mass balance and mass change per time:

`m_ELM_01.txt`	mass of element 1	(in mol)
`j_ELM_01.txt`	mass change of element 1	(in mol/h)
...		
`m_ELM_NB.txt`	mass of element NB	(in mol)
`j_ELM_NB.txt`	mass change of element NB	(in mol/h)

The elements are defined in `trn.ini` (see Sec. B.3.1).

B.4.3 Output Tables for Chemical Species

The file structure of all concentration tables is the same. There are two header lines: the first line defines the parameters, the second line defines the units. For example, the parameters (columns) of the *temporal*-distribution files are:

`t`	time variable	t	in h
`x`	cell midpoint	x_n	in m
`temp`	water temperature	T	in °C
`pH`	pH value		
`pE`	pe value		
`#ion`	ion strength (which is proportional to salinity)		
`elem_1`	element concentration		in mmol/L
`elem_2`	element concentration		in mmol/L
...			
`ions_1`	chemical species concentration		in mmol/L
`ions_2`	chemical species concentration		in mmol/L
...			
`secm_1`	amount of secondary minerals		in mmol/L
`secm_2`	amount of secondary minerals		in mmol/L
...			
`SI_1`	saturation index of secondary and primary minerals		
`SI_2`	saturation index of secondary and primary minerals		
...			
`exch_1`	ion-exchange concentration		in meq/L

`exch_2`	ion-exchange concentration	in meq/L
...		
`CTOT/PORE`	total ion-exchange capacity per Liter pore volume	in meq/L

The *spatial*-distribution tables differ from this example only in the first column where the time variable, t, is replaced by the cell name (cell number).

The number of elements and their order in the list are defined in `elem.dat`, `ions.dat`, `secm.dat`, and `exch.dat` (see Sec. B.3.4).

B.5 Program Crash and Error Message

In case of a program crash usually an error message file, `error.txt`, will be released in the root directory. Common errors are due to

- wrong input data (e.g., negative values)
- missing input files
- convergence problems within PHREEQC calculations

The error message will help you to detect the real cause.

C CORE COMPOSITION [AN07]

Sample No.	From	To	Mass	Mg	Al	Si	P	S	K	Ca	Sc	Ti	V	Cr	Mn	Fe
			g	(%)	(%)	(%)	(%)	(%)	(%)	(%)	(%)	(%)	(%)	(%)	(%)	(%)
AKC028	**Col 1**															
84856	188,25	188,51	496	0	1,07	43,3	0,006	0,027	0,086	0,023	0,003	0,281	0,002	0	0,002	1,10
84857	188,51	188,82	680	0,009	2,56	43,3	0,005	0,026	0,107	0,023	0,004	0,323	0,002	0	0,002	0,37
84858	188,82	189,15	804	0,005	1,87	44,3	0,005	0,031	0,100	0,024	0,003	0,320	0,001	0	0,002	0,25
84859	189,40	189,70	696	0,005	2,02	44,9	0,006	0,030	0,094	0,022	0,003	0,323	0,001	0,015	0,003	0,49
84860	189,70	190,03	786	0	1,79	43,9	0,005	0,033	0,104	0,022	0,003	0,294	0,001	0	0,002	0,41
84861	190,03	190,34	672	0,001	1,58	43,9	0,004	0,031	0,082	0,025	0,004	0,339	0,001	0,014	0,003	0,41
84862	190,34	190,57	510	0,001	0,78	45,8	0,004	0,030	0,082	0,021	0,004	0,413	0,001	0,002	0,003	0,14
84863	190,57	190,83	664	0,005	1,50	44,6	0,004	0,032	0,090	0,022	0,003	0,387	0,001	0,005	0,003	0,20
Mean	188,25	190,83	664	0,003	1,65	44,3	0,005	0,030	0,093	0,023	0,003	0,335	0,001	0,005	0,003	0,420
AKC029	**Col 2**															
80910	196,43	196,60	412	0	0,90	41,9	0,009	0,033	0,077	0,017	0,002	0,329	0,004	0	0,002	0,804
80911	196,60	196,72	296	0,016	1,92	41,5	0,007	0,030	0,083	0,023	0,003	0,544	0,003	0,008	0,005	0,476
80912	196,72	196,79	912	0,046	6,42	36,6	0,015	0,044	0,247	0,044	0,004	0,536	0,003	0,006	0,002	0,930
80913	196,79	196,84	108	0	0,98	38,6	0,008	0,030	0,072	0,017	0,003	0,727	0,002	0,024	0,008	1,170
80914	196,84	197,08	588	0,011	2,06	39,0	0,005	0,034	0,203	0,024	0,002	0,485	0,000	0	0,003	0,202
80915	197,08	197,33	672	0,01	2,07	43,1	0,004	0,042	0,101	0,026	0,003	0,320	0,001	0	0,002	0,211
80916	197,33	197,65	752	0,015	2,71	43,5	0,007	0,052	0,125	0,034	0,004	0,336	0,002	0	0,002	0,213
80917	197,65	197,81	316	0,013	2,58	43,5	0,005	0,074	0,117	0,046	0,004	0,349	0,004	0,001	0,002	0,197
80918	197,81	197,86	138	0,048	5,32	38,3	0,007	0,060	0,235	0,071	0,003	0,483	0,006	0,029	0,002	0,282
80919	197,86	197,90	90	0,019	2,41	42,0	0,006	0,045	0,126	0,039	0,004	0,356	0,002	0,021	0,003	0,232
80920	197,90	197,94	148	0,075	6,65	36,8	0,01	0,062	0,286	0,078	0,003	0,512	0,010	0,015	0,003	0,293
80921	197,94	198,40	234	0	0,90	43,1	0,004	0,546	0,128	0,029	0,005	0,292	0,002	0,006	0,002	1,321
Mean	196,43	198,40	389	0,021	2,91	40,7	0,007	0,088	0,150	0,037	0,003	0,439	0,003	0,009	0,003	0,528
AKC030	**Col 3**															
83837	213,40	214,00	1548	0,024	0,41	43,5	0,005	0,167	0,045	0,031	0,003	0,037	0,000	0,02	0,001	0,22
83838	214,00	214,50	1244	0,014	0,31	46,8	0,006	0,121	0,052	0,030	0,003	0,035	0,000	0,039	0,002	0,15
83839	214,50	215,00	1296	0,019	0,32	42,5	0,007	0,112	0,072	0,027	0,002	0,031	0,000	0,088	0,002	0,14
83840	215,00	215,50	1272	0	0,31	48,0	0,003	0,162	0,030	0,014	0,004	0,038	0,000	0,003	0	0,11
Mean	213,40	215,50	1340	0,014	0,34	45,2	0,005	0,141	0,050	0,026	0,003	0,035	0,000	0,038	0,001	0,154
AKC033	**Col 4**															
83944	191,40	192,00	1288	0,035	3,99	41,3	0,008	0,031	0,244	0,037	0,004	0,471	0,002	0,039	0,003	0,24
83945	192,00	192,55	1242	0,017	2,79	42,6	0,009	0,027	0,222	0,025	0,004	0,426	0,003	0,014	0,004	0,88
83946	192,55	193,00	290	0,001	0,82	45,2	0,009	0,031	0,092	0,023	0,005	0,315	0,002	0,021	0,003	1,04
83947	193,00	193,45	1080	0,003	2,05	43,2	0,006	0,023	0,107	0,020	0,004	0,414	0,000	0,004	0,004	0,40
83948	193,45	193,90	1214	0	1,18	44,6	0,006	0,024	0,085	0,019	0,003	0,376	0,002	0,019	0,003	0,55
Mean	191,40	193,90	1023	0,011	2,17	43,3	0,008	0,027	0,150	0,025	0,004	0,400	0,002	0,019	0,003	0,621

Sample No.	From	To	Co	Ni	Cu	Zn	As	Sr	Y	Zr	Nb	Ba	Pb	Th	U	U3O8	U3O8	C	S
			(%)	(%)	(%)	(%)	(%)	(%)	(%)	(%)	(%)	(%)	(%)	(%)	DNA(ppm)	DNA(ppm)	XRF(ppm)	%	%
AKC028	**Col 1**																		
84856	188,25	188,51	0	0,002	0,004	0,003	0,000	0,152	0,006	0,167	0,000	0,027	0,000	0,003	18	21	24	0,06	0,02
84857	188,51	188,82	0	0,002	0,002	0,001	0,000	0,152	0,008	0,201	0,000	0,030	0,001	0,004	9	11	35	0,03	0,02
84858	188,82	189,15	0	0,001	0,002	0,001	0,000	0,157	0,008	0,182	0,000	0,030	0,001	0,004	7	8	24	0,04	0,02
84859	189,40	189,70	0	0,001	0,005	0,002	0,000	0,157	0,007	0,185	0,000	0,029	0,001	0,005	9	11	24	0,04	0,02
84860	189,70	190,03	0	0,001	0,005	0,001	0,000	0,157	0,005	0,174	0,000	0,028	0,001	0,005	7	8	24	0,05	0,03
84861	190,03	190,34	0	0,001	0,004	0,001	0,000	0,151	0,006	0,190	0,001	0,028	0,000	0,004	7	8	12	0,04	0,03
84862	190,34	190,57	0	0,001	0,003	0,000	0,000	0,151	0,007	0,197	0,000	0,028	0,001	0,004	6	7	24	0,05	0,02
84863	190,57	190,83	0	0,003	0,007	0,002	0,000	0,162	0,007	0,198	0,000	0,030	0,001	0,006	6	7	24	0,04	0,02
Mean	188,25	190,83	0	0,002	0,004	0,001	0,000	0,155	0,007	0,187	0,000	0,029	0,001	0,004	9	10	24	0,04	0,02
AKC029	**Col 2**																		
80910	196,43	196,60	0	0,000	0,008	0,004	0,001	0,148	0,007	0,181	0,000	0,014	0,000	0,002	21	25	36	0,04	0,03
80911	196,60	196,72	0	0,000	0,003	0,002	0,000	0,150	0,005	0,248	0,000	0,020	0,000	0,004	12	14	29	0,00	0,03
80912	196,72	196,79	0	0,000	0,005	0,004	0,000	0,157	0,005	0,189	0,000	0,016	0,000	0,004	14	17	29	0,11	0,03
80913	196,79	196,84	0	0,000	0,008	0,007	0,000	0,131	0,006	0,215	0,000	0,022	0,000	0	15	18	10	0,05	0,01
80914	196,84	197,08	0	0,000	0,003	0,000	0,000	0,147	0,004	0,194	0,000	0,015	0,000	0	6	7	2	0,08	0,02
80915	197,08	197,33	0	0,000	0,004	0,000	0,000	0,142	0,005	0,173	0,000	0,013	0,000	0,001	10	12	16	0,09	0,02
80916	197,33	197,65	0	0,000	0,009	0,003	0,000	0,159	0,005	0,179	0,000	0,015	0,002	0,004	24	28	39	0,17	0,03
80917	197,65	197,81	0	0,000	0,018	0,027	0,000	0,151	0,006	0,189	0,000	0,015	0,000	0,004	124	146	151	0,60	0,07
80918	197,81	197,86	0	0,014	0,000	0,043	0,000	0,163	0,005	0,185	0,000	0,017	0,000	0,004	237	279	277	1,08	0,07
80919	197,86	197,90	0	0,004	0,000	0,004	0,000	0,152	0,007	0,191	0,000	0,015	0,000	0,004	113	133	137	0,43	0,03
80920	197,90	197,94	0	0,010	0,000	0,060	0,000	0,164	0,005	0,183	0,000	0,020	0,001	0,006	577	680	673	1,86	0,11
80921	197,94	198,40	0	0,007	0,000	0,035	0,014	0,149	0,006	0,171	0,000	0,014	0,001	0,004	1990	2347	2287	0,34	1,39
Mean	196,43	198,40	0	0,003	0,005	0,016	0,001	0,151	0,006	0,192	0,000	0,016	0,000	0,003	262	309	307	0,40	0,15
AKC030	**Col 3**																		
83837	213,40	214,00	0	0,028	0,000	0,011	0,002	0,160	0,006	0,158	0,017	0,011	0,000	0,003	2	2	11	0,07	0,16
83838	214,00	214,50	0	0,007	0,001	0,001	0,000	0,156	0,006	0,157	0,002	0,011	0,000	0,003	1	1	8	0,04	0,12
83839	214,50	215,00	0	0,031	0,000	0,000	0,001	0,152	0,005	0,156	0,033	0,009	0,000	0,001	1	1	9	0,05	0,10
83840	215,00	215,50	0	0,000	0,000	0,001	0,000	0,149	0,005	0,167	0,001	0,012	0,003	0,006	0	0	26	0,07	0,03
Mean	213,40	215,50	0	0,017	0,000	0,003	0,001	0,154	0,006	0,160	0,013	0,011	0,001	0,003	1	1	14	0,06	0,10
AKC033	**Col 4**																		
83944	191,40	192,00	0	0,005	0,017	0,001	0,000	0,160	0,005	0,209	0,000	0,028	0,001	0,007	8	9	33	0,02	0,03
83945	192,00	192,55	0	0,005	0,016	0,002	0,000	0,158	0,008	0,206	0,000	0,027	0,001	0,006	12	14	39	0,01	0,02
83946	192,55	193,00	0	0,008	0,019	0,003	0,001	0,153	0,008	0,189	0,000	0,025	0,002	0,006	9	11	35	0	0,03
83947	193,00	193,45	0	0,000	0,011	0,000	0,000	0,154	0,007	0,194	0,000	0,023	0,000	0,004	14	17	21	0	0,02
83948	193,45	193,90	0	0,000	0,014	0,003	0,000	0,150	0,008	0,190	0,000	0,024	0,001	0,005	12	14	37	0	0,02
Mean	191,40	193,90	0	0,004	0,015	0,002	0,000	0,155	0,007	0,198	0	0,025	0,001	0,006	11	13	33	0,006	0,024

D AQUIFER SIMULATIONS – MODEL RESULTS

The following four Post-Mining scenarios are considered:

Scenario		transversal dilution	solution in ore zone	solution pH in ore zone
D.1	Worst Case / No Dilution	no	lix	1.7
D.2	Worst Case with dilution	yes	lix	1.7
D.3	Real Case / No Dilution	no	lix_R	2.0
D.4	Real Case with dilution	yes	lix_R	2.0

Thereby is:

most improbable case:	Worst Case / No Dilution	in Sec. D.1
most probable case:	Real Case with dilution	in Sec. D.4

A detailed description is presented in Chapter 4.

D.1 Scenario – Worst Case / No Dilution

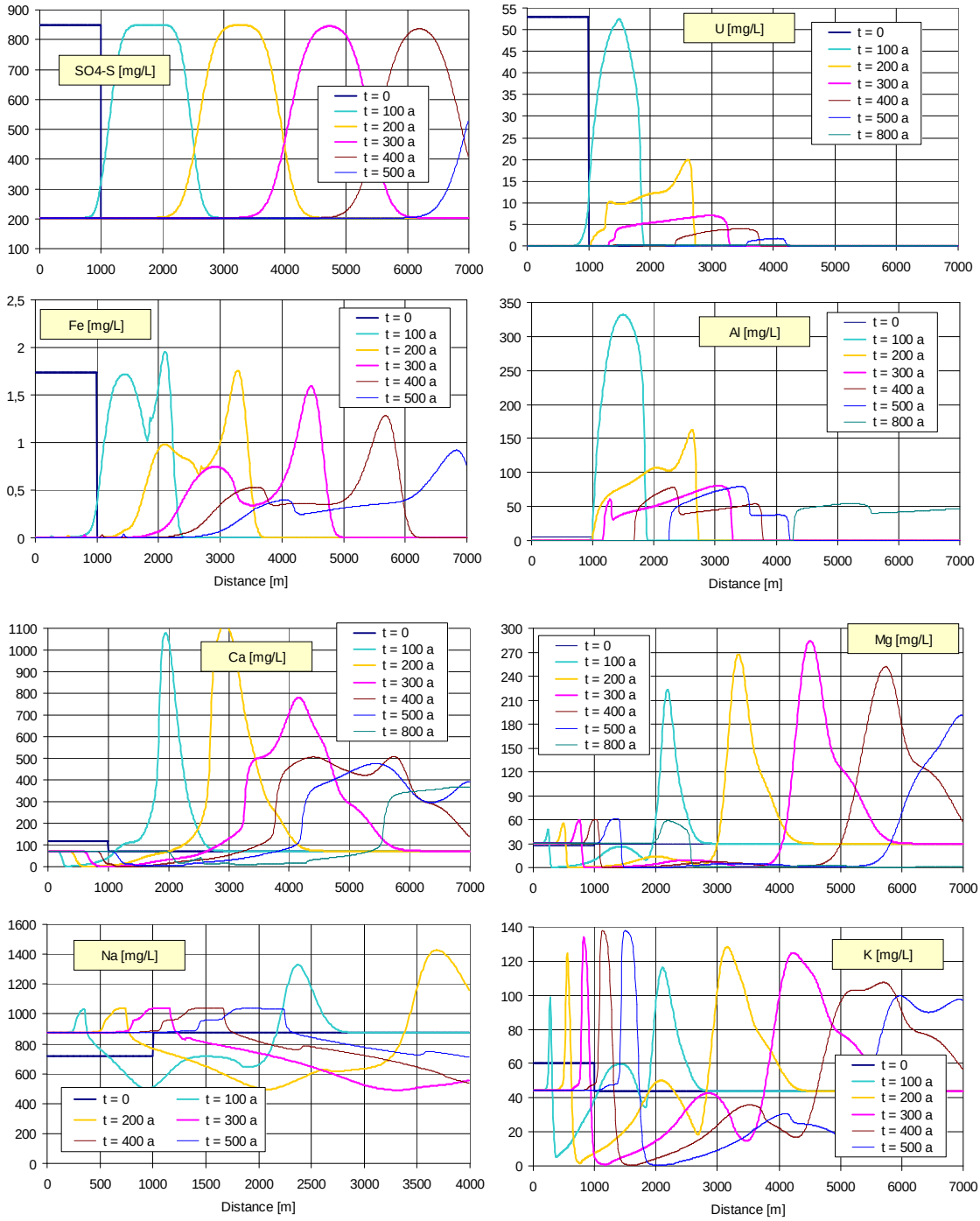

Fig. D.1 Element concentrations [mg/L] as a function of distance x – Worst Case / No dilution

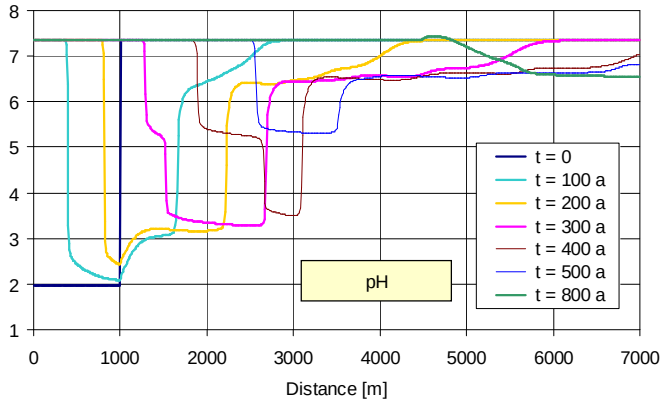

Fig. D.2 pH as a function of distance x – Worst Case / No dilution

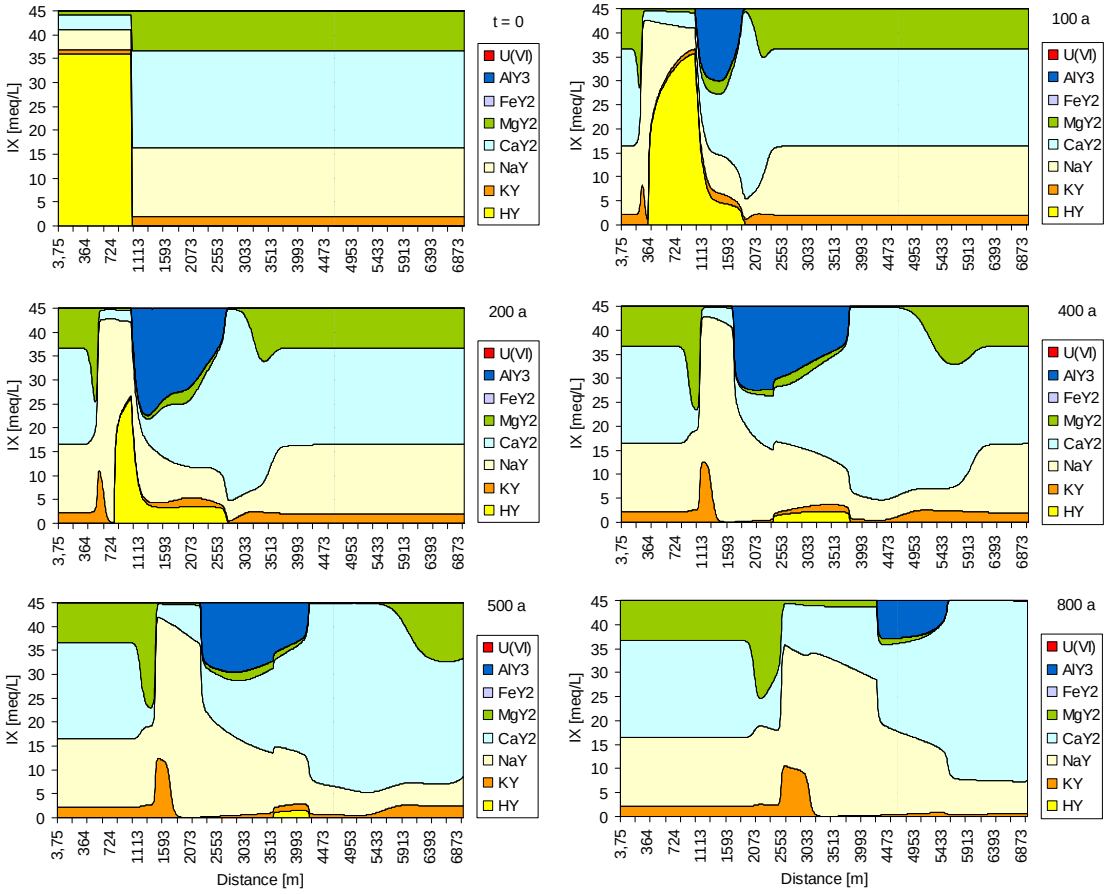

Fig. D.3 Cation distribution on ion exchanger as a function of distance x – Worst case / No dilution

D.2 Scenario – Worst Case with Dilution

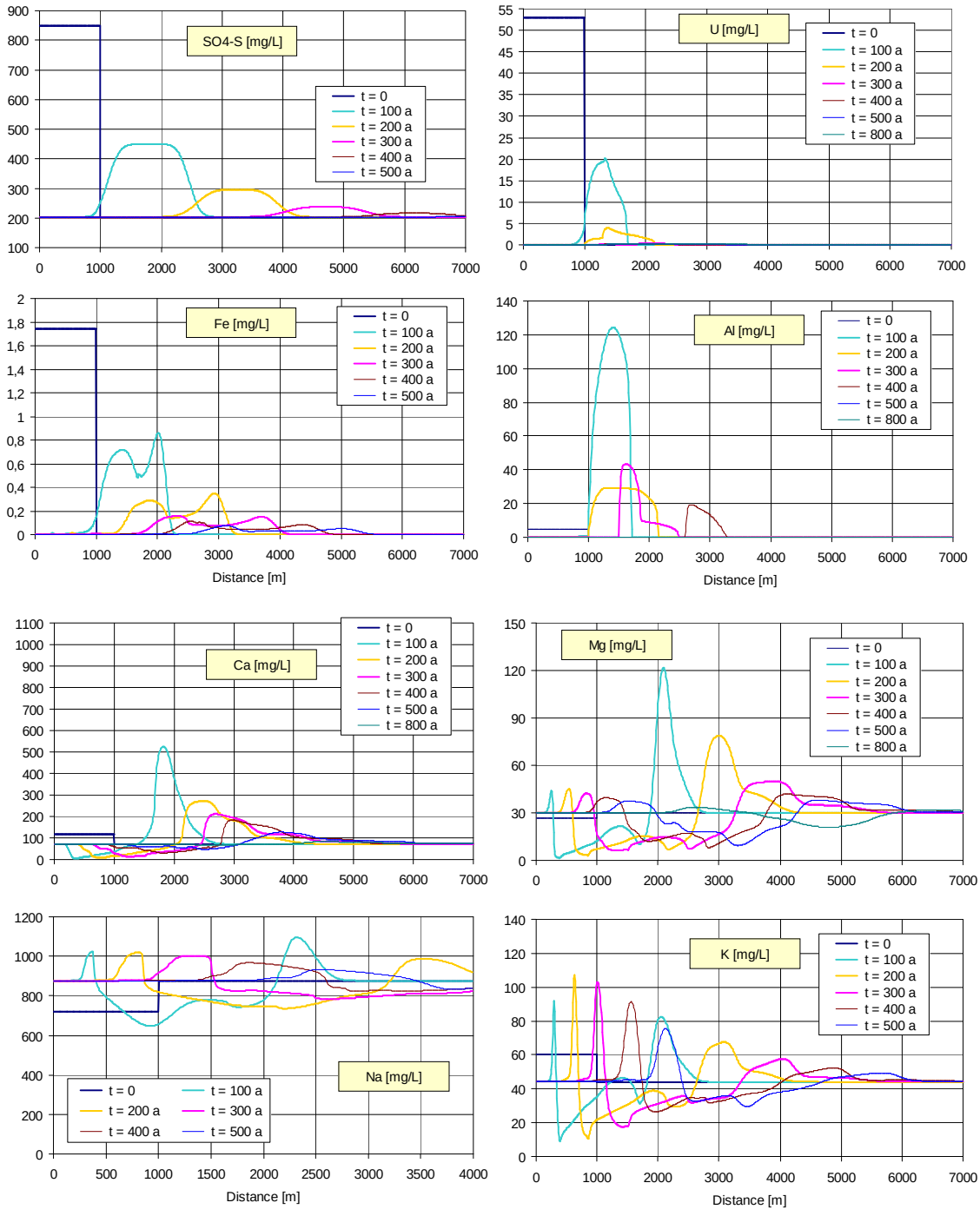

Fig. D.4 Element concentrations [mg/L] as a function of distance x – Worst Case with Dilution

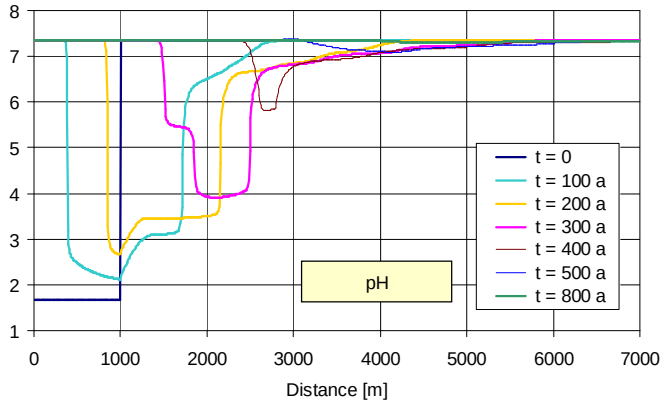

Fig. D.5 pH as a function of distance x – Worst Case with Dilution

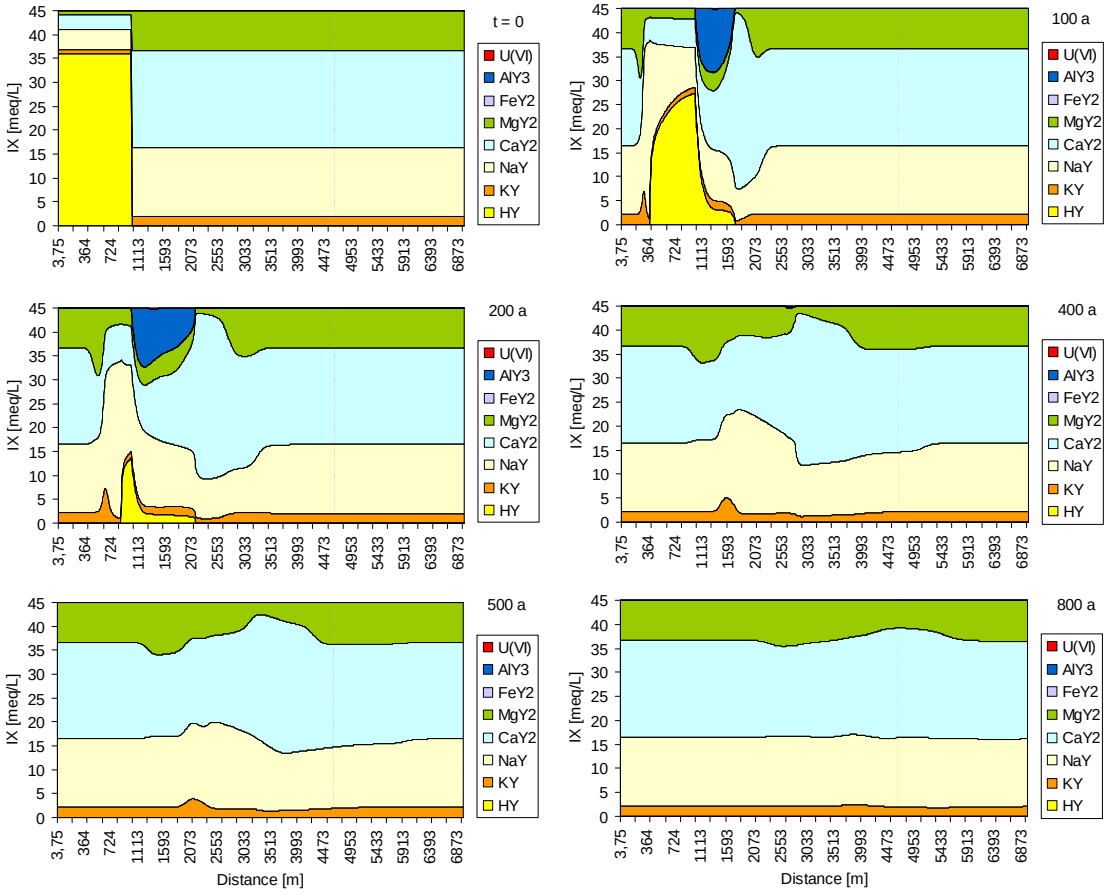

Fig. D.6 Cation distribution on ion exchanger as a function of distance x – Worst case with Dilution

D.3 Scenario – Real Case / No Dilution

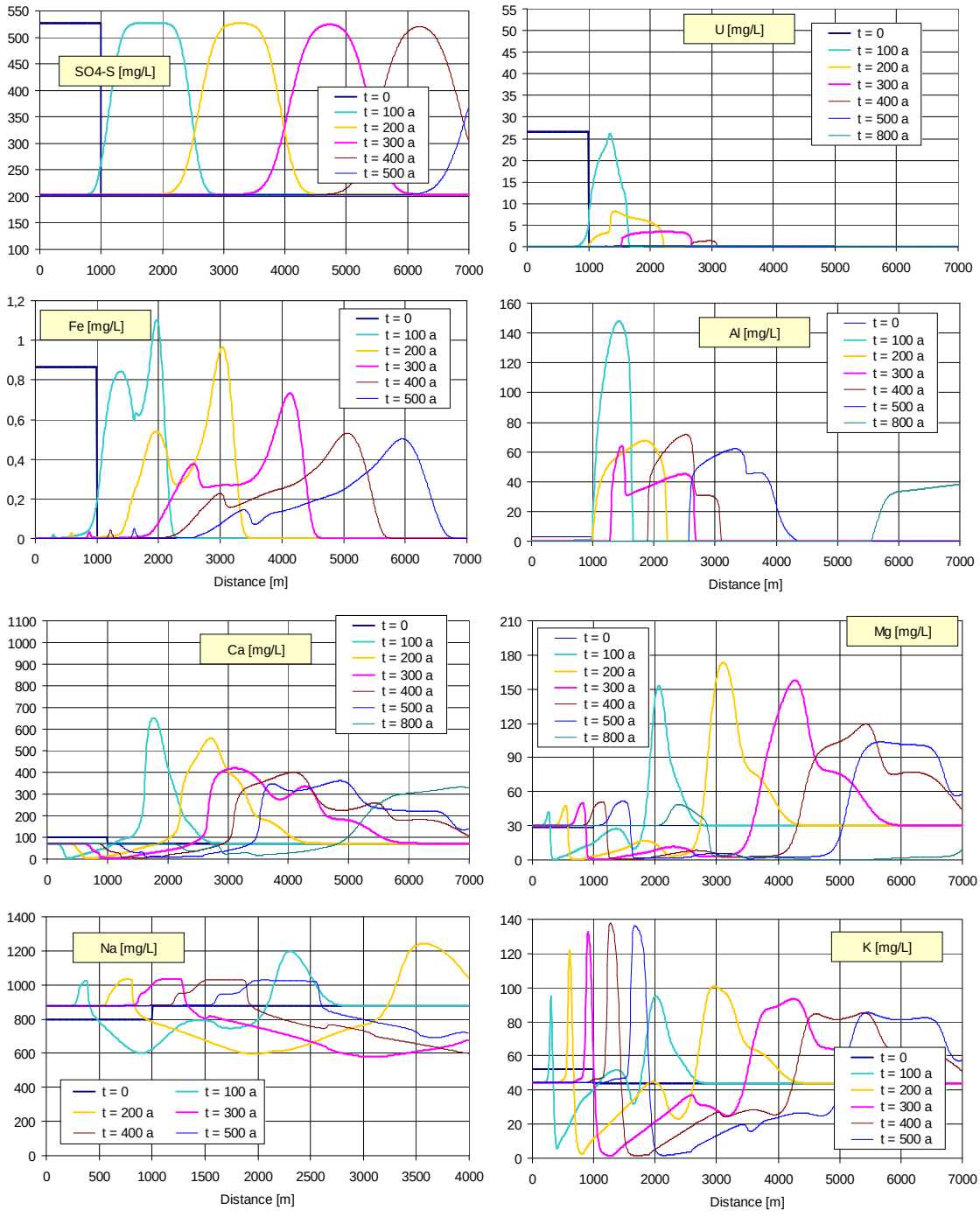

Fig. D.7 Element concentrations [mg/L] as a function of distance x – Real Case / No dilution

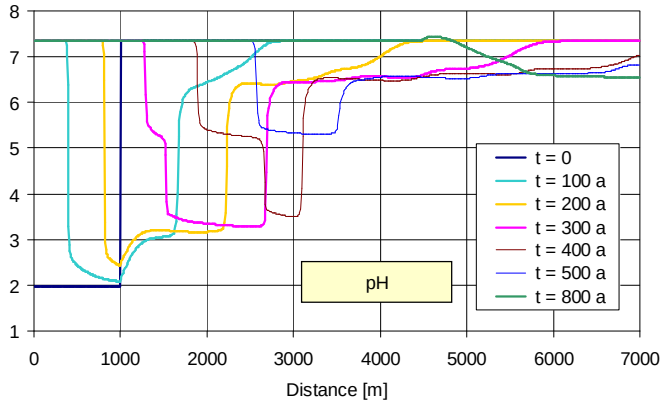

Fig. D.8 pH as a function of distance x – Real Case / No dilution

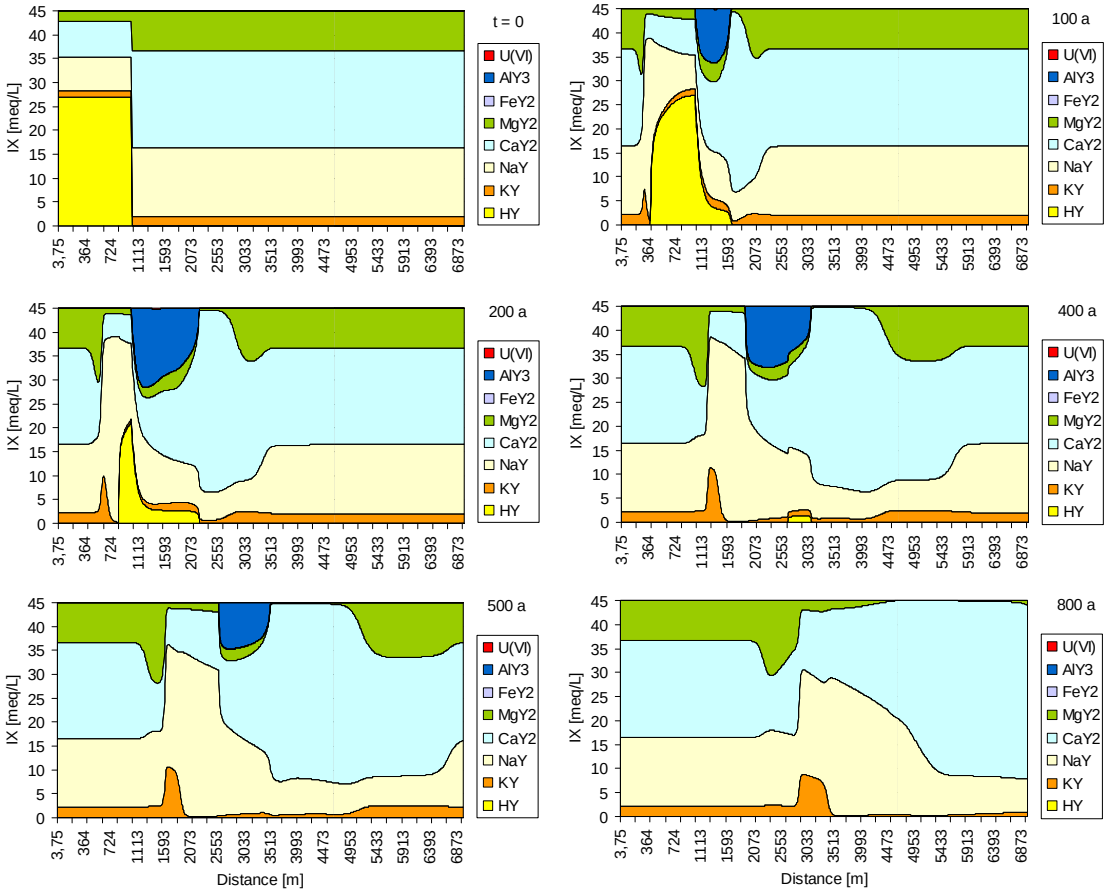

Fig. D.9 Cation distribution on ion exchanger as a function of distance x – Real Case / No dilution

D.4 Scenario – Real Case with Dilution

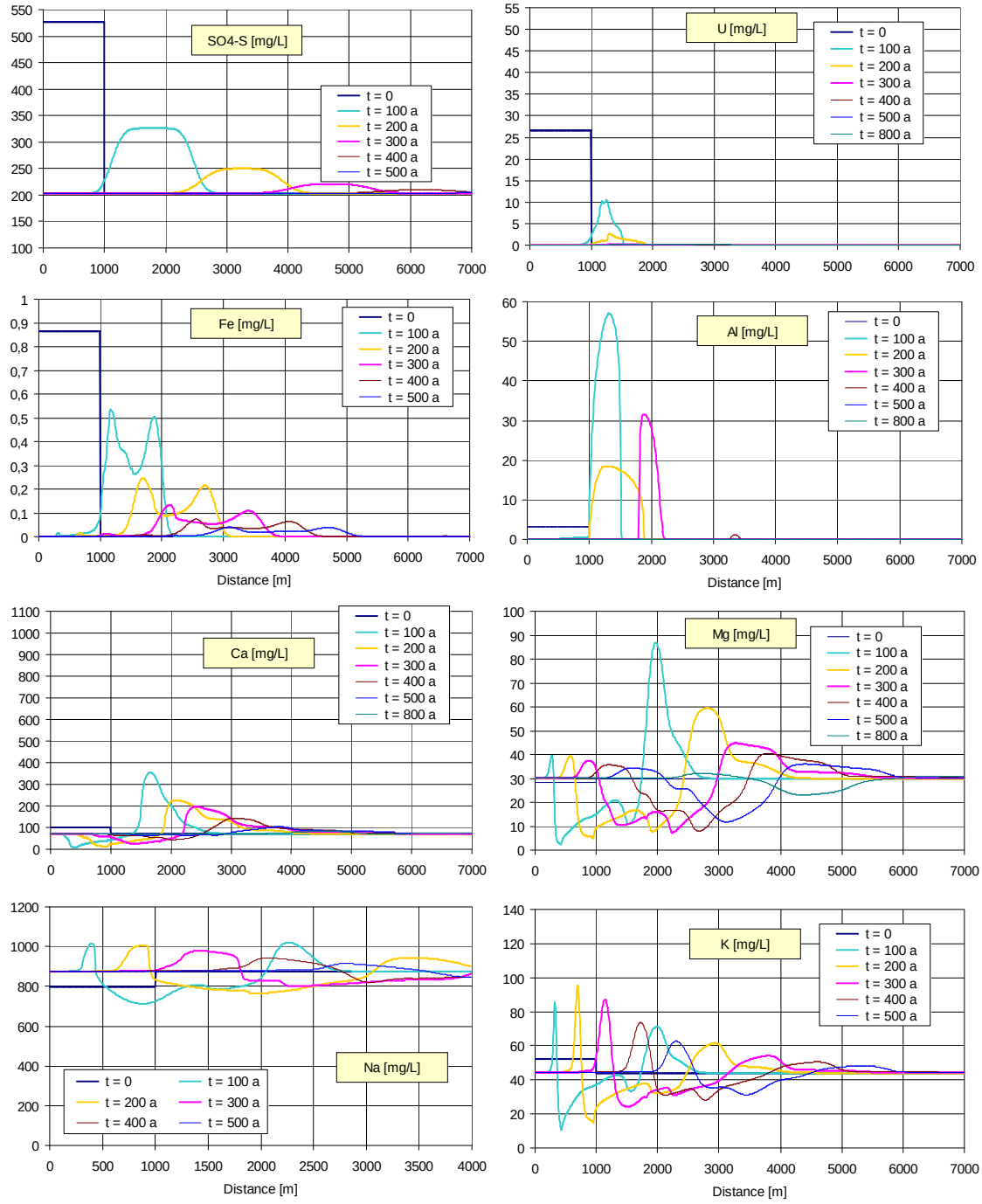

Fig. D.10 Element concentrations [mg/L] as a function of distance x – Real Case with Dilution

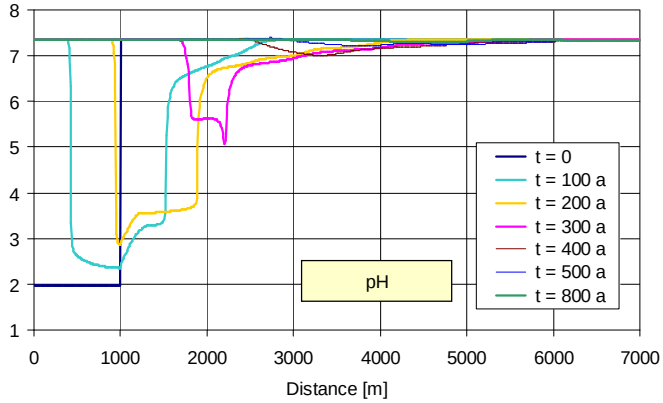

Fig. D.11 pH as a function of distance x – Real Case with Dilution

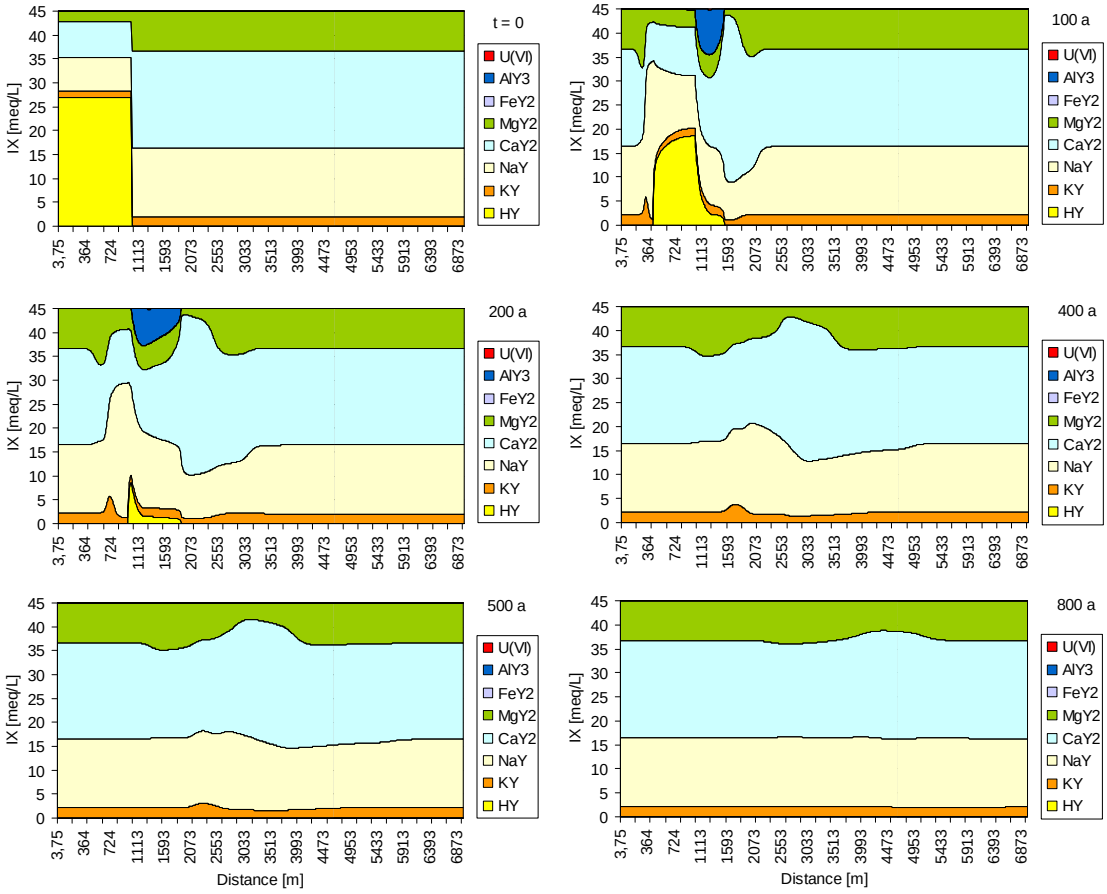

Fig. D.12 Cation distribution on ion exchanger as a function of distance x – Real Case with Dilution

E IMPACT OF FRACTURED ROCK FLOW

The aim of the following consideration is to estimate the impact of an uncontrolled flow from the ore zone into the FM Embayment via fractured rocks. Fig. E.1 illustrates a typical by-pass where lixiviant taken from a cell in the ore-zone is directed into an embayment cell that is 5 km away (downstream).

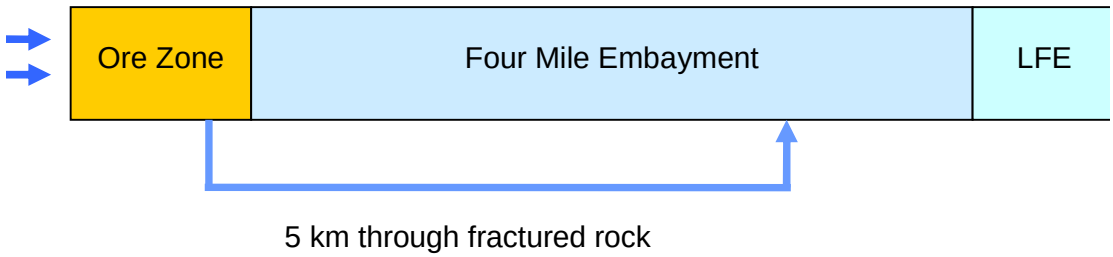

Fig. E.1 Scenario with lix flow through fractured rocks

The crucial parameter for the simulation is the mix ratio between the solution inside the embayment cell and the incoming lix. This ratio is given by the volumetric flow through fractured rocks, Q_F, and through the sandy aquifer, Q:

(E.1) $$\text{mix} = \frac{Q_F}{Q}$$

with (see [DS97] pp. 44-55)

(E.2) $$Q = k \frac{g \rho_W}{\mu} A \left| \frac{\partial h}{\partial x} \right| \quad \text{and} \quad k = c_k d_{10}^2 \quad \text{with} \quad c_k = 6.5 \cdot 10^{-4}$$

(E.3) $$Q_F = k_F \frac{g \rho_W}{\mu} A_F \left| \frac{\partial h}{\partial x} \right|_F \quad \text{and} \quad k_F = \frac{N b^3}{12}$$

Here, k and k_F are the intrinsic permeabilities (in units L^2) of the sandy aquifer and of the fractured rock. The other quantities are

$\lvert\partial h/\partial x\rvert = 0.00025$	hydraulic gradient in sandy aquifer
$\lvert\partial h/\partial x\rvert_F$	hydraulic gradient for fractured-rock pathway
$g = 9.81\ m/s^2$	acceleration due to gravity
$\mu = 8.9 \cdot 10^{-4}$ Pa s	viscosity of water (at 25 °C)
$\rho_W = 1.0 \cdot 10^3\ kg/m^3$	density of water
d_{10}	grain size (10 % particles are finer, 90 % are coarser)
$A = W Z$	cross section of flow path in sandy aquifer (in L^2)

$A_F = W\ b$	cross section of flow path in fractured rocks (in L^2)
W	width of flow path (in L)
Z = 10 m	thickness of flow path in sandy aquifer (= Z_{ore})
b	joint opening (in L)
N	number of joints per unit distance (in L^{-1})

The factor $g\rho_W/\mu$ describes the fluid and is given by

$$\text{(E.4)} \qquad \frac{g\rho_W}{\mu} = \frac{9.81\,m/s^2 \cdot 10^3\,kg/m^3}{8.9\cdot10^{-4}\,Pa\,s} = 1.1\cdot10^{-7}\ m^{-1}s^{-1}$$

[For example, using d_{10} = 0.1 mm and porosity ε = 0.30 we get a pore velocity in the sandy aquifer of

$$\text{(E.5)} \qquad v = \frac{Q}{A\,\varepsilon} = c_k d_{10}^2 \frac{g\rho_W}{\mu}\left|\frac{\partial h}{\partial x}\right| = 20\,\frac{m}{a} \quad]$$

If we quantities described above are inserted into Eq. (E.1) we obtain

$$\text{(E.6)} \qquad mix = \frac{k_F\,A_F}{k\,A}\cdot\beta \qquad \text{with} \qquad \beta = \frac{\left|\partial h/\partial x\right|_F}{\left|\partial h/\partial x\right|}$$

From hydrogeological modeling (MODFLOW calculations) is known that an opposite hydraulic gradient prevents the lixiviant from entering the fractured rock (i.e. β = 0). Now, with the condition that there is still an uncontrolled inflow it is assumed that

$\beta \approx 0.1$	(i.e. 10 % of the aquifer gradient)
N = 10 joints per meter	(worst case)
b = 1 mm	(worst case)

Therewith it results a mix factor of

$$\text{(E.7)} \qquad mix = \frac{Nb^3/12}{6.5\cdot10^{-4}\,d_{10}^2}\cdot\frac{b}{Z}\cdot\beta = 1.3\cdot10^{-3}$$

Compared to the mix factor due to transversal dispersion in Eq. (4.9) this impact is 3 times smaller. In relation to the groundwater within the embayment the order of magnitude is within the uncertainty of the data.

In conclusion, the small impact of lixiviant intrusion into the FM Embayment via fractured rocks can be neglected in the aquifer simulations.